

Recent Discovery of a New Geothermal Field in Italy: Alfina

R. CATALDI * AND M. RENDINA *

ABSTRACT

Research and initial exploration drilling carried out in the Alfina geothermal area are dealt with in this paper.

The Alfina area, located in northern Latium (central Italy), is almost lacking in hydrothermal manifestations at the surface. The research approach included two main steps: the first consisting of studies and investigations on a regional basis (geology, photogeology, hydrogeochemistry, gravimetry and shallow resistivity prospecting); the second consisting of specific surveys (geothermal gradient, heat flow, deep geoelectric prospecting, etc.). The latter surveys were conducted only in the preferential areas which had been singled out by means of regional investigations. The regional and specific survey pointed out that the Alfina area is characterized by a convergence of different geological factors favourable to the existence of geothermal fluids at depth; thus, the first exploration well in this area was drilled and completed in the summer of 1973.

The results of this well confirm that a geothermal reservoir exists in the Alfina area at depths below 600 m.

An outline is finally given of the future development of the new geothermal field.

Introduction

Interest in developing geothermal research in the pre-Appennine belt of central Italy, facing the Tyrrhenian coast, dates back to more than a decade. But only in 1965 approximately, a few years after the merging of the previous electric energy utilities into ENEL (Italian Electric Energy Agency), was it possible to plan an extensive programme of geothermal research on a national basis.

Following this programme, different projects were set up on a regional basis for investigating the geothermal potentiality of some Italian regions.

The « Monti Volsini geothermal project », including the Alfina area, is one of these projects. It concerns the region surrounding lake Bolsena (northern Latium) and covers a total surface exceeding 1500 km².

A geothermal prefeasibility study was thus undertaken in this region by ENEL about 8 years ago which aimed at determining whether the area featured any geological element encouraging the development of the Monti Volsini project.

Research approach

Based on the literature existing at that time and on a series of on the spot inspections, the prefeasibility

* ENEL, Direzione Studi e Ricerche, Centro di Ricerca Geotermica, Pisa, Italy.

study concluded that the Monti Volsini region was characterized geologically by

- wide effusions of Quaternary volcanic rocks;
- active faulting of Upper Miocene-Quaternary;
- a thick impermeable complex at the bottom of the volcanic cover;
- a confined aquifer underlying the above-mentioned complex;
- sporadic spots of hydrothermal manifestations.

These elements, of course, neither proved nor disproved the existence of hyperthermal fluids at depth; they only indicated that it was worthwhile continuing the geothermal project and passing to the feasibility study proper.

Research was then organized according to a criterion of step-by-step development, from regional low-cost studies to local specific surveys.

Regional approach

The group of regional studies, started in 1968 and concluded in 1970, consisted of the following investigations.

Geological study

It mainly involved volcanology, petrology and the volcano-tectonic setting, since volcanism is the dominant geological feature of the Monti Volsini region. Indeed, as Figure 1 shows, sedimentary terrains outcrop only at the borders of the region, evidencing the different geological formations which represent the substratum of the thin volcanic cover.

Tectonic attitude, lithology and the stratigraphic sequence of sedimentary rocks were also studied over a sufficiently wide area, in order to fit the situation of the region within a more complete geological frame.

Photogeological study

It included an analysis and a density map of the total field of fractures, selection and density maps of the main trends of fractures, selection of « long linears », study of the drainage pattern etc.

Besides such elements, the study of air photo-coverage enabled the detection and analysis of all « circular features » occurring in the region. Studying these fea-

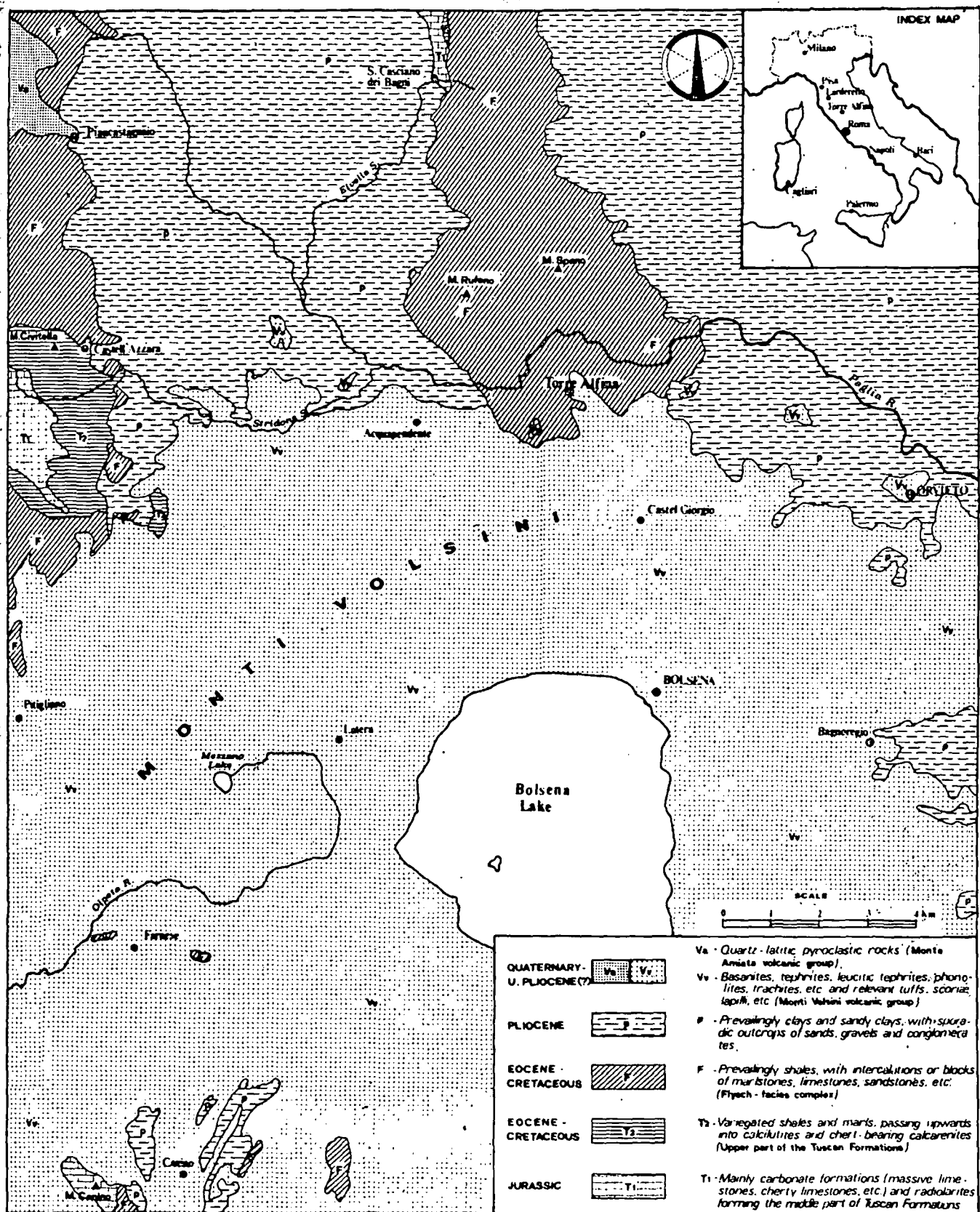


FIG. 1. — Schematic geological map of the Monti Volsini region.

tures (extrusion chimneys, crater edges, calderas, domes, etc.) is particularly important in such a volcanic region as that of Monti Volsini because of the role they play as local absorption areas of cold rain-water into the reservoir.

Figure 2 represents a portion of the area covered by the photogeological study. It shows the density of N-S and E-W fracture trends obtained from selection of the total field of fractures, and evidences that the geothermal area of Alfina is located on the western side of a buried geological feature connected with a densely fractured area at the surface.

Gravity prospecting

It was principally aimed at reconstructing the regional attitude of deep tectonic features. The average spacing of prospection is 1 point per 2 km² approx.

As can be seen in Figure 3, Monti Volsini region has a rather contrasting gravimetric attitude, with a series of positive and negative anomalies roughly trending N-S or NNW - SSE.

The two main positive anomalies, evidenced by values exceeding 25 milligals, are situated near Mt. Canino (the first) and in the Alfina area (the second). The latter anomaly has a local closure of about 5 milligals, which can be attributed to a positive feature of the carbonate formations underlying the impermeable flysch-facies terrains.

Special mention should be made of two low-density sub-circular anomalies, discovered south of Mezzano lake and near Bagnoregio. Both anomalies are marked by gravimetric values lower than 15 milligals. The first anomaly is certainly related to the volcanic extrusion of the Latera caldera; the second and round-shaped anomaly, on the contrary, may be interpreted as a mass deficit which is the result of an acid stock probably buried in the region, at a depth of 2.5 - 3 km.

Shallow resistivity survey

Like other similar surveys performed in different Italian geothermal areas, this survey was planned on a multi-purpose basis: firstly, to determine the depth and attitude of the top of the argillaceous or shaly formations underlying the volcanic cover; secondly, to determine the thickness of this cover and the attitude of the unconfined water level contained therein; thirdly, to single out low-resistivity areas. Taking into account that the thickness of the volcanic cover was expected to be in general less than 300 m, an electrode AB distance of up to 1 km was adopted according to the quadripôle Schlumberger array.

The distribution of resistivity values for the maximum depth investigated (i. e. corresponding to an AB distance of 1 km) is provided in Figure 4. This figure indicates that three low-resistivity areas (with values less than 10 ohm·m) exist in the Monti Volsini region.

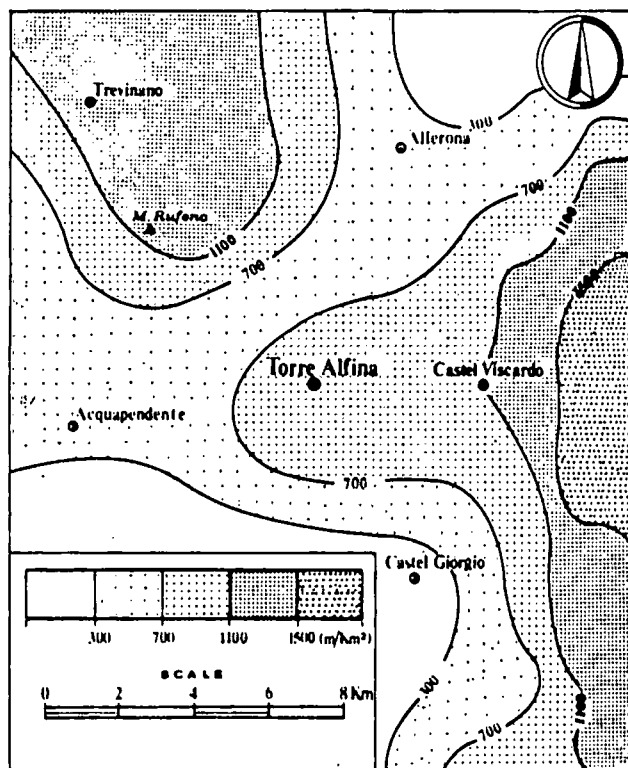


FIG. 2. — Density map of fractures (Selection N-S and E-W).

They are located as follows: the first near Alfina, the second west of Bolsena lake (near Latera) and the third a few kilometres west of Mt. Canino. These three areas are separated by high-resistivity values (100 ohm·m or more) but are all placed along a belt, whose direction (NE - SW) follows the pre-Apennine structural trend and is, therefore, of tectonic significance.

Hydrogeochemical study

It was initially planned as a regional hydrogeological survey of hydrothermal manifestations occurring in the whole volcanic area between Mt. Amiata and Rome. Subsequently, based on this survey, water, gas, incrustations, etc. of the principal manifestation spots were chemically (and sometimes also isotopically) analyzed to reconstruct the geochemical environment of the potential reservoir and to outline the patterns of water circulation.

Complete results of the hydrogeochemical study are contained in this issue in a paper by BALDI ET AL., which the interested reader is referred to. The main conclusions can be summarized as follows.

Two principal patterns of circulation exist in the region: a shallow one, developing essentially within the volcanic cover, and a deep one, involving the carbonate and evaporitic formations which represent the confined aquifer overlain by the flysch-facies complex. Thus, broadly speaking, the whole region between Mon-

ti V
inat
genc
emp
abo
that
man

Vols
fails
sign

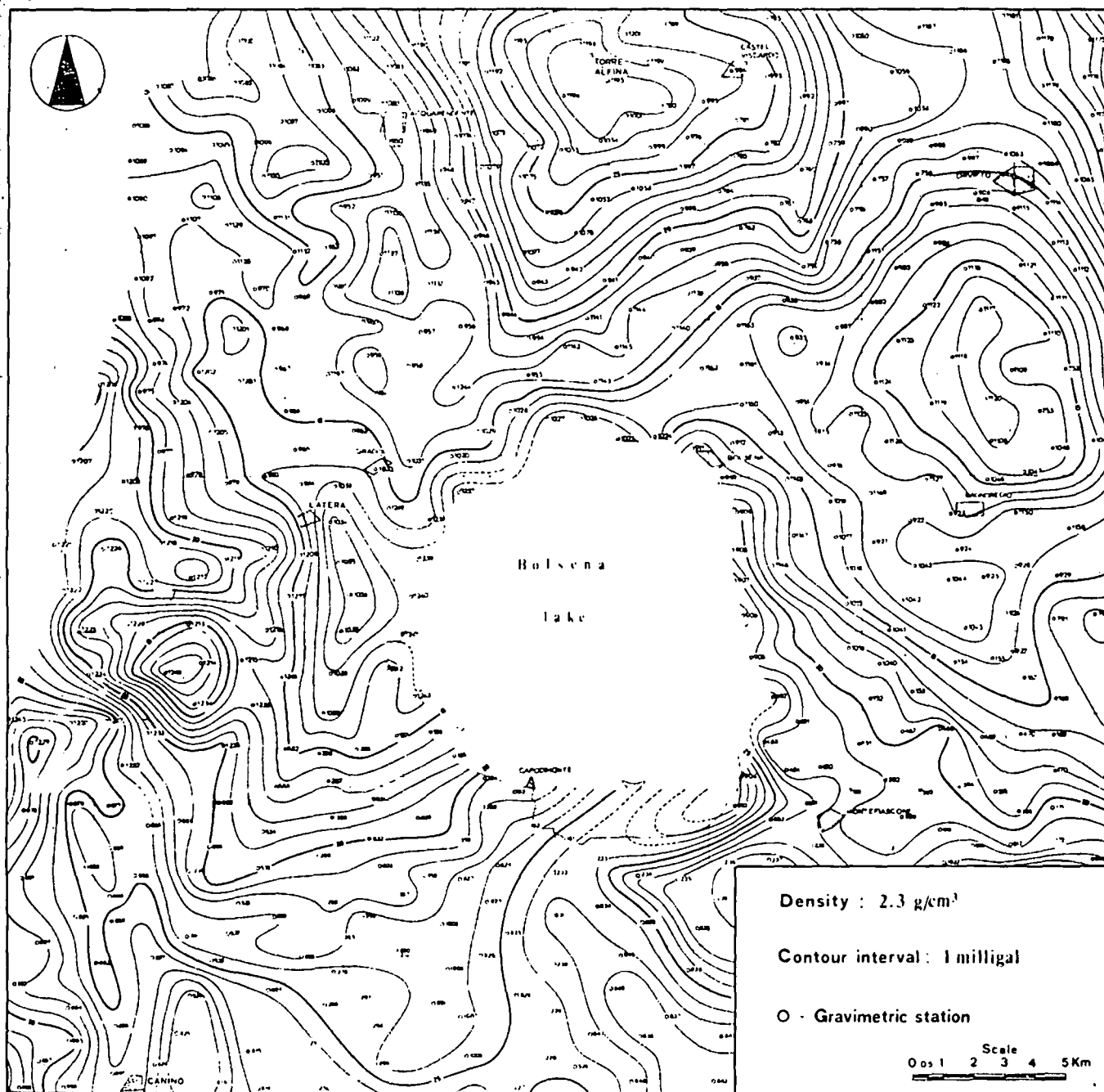


FIG. 3. — Bouguer anomaly map of the Monti Volsini region.

ti Volsini and Rome may be regarded as a « water-dominated geothermal system », with base temperature generally lower than 100°C. However, it should be emphasized that spots of hot manifestations in the above-said region have such a scattered distribution that vast areas remain entirely void of hydrothermal manifestations at the surface.

As a matter of fact, the northern part of the Monti Volsini region (and the area of Alfina in particular) fails to display, over an area exceeding 300 km², any significant surface trace of hydrothermal circulation;

consequently, the general conclusions of the hydrogeochemical study left open the possibility that the Alfina area might have a reservoir temperature over 100°C.

Other investigations

In addition to the investigations outlined above, which covered the whole (or most of) Monti Volsini project area two other kinds of investigations were conducted on a preliminary basis during the regional approach stage.

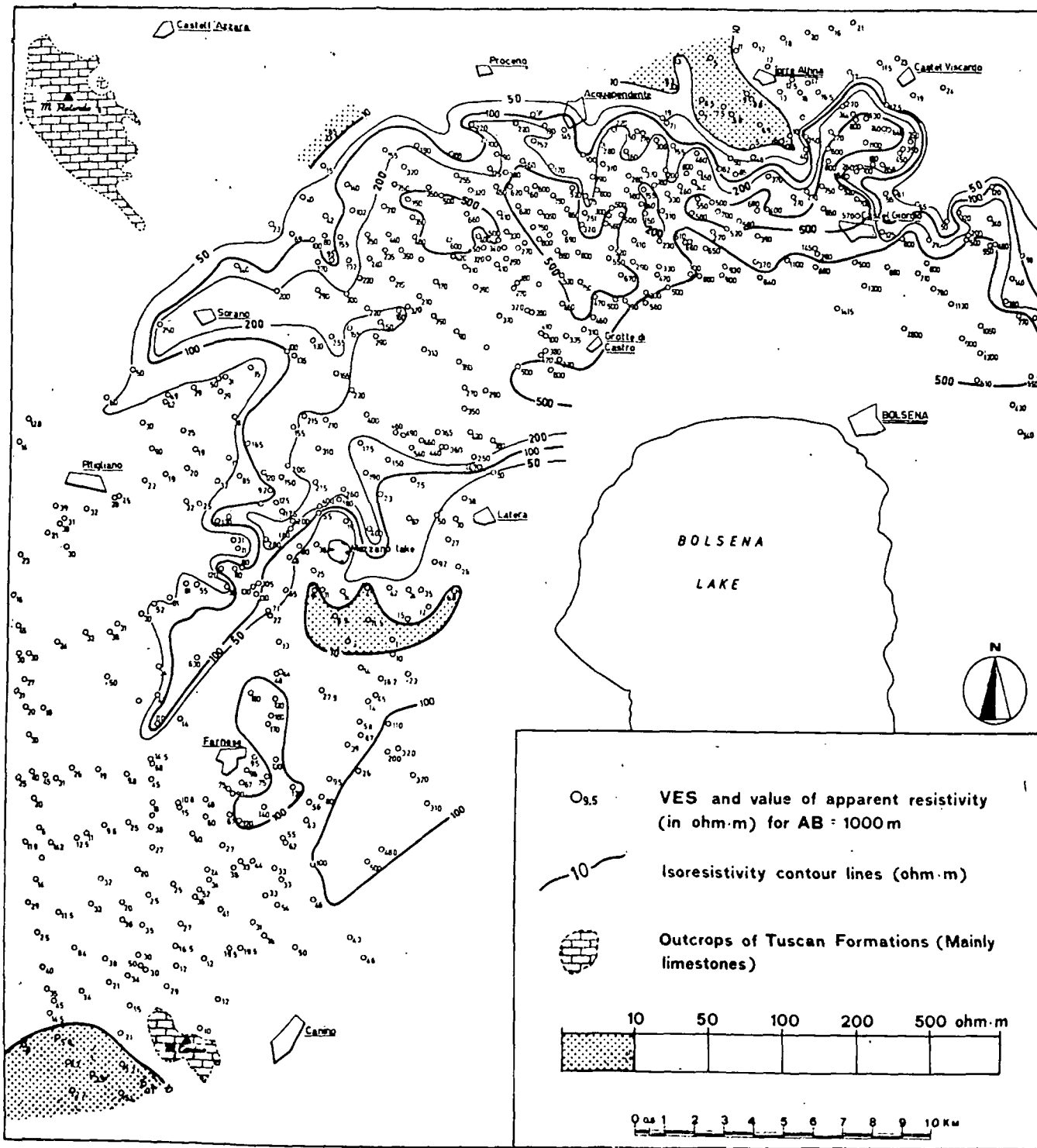


FIG. 4. — Shallow resistivity map of the northern and western part of the Monti Volsini region (AB=1000 m).

They are

- a number of *deep electric soundings* (AB of between 2 and 6 km) to evaluate at certain points the depth of the resistive substratum possibly corresponding to permeable carbonate formations;
- a few *geothermal test-holes* to determine the feasibility of applying geothermal prospection to such a region as that of Monti Volsini, where permeable volcanic rocks widely outcrop.

Specific surveys

The integrated evaluation of all the above-mentioned regional investigations enabled to conclude that two areas of the project might deserve further attention for additional and more specific prospections.

These two preferential areas, shown in Figure 5, cover aggregately a surface of about 500 km², which



FIG. 5. — *Two preferential areas for geothermal investigations.* The dashed areas are the two preferential areas for geothermal investigations.

represent about 17% of the total area of the Volsini project. The following sections were drilled in the spring of 1972 in the two preferential areas.

Geothermal gradient

It was determined that the geothermal gradient at depths of between 100 and 200 m is about 0.05°C/m. The local geothermal gradient is higher in the area of regional interest (see Figure 5) and lower in the area of minimum thickness of the volcanic formations.

The final results of the geothermal gradient survey, for the two preferential areas, are shown in Figure 6. The terrain lying between the two preferential areas is also covered by the geothermal gradient survey.

The average geothermal gradient in the two preferential areas is 0.05°C/m. The average geothermal gradient in the area of minimum thickness of the volcanic formations is 0.03°C/m.

Three additional geothermal test-holes were drilled in the Volsini region. The results of these test-holes are shown in Figure 7. The geothermal gradient in the Canino, Latera, and Fardome areas is 0.03°C/m. The geothermal gradient in the area of minimum thickness of the volcanic formations is 0.03°C/m.

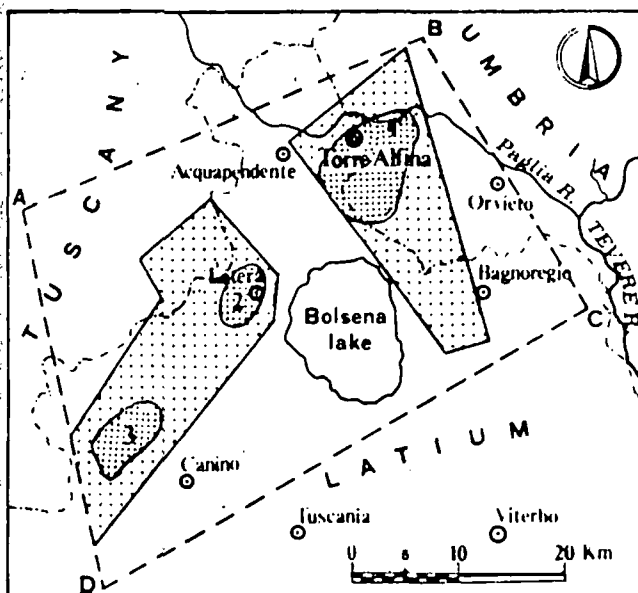


FIG. 5. — Area of the Monti Volsini geothermal project. The dashed line outlines the whole project area; dotted areas are the preferential ones singled out by regional investigations.

represent about 30% of the total area of the Monti Volsini project.

The following specific surveys were thus started in the spring of 1971 and completed in the summer of 1972 in the two preferential areas.

Geothermal gradient survey

It was carried out by drilling 30 shallow holes at depths of between 60 and 250 m, thus giving an average depth of 120 m.

The location of each hole was chosen on the basis of regional investigations (especially the shallow resistivity survey), which allowed to select the areas with a minimum thickness and the least possible permeability of the volcanic rocks.

The final depth of each hole was such as to reach and cross, for at least 30 m, the argillaceous or shaly terrains lying under the volcanic cover.

The average density of geothermal holes is 1 per 17 km² approx., but their distribution over the two preferential areas is not homogeneous due to geological and operative reasons. Despite this seemingly low density, all the geological features of potential interest were covered by many geothermal holes.

Three chief anomalies were detected in the Monti Volsini region, which are located in the areas near Mt. Canino, Latera and Alfina. These areas, with geothermal gradient values between 0.1 and 0.2°C/m, stand out over the surrounding ones, whose regional value is 0.05°C/m. All three anomalous areas are aligned along the same NE-SW belt described for the shallow resistivity survey.

Heat-flow survey

This was another specific investigation carried out in the preferential areas. It was, however, an indirect survey, as it was based upon the geothermal gradient survey and thermal conductivity measurements executed in laboratory.

These measurements were carried out according to the « needle probe method » on soft rock samples cored in each hole in correspondence to the depths at which temperature had to be measured.

The heat-flow map (Figure 6) basically reflects the gradient map. This has nothing surprising, since about 85% of conductivity values are concentrated in the range $3.25-4.75 \cdot 10^{-3}$ cal/°C cm s (1.36 to 1.99 W/m K approx.). This concentration depends in turn upon the location of geothermal holes, which were drilled in as-impervious-as-possible terrains (clays, shales, etc.).

As a consequence, the same anomalous areas mentioned for the geothermal gradient survey (i. e. Canino, Latera and Alfina) stand out in the heat-flow map. These areas are all marked by values exceeding $3 \mu\text{cal}/\text{cm}^2\text{s}$ ($0.13 \text{ W}/\text{m}^2$), but those of Canino and Alfina (6 to $8 \mu\text{cal}/\text{cm}^2\text{s}$, or $0.25-0.33 \text{ W}/\text{m}^2$) are even more marked than that of Latera (4 to $5 \mu\text{cal}/\text{cm}^2\text{s}$, or $0.17-0.21 \text{ W}/\text{m}^2$).

Deep geoelectrical prospecting

It was mainly directed at detecting the resistive substratum which was likely to correspond to the top of the carbonate formations lying under the flysch-facies complex. Like the shallow resistivity survey, this

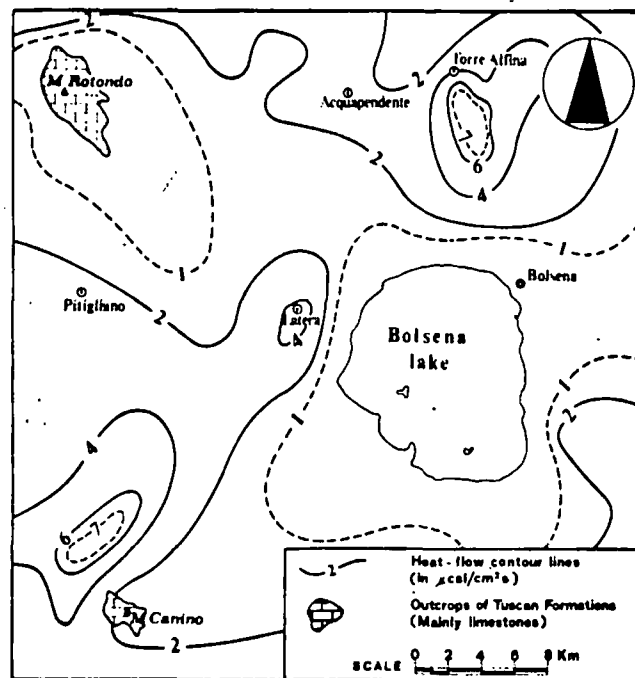


FIG. 6. — Heat-flow map of the Monti Volsini region.

prospecting was performed following the Schlumberger quadripôle method, with a max. AB electrode distance of 4-6 km, which was considered sufficient for average depths (1000-1500 m) of the resistive substratum. Considering that the main structural trend of the Monti Volsini region is NNW-SSE, the geoelectric profiles were carried out, as far as possible, along a NE-SW direction, in order to « cross » deep-seated resistive features.

The spacing between electric soundings is on the average 1 km approx. along each profile; while the distance from one profile to the other is about 2 km. A greater density was adopted in correspondence to the areas of geothermal anomaly.

Part of the deep geoelectric prospecting results is shown in Figure 7, which represents the attitude of the resistive substratum in the Alfina area proper. It can be noted that in the very central part of this area the resistive substratum is framed as a closed positive feature, adjoined by a series of smaller down-thrown blocks. In the central part of this feature, the average elevations of between -200 and -500 m with respect to datum plane (s. l.) correspond to depths of 600-1000 m, which are very suitable for drilling exploration. Other positive features of the resistive substratum, comparable to that of Alfina, were found in the areas near Mt. Canino and Latera.

Other surveys

Some additional investigations, besides the above-said surveys, were performed on a local scale in correspondence to the preferential areas shown in Figure 5.

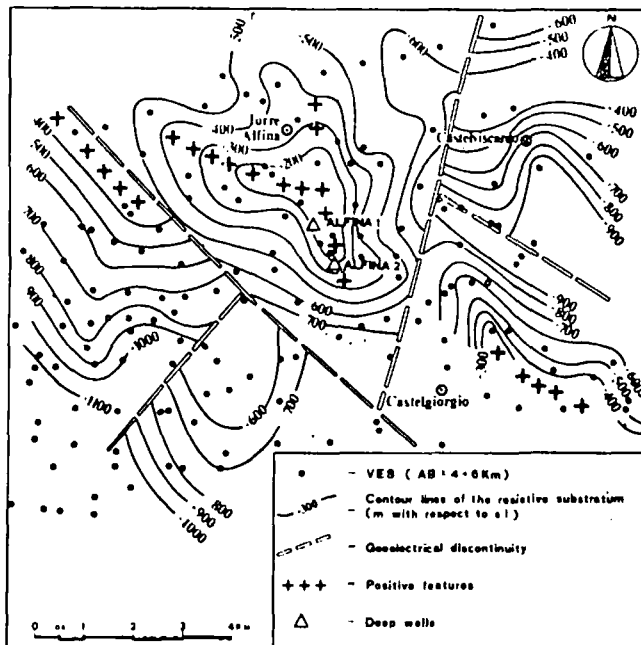


FIG. 7. — Attitude of the resistive substratum in the Alfina geothermal area.

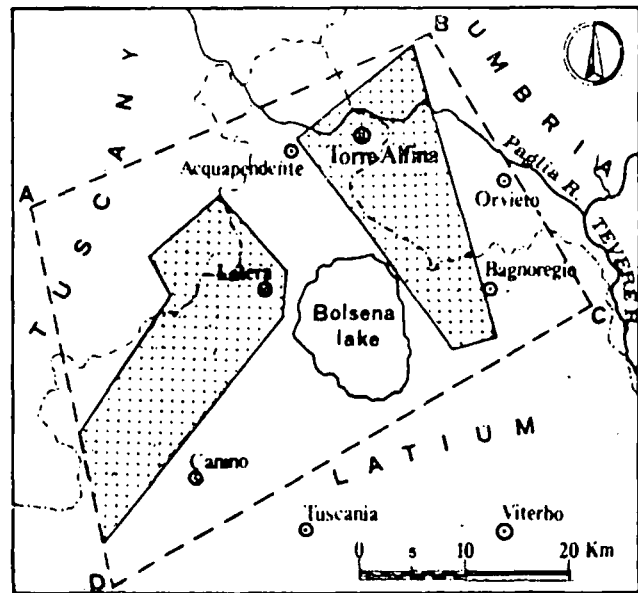


FIG. 8. — Areas selected for deep exploration. 1) Torre Alfina; 2) Latera; 3) Canino.

In short, these additional investigations include: detailed stratigraphic series of volcanic and sedimentary sequences; hydrogeology and chemical analyses of cold springs; repeated geochemistry of manifestations.

As regards the Alfina area proper, which is almost completely lacking in hydrothermal manifestations, as previously said, geochemical investigations could supply only indirect information, based essentially on a gas escape existing near the Alfina village.

This escape occurs in a few small pools of cold water, from which sporadic bubbles of gas (mainly CO₂, as Table 1 shows) are weakly released. Considering jointly the chemical nature of the gas and the geological structure of the area, as well as the hydrogeological situation, the hypothesis could be put forward that a gas cap was likely to exist within the upper part of the closed feature detected by the deep geoelectric prospecting.

Selection of promising areas

Comparison and integrated interpretation of all the regional and specific surveys enabled to focus attention on the three areas shown in Figure 8: Canino, Latera and Alfina.

In fact, by comparing the results of each survey or study, it can be noticed that these three areas are characterized by a remarkable convergence of the following geological features

- high values of geothermal gradient (0.1-0.2 °C/m);
- high values of conductive heat flow (> 3 μcal/cm²s);
- elongated gravity highs of a structural type;
- positive features of resistive substratum (probably corresponding to permeable carbonate rocks), whose top lies at depths of 600-1000 m;

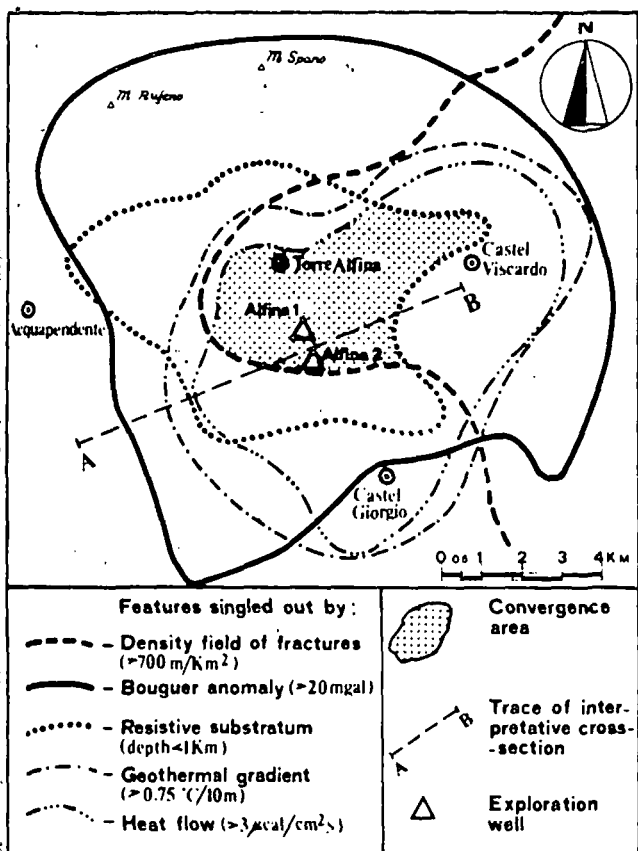


FIG. 9. — Preferential features of the Alfina geothermal area.

- a sufficient thickness (500 m or more) of the impermeable complex sealing the underlying resistive complex;
- high density of fracture field ($> 700 \text{ m/km}^2$);
- scattered spots of hydrothermal manifestations (except for the Alfina area);
- probable presence of a gas cap at the top of uplifted features.

Due to the coexistence of these geological features, the area which appeared to be promising for undertaking drilling exploration was that of Alfina. Here, furthermore, as was pointed out for the hydrogeochemical study, the absence of hydrothermal manifestations at the surface was considered an additional favourable factor for proceeding to the deep exploration stage.

The planimetric projection of the different geological features singled out in the Alfina area is shown in Figure 9, where the overlapping zone can be regarded as preferential for starting drilling exploration. The interpretation given to this area before starting drilling is represented in the cross-section of Figure 10.

Exploration of the Alfina area

Exploration of the Alfina area began in the spring of 1973 and is still at an early stage. The first test-well, whose location and projection are shown in Figures 9 and 10 respectively, began in May 1973 and was completed in about one month in June 1973, at the final

depth of 633 m. Figure 11 displays the geological situation of this well, together with some thermometric and geoelectric logs.

As the latter figure shows, the lithostratigraphic sequence of the well is quite simple and is made up of a flysch-facies complex lying under a few metres of volcanic rocks and probably over carbonate formations.

Regardless of the fact that two different formations (each including two different members) can be distinguished within the flysch-facies complex, it can be claimed that shale is the dominant lithotype of the sequence, with thin intercalations of marls, marlstones and limestones. This dominance accounts in turn for the complete absence of circulation losses or mud absorption down to the bottom of flysch terrains, as well as for the remarkable constance of geothermal gradient.

At a depth of 633 m, however, where the cap-rock is likely to come into contact with the reservoir, a sudden circulation loss occurred during drilling, which resulted in a rapid and violent eruption, in spite of the many attempts made at removing the drill string and at introducing the production casing.

The flow rate increased significantly in a few hours and a considerable amount of dust and chips, torn away from the uncased walls of the well by the endogenous fluid, added to the same fluid, thereby producing a scene far more impressive than that shown in Figure 12.

The fluid yielded by the well was, from the very beginning of the eruption, a dry fluid, prevalently made up of CO_2 and a minor percentage of steam. In the course of the following 2-3 days, however, the gaseous rate underwent an evident decrease, whilst temperature, total amount of fluid and steam percentage were rising. At the same time, dust and chips diminished and the gas-steam jet became increasingly high and clean (Figure 13).

Owing to very hazardous working conditions, the need arose to repair or to collapse the well; therefore it was absolutely impossible to undertake the usual measurements for obtaining the actual values of flow-rate, pressure, gas-steam ratio and temperature. Consequently, for the initial conditions of production, only some estimated values can be provided, i. e. 300-400 t/h for flow rate and 70-80% by weight for gas-steam ratio.

Moreover, shut-in pressure certainly exceeded 33 kg/cm^2 , since this value was recorded during shutting operations aimed at causing the walls of the well to collapse.

The chemical composition of the gas exhausted by the well Alfina 1 (Table 1) is practically the same as that of the surface escape of cold gas occurring about 2 km away from the well site, so confirming their common origin.

By comparing the gas composition given in Table 1, it can be noted that hydrogen sulphide is practically

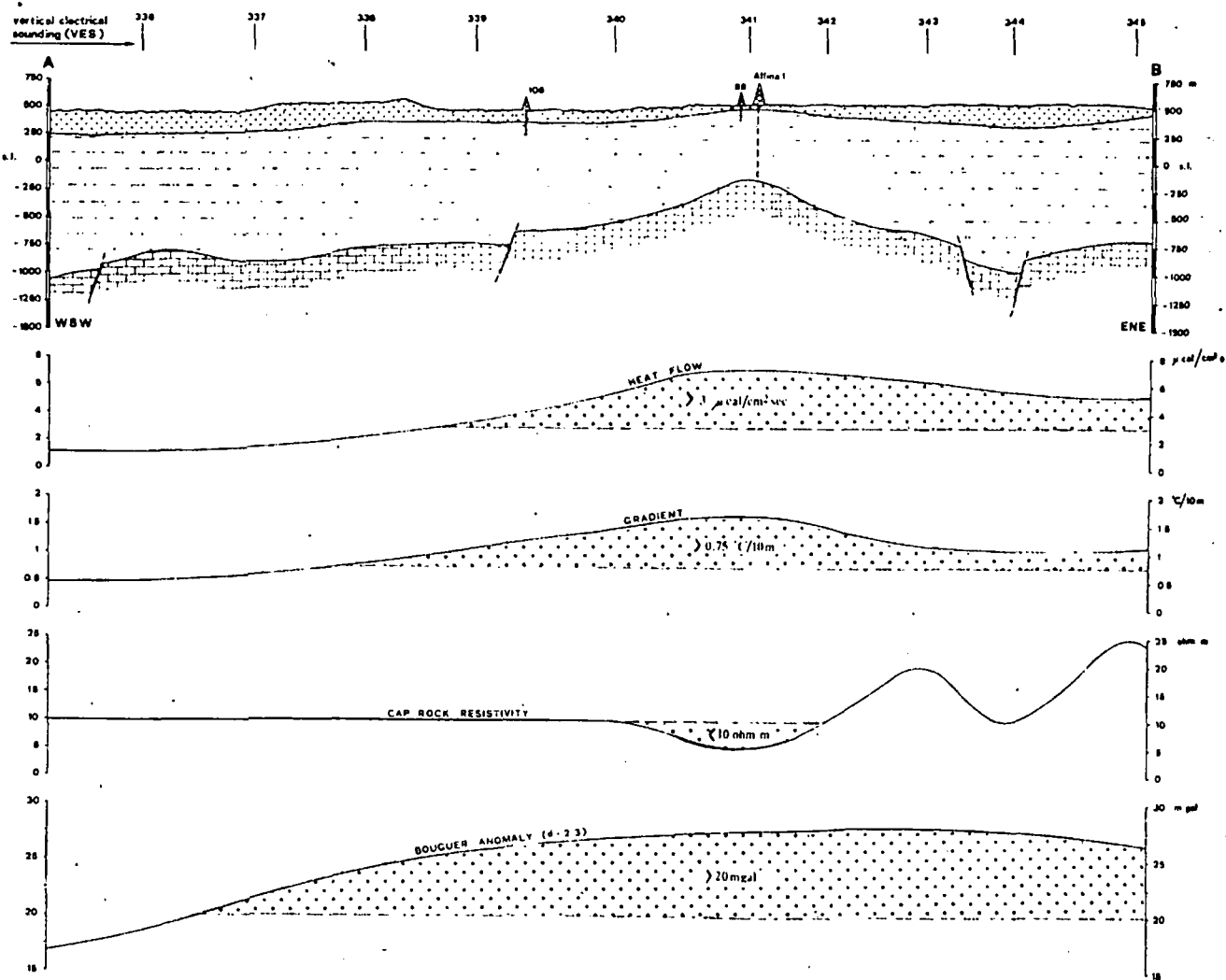


FIG. 10. — Interpretative cross-section of the Alfina geothermal area.

TABLE 1. — Gas composition of the Alfina well as compared to that of a nearby gas-escape and of the Mt. Amiata geothermal fields (% in volume).

Compo- nents	Superfi- cial gas escape near Alfina	ALFINA WELL					Mt. Amiata (average)
		Sample 1	Sample 2	Sample 3	Sample 4	Sample 5	
CO ₂	98.62	98.54	98.54	98.59	98.65	98.65	94.91
CH ₄	0.20	0.15	0.17	0.18	0.17	0.17	3.64
N ₂	1.12	1.31	1.29	1.23	1.18	1.18	0.76
H ₂	traces	nil	nil	nil	nil	nil	0.36
O ₂	0.06	traces	traces	traces	traces	traces	nil
H ₂ S	nil	traces	nil	nil	nil	nil	0.33

missing in the Alfina area and that methane is significantly lower in this area with respect to that on average contained in the gas mixture of the Mt. Amiata geothermal fields. These differences lead to the hypothesis that reservoir conditions in the Alfina area are some-

what different from those of the Mt. Amiata geothermal fields, the nearest of which (Piancastagnaio) is located at a distance of over 25 km.

Next development of the area

The technical work required to control the violent eruption of Alfina 1 well severely restricted the possibility of obtaining the physical characteristics of the fluid during the initial period of production and subsequently hindered the possibility of carrying on systematic measurements.

Despite this, it can be deemed that the data and information provided by Alfina 1 well fully support the previous interpretation based on surface surveys and confirm that a new geothermal field was discovered by ENEL in Italy.

The extension and potentiality of this new field are yet to be determined. As concerns extension, Figure 9 enables a first work hypothesis by considering the area where different geological features overlap

and which, however, in the limits of interpretation and conservative reservoir calculations, are indeed, are i calculations of the field.

AGE	COMPLEX
QUAT.	VOLC.
CRETACEOUS - L. TERTIARY (?)	
FLYSCH FACIES COMPLEX	
M. CRETAC.	M. CRETAC.
M. CRETAC.	M. CRETAC.

FIG. 11. — flows in shales, and calc nites, in shales formations.

and which covers a surface of 15-20 km². The latter, however, might be an underestimated figure since the limits of interest for some features (such as gravimetry and reservoir depth) have been considered following conservative assumptions.

As to the potentiality of the field, estimates are even more difficult due to the lack of tested values for some physical parameters of the reservoir. These values, indeed, are indispensable in approaching thermodynamic calculations aimed at shaping a realistic physical model of the field. In this respect, by analogy with other Italian

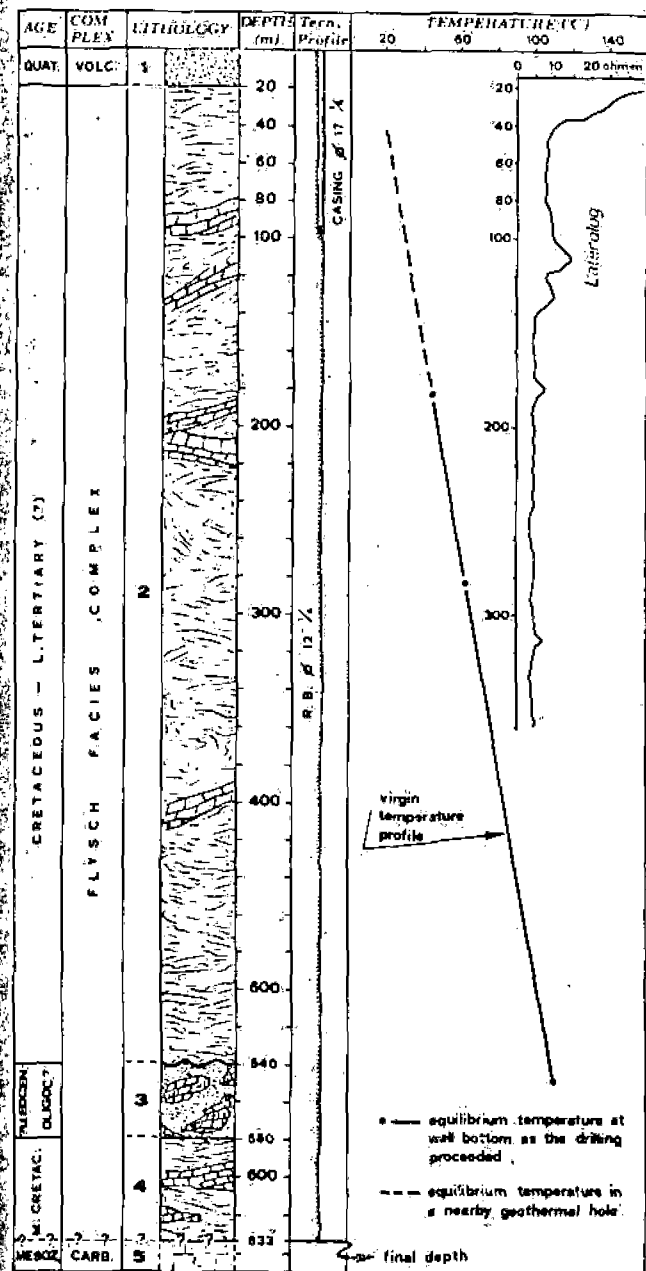


Fig. 11. — Exploration well Alfina 1. 1) Trachybasaltic lava flows and related scoriae; 2) Variegated shales and sandy shales, with thin intercalations of marlstones, limestones and calcarenites; 3) Chert-bearing calcilutites and calcarenites, embedded in a shaly-marly matrix; 4) Variegated shales with grey and pink marlstones; 5) Carbonate formations.



Fig. 12. — View of the Alfina 1 well, 36 hours after explosion. The steam-gas jet is carrying a remarkable amount of dust and chips.

fields, it should be supposed that at least six months of exploration and production are needed to obtain the physical parameters of the reservoir (porosity, water balance, base temperature, thickness, etc.) and to allow a substantial drainage of the gas cap.

With reference to the above-mentioned problems (extension and potentiality) and to those connected with industrial exploitation of the new field, a detailed project (called « Alfina geothermal project ») has been set up by ENEL, which will be implemented on a step-by-step basis.

As regards the exploration area only, the first step, which is scheduled for the 1974-76 period, includes

- an exploration research program, implying detailed studies and investigations on deep and surface geology, hydrogeology, geochemistry, geophysics and reservoir engineering;
- a drilling program, including 5-10 test-wells and one or two deep well(s) for disposing of geothermal waters (if necessary);
- an ecological program, aimed at studying and experimenting different alternatives of utilization and/or disposal of geothermal waters and gaseous effluents.

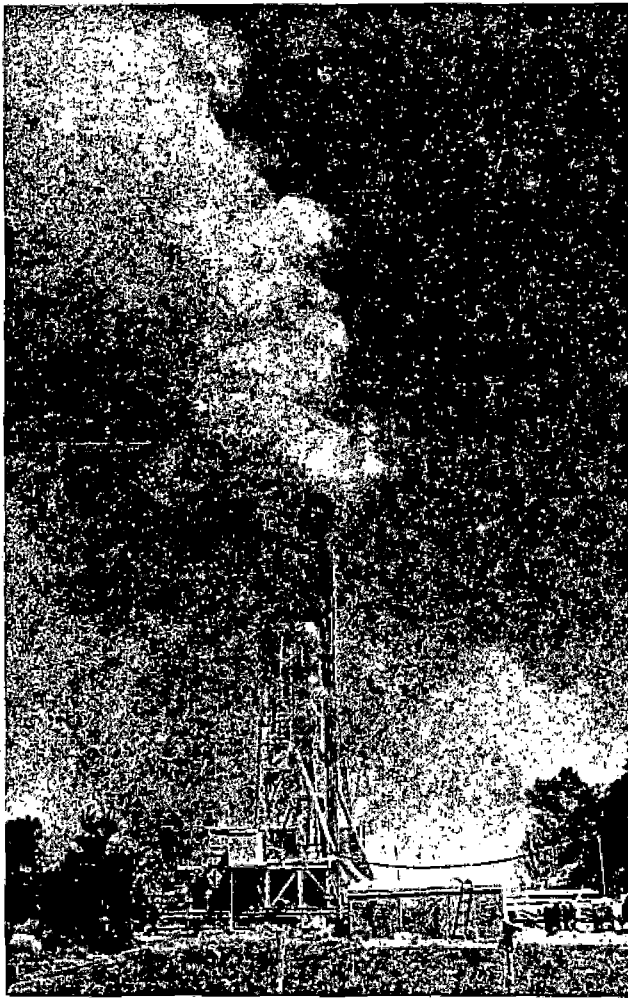


FIG. 13: — View of the Alfina 1 well, 3 days after explosion. Note the different height and cleanliness of the gas-steam jet in respect to that of Fig. 12.

Reference note

The region of Monti Volsini, and particularly the area of Alfina, were, until a few years ago, sufficiently studied from the volcanological standpoint, but poorly known from the general and structural geological standpoint. As a result, basic literature was also rather reduced.

As a consequence, when shaping the Monti Volsini geothermal project, ENEL was confronted with the need to perform not only specific surveys and prospections applied to geothermal exploration, but also basic studies and investigations with a view to obtaining an improved regional picture of the various geological problems. Most of the geological, geophysical and geochemical results gathered during the research concerning the area of the Monti Volsini project are therefore unpublished and available from ENEL — Centro di Ricerca Geotermica — files.

Since this note is practically based on unpublished literature we have preferred to avoid specific References in order not to burden the text with frequent quotations of unpublished reports.

However, the main reports of this type are quoted in the list of selected references.

Acknowledgements

The Monti Volsini geothermal project was conducted and implemented by the Centro di Ricerca Geotermica (CRG), ENEL, directed by Dr. P. CERON.

University institutes or service companies were entrusted with some studies or geophysical prospectings; other studies and prospectings, as well as the integrated interpretation of all surveys, have been carried out by the whole technical staff of CRG.

We are indebted in particular to A. CALAMAI for his assistance in preparing part of the drawings and for the critical reading of the manuscript.

REFERENCES

BURGASSI P. D., CERON P., FERRARA G. C., SESTINI G. and TORO B. 1970 — Geothermal gradient and heat flow in the Radicofani region (east of Mt. Amiata, Italy). *Geothermics, special issue 2, Pisa.*

CALAMAI A., CATALDI R., SQUARCI P., TAFI L. 1970 — Geology, Geophysics and Hydrogeology of the Monte Amiata geothermal fields. *Geothermics, special issue 1, Pisa.*

CATALDI R. 1967. — Remarks on the geothermal research in the region of Mt. Amiata (Tuscany, Italy). *Bull. volc., 30.*

CENTRO RICERCHÉ GEOLOGICHE 1969 — Studio fotogeologico della zona Volsina-Cimina-Sabatina. *Florence, (Study carried out for ENEL - Centro di Ricerca Geotermica - Unpublished report).*

COMPAGNIA GENERALE DI GEOFISICA 1970 — Studio gravimetrico della zona Volsino-Cimina. *Rome, (Study carried out for ENEL - Centro di Ricerca Geotermica - Unpublished report).*

COMPAGNIA MEDITERRANEA PROSPEZIONI 1970 — Studio geoelettrico nella zona a Nord ed Ovest del lago di Bolsena. *Rome, (Study carried out for ENEL - Centro di Ricerca Geotermica - Unpublished report).*

COMPAGNIA MEDITERRANEA PROSPEZIONI 1972 — Studio geoelettrico strutturale nella parte settentrionale ed occidentale dei Monti Volsini. *Rome, (Study carried out for ENEL - Centro di Ricerca Geotermica - Unpublished report).*

ENEL - CENTRO DI RICERCA GEOTERMICA 1972 — Rapporto sulle prospezioni geofisiche eseguite nel 1971 nella regione dei Monti Volsini. *Pisa, (Unpublished report).*

ENEL - CENTRO DI RICERCA GEOTERMICA 1973 — Prospezione geotermica nella regione dei Monti Volsini. *Pisa, (Unpublished report).*

ENEL - CENTRO DI RICERCA GEOTERMICA 1973 — Studio idrogeochimico delle regioni volsina, cimina e sabatina. *Pisa, (Unpublished report).*

ENEL - CENTRO DI RICERCA GEOTERMICA 1973 — Rapporto sul sondaggio di ricerca Alfina 1. *Pisa, (Unpublished report).*

MOUTON J. 1969 — Contribution des méthodes de prospections géothermique, électrique et gravimétrique à l'étude des champs géothermiques de Toscane. *Bull. volcan., 33.*

NAPPI G. 1969 — Stratigrafia e petrografia dei Volsini sud-occidentali (Caldera di Latera). *Boll. Soc. Geol. Ital., v. LXXXVIII, 1, 171-181.*

SERVIZIO GEOLOGICO D'ITALIA - Carta geologica d'Italia: sheets 1:100.000 - n. 129 « S. Fiora » - n. 130 « Orvieto » - n. 136 « Tuscania » - n. 137 « Viterbo » and respective sheets remarks.

UNIVERSITY OF PARMA, INSTITUTE OF PETROGRAPHY, MINERALOGY AND MINERAL DEPOSITS 1970 — Relazione sul vulcanismo volsino. *Parma, (Study carried out for ENEL - Centro di Ricerca Geotermica - Unpublished report).*

UNIVERSITY OF PISA, INSTITUTE OF GEOLOGY 1970 — Rilevamento e studio geologico della regione volsina. *Pisa, (Study carried out for ENEL - Centro di Ricerca Geotermica - Unpublished report).*

A R
A. C.
ABST
which
Italy;
ing of
exploit
genera
respec
I
Studi
ments
These
ly, hav
a) to a
whie
repre
b) to tr
study
also
c) to re
possi
rocks
Fa
ments
the geo
T)
tember
the foll
curs
— 0-
— 170-
— 715-
— 800-11
The
of 890
of threa
drilling
* E
Geotermi

Remarks on the Geothermal Research in the Region of Monte Amiata (Tuscany - Italy) *

R. CATALDI

E.N.E.L. - Direzione Studi e Ricerche

Introduction

Position and limits of the region

The geothermal region which will be discussed in this paper is located in southern Tuscany, at approximately 80 km SE of Lardello and 120 km NW of Rome. It is limited by: the Orcia river to the North, the Formone stream and the superior course of the Paglia river to the East, the alignment Montebuono-Catoggio to the South, the superior part of the Albegna river, the range Rocchette-Poggio Sasso-Poggio Volturaie-Mt. Aquilaia and the Ente stream to the West (see Fig. 1).

The volcanic massif of Mount Amiata stands isolated in approximately the center of this region. This massif, which is over 1700 meters high, dominates the whole large surrounding region, which slopes down towards the valleys of the Orcia river to the North, of the Paglia river to the East, of the Fiora and Albegna rivers to the South. Around the main central mountain, there are the reliefs of Poggio Zoccolino (1035 m) to the NE, of Mt. Civitella (1107 m) and Mt. Rotondo (951 m) to the S-SE, of Mt. Labbro (1193 m) and of the range Volturaie-Mt. Buceto-Mt. Aquilaia (1050 ÷ 1150 m) to the W and SW, and other minor hills. All together, such reliefs form the main morphologic frame of the region.

* Paper presented at the IAV International Symposium on Volcanology (New Zealand), Nov. 1965.

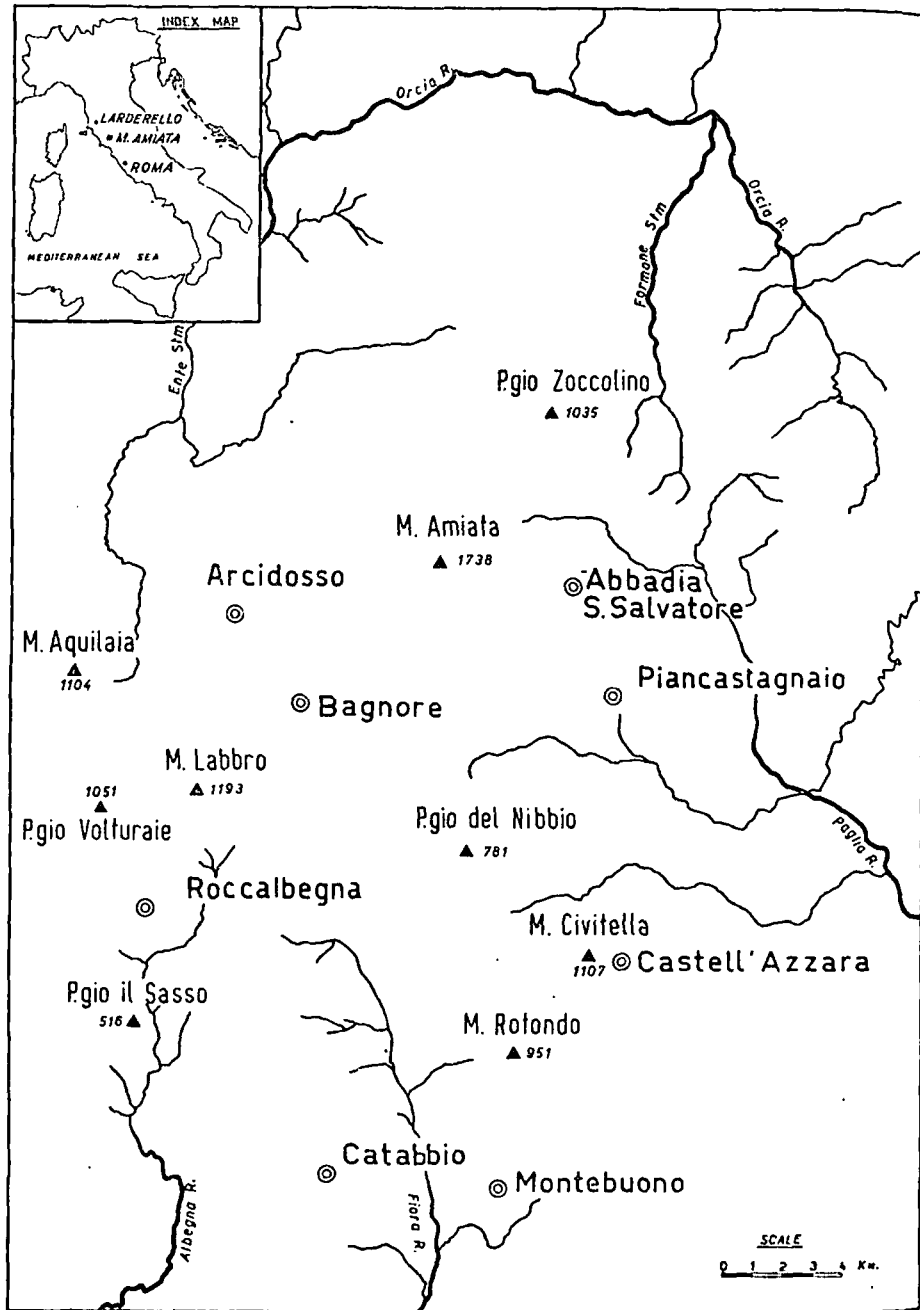


FIG. 1 - Schematic map of Mt. Amiata region.

Brief history of the region

The geothermal phase of the geological Development series of the region took project level and local stratigraphic conditions. They were then the of analog out on the derello re as the m exploratic

The of the w results. T SW flank drilling o ments of was local of this at 16 wells:

From tested by Nibbio o the drilli

The associatic

(1) Note in the Poggi new product

Brief historical outline of the geothermal research in the Mt. Amiata region

The exploration drilling, the discovery and exploitation of the geothermal steam in the Mt. Amiata region belong to a quite recent phase of research. Already in the years 1953-1956 however, the Geological Department of the ex « Larderello Company » had started a series of preliminary studies to find out whether, in the Mt. Amiata region too, there existed such elements as to justify an exploration project for the research of natural steam. To this purpose, regional and local studies were planned and carried out on the lithology, the stratigraphy and the structure, on the surface and deep hydrological conditions, on the volcanology and on the surface mineralisations. They were followed by geophysical surveys; first the gravimetrical, then the electrical and, more recently, the thermal one. On the basis of analogical criteria the results of the preliminary studies carried out on the Mt. Amiata region were compared with those of the Larderello region and of its producing areas; then, the areas considered as the most favourable were chosen and the locations of the first exploration wells selected.

The research, started in the summer of 1958 with the drilling of the wells St. Filippo 1 and Bagnore 1, immediately gave positive results. The exploration of the producing area of Bagnore, on the SW flank of the Amiata volcano, was completed in 1962 with the drilling of 21 wells. In the summer of 1961, after the latest developments of the surface studies, the producing area of Piancastagnaio was located in the southern slopes of Mt. Amiata. The exploration of this area has not been completed yet: up to September 1965 only 16 wells have been drilled.

From 1963 onwards, other areas of the Amiata region have been tested by exploration wells: Roccalbegna and, above all, the Poggio Nibbio ones have been considered sufficiently interesting to justify the drilling of additional test wells⁽¹⁾.

Geological Conditions

The existence of a « steam-field » is strictly conditioned by the association of various geological factors. Among them it is indispen-

⁽¹⁾ Note added in proof - As a matter of fact, in April, 1966 a second well drilled in the Poggio Nibbio area resulted productive. Data concerning the exploitation of this new productive area will be given in a future paper.



ata region.

sable to have: an efficient cap-rock, an underlying permeable complex, a favourable geologic structure, a substantial thermic anomaly and an adequate water supply. Therefore, owing to the necessary brevity of this note, the geological conditions of the Amiata region will be described only in the main features with special reference to those aspects considered as the most important for the applied research of endogenous fluids.

STRATIGRAPHY

From a geohydrological point of view, the stratigraphic units of the Amiata region can be grouped into four complexes (see Fig. 2). From top to bottom they are:

i) *Complex I*: permeable. It is made up of Quaternary volcanic rocks only and includes the volcanics of Mt. Amiata (quartz-latic ignimbrites, rheoignimbrites and lavas as well as two small trachytic lava flows) and the « selagites » outcropping in the Senna stream valley. The surface extension of the latter is rather limited: the volcanics of the Mt. Amiata massif, on the contrary, stretch out over an area of about 90 km²;

ii) *Complex II*: impermeable. Includes the clastic deposits of the Neogene (clays, sands and gravels) and the underlying rocks of the Cretaceous-Eocene flysch (mainly shales and besides marls, limestones and sandstones). The latter, more commonly known under the inclusive name of « *argille scagliose* », form the real and proper cap-rock. The Neogenic deposits, although often coarse (and therefore permeable) have also been included in Complex II because they generally lie on the impermeable flysch;

iii) *Complex III*: generally impermeable. It consists of marls, marly limestones and lithographic limestones interbedded with varicoloured shales. This formation, known in Tuscany under the name of « *Scisti policromi* », that is polychromous shales, passes upwards into nummulitic calcarenites.

The terrains of this complex range in age from Cretaceous to Eocene (?).

(?) Part of such complex is certainly in stratigraphic continuity with the permeable Complex IV on which it lies; on the other hand, part of it is probably stratigraphically connected with the overlying flyschoid formations of Complex II.

As up to now there are not sufficient data to ascribe with certainty the two parts of Complex III to Complexes IV and II respectively, the writer thinks it more advisable to group the « polychromous shales » and the overlying nummulitic calcarenites in a separate complex.

Before
cance, in ti
of the rock
and upper
rary in it

In son
section is
IV, and as
tween then
the Comple
alter the g
basal main
on the wh

iv) Co
from Upp
From
follows:

- upj
- rad
- ma
- lov
- yel
- ma
- eva
- Ne

In the
at the surt
15 ÷ 20 s

There
sporadical
meable fo

STRUCTURE

The s
all in the
a well dri
it results

(?) Data
paper by R

Before ascribing to this complex a precise hydrologic significance, in terms of permeability or of impermeability, on the basis of the rocks which form it, some remarks are necessary. The middle and upper part of this complex are very often calcareous: on the contrary in its basal part the argillaceous beds are clearly prevailing.

In some places, owing to tectonic movements, the calcareous section is in direct contact with the underlying permeable Complex IV, and as a result of the hydrological connection which arises between them, the calcareous section of Complex III becomes a part of the Complex IV. In general, however, the tectonic movements do not alter the geometrical relation between the middle-top part and the basal mainly argillaceous one of the Complex III, so that it behaves, on the whole, as a cap-rock of the permeable underlying terrains;

iv) *Complex IV*: permeable. Includes all the formations ranging from Upper Triassic (Noric) to Tithonic.

From top to bottom the sequence, when complete, is made up as follows:

- upper cherty limestones (« *maiolica* »): Tithonic;
- radiolarites;
- marly limestones and marls with *Posidonomya alp.*;
- lower cherty limestones;
- yellowish-pink-reddish limestones with *Ariethites*;
- massive reef limestones;
- evaporitic formation (dolomitic limestones with anhydrite): Noric-Rhaetic.

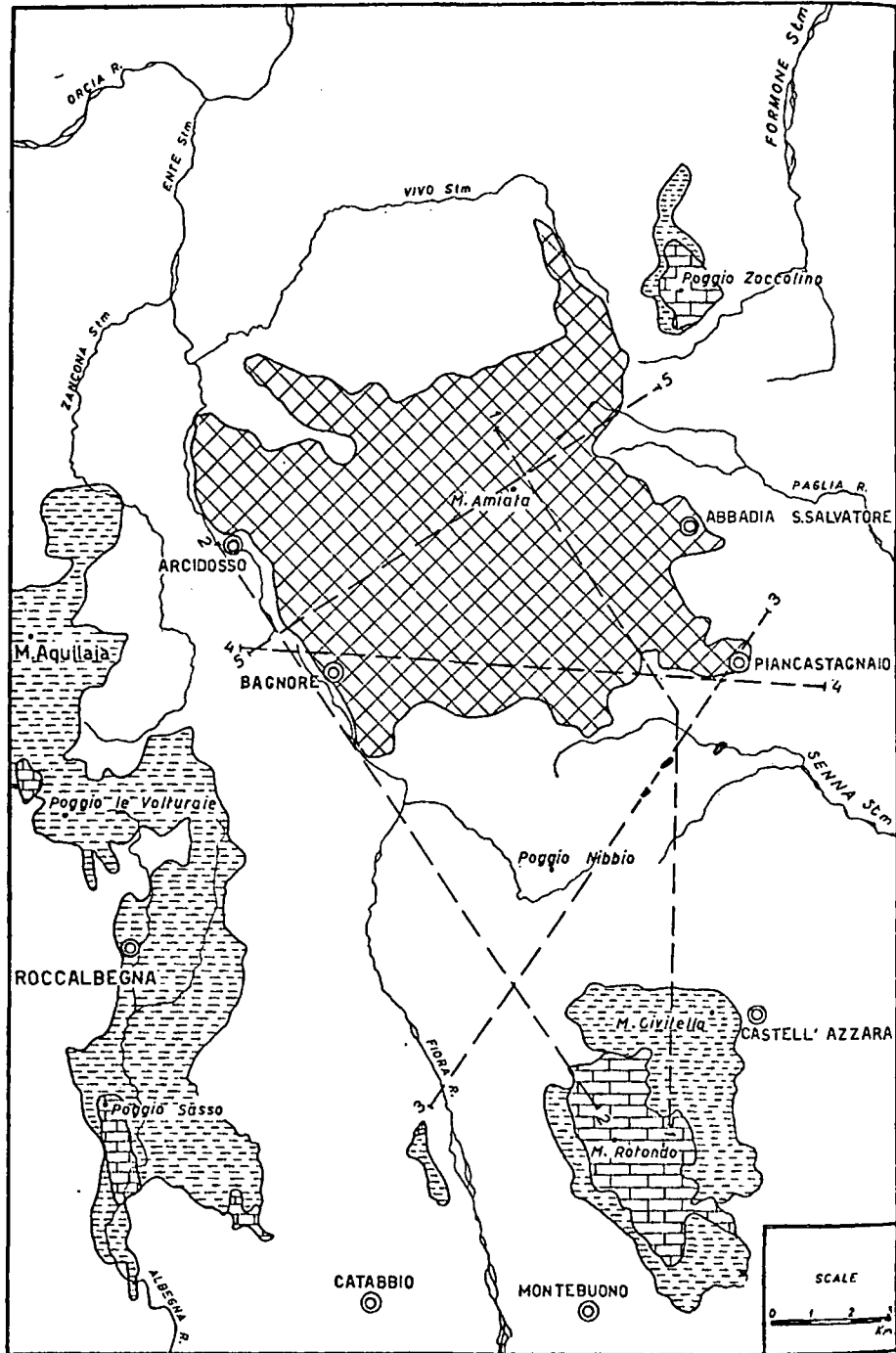
In the Amiata region, this complex has a rather limited extension at the surface: out of a total area of about 1000 sq.km, it covers only 15 ÷ 20 sq.km (see Fig. 2).

Therefore, the permeable terrains of Complex IV outcrop only sporadically, like rigid islands, completely surrounded by the impermeable formations of the Complexes II and III.

STRUCTURE

The substratum of the evaporitic formation does not outcrop at all in the Amiata region. It has been reached however by means of a well drilled in the southern part of the region here considered, and it results to be made up of greenish sericitic schists of Carnic age⁽¹⁾.

(¹) Data published for the courtesy of « Monte Amiata S.M.p.A. » in a previous paper by R. BURGASSI, R. CATALDI, J. MOUTON, F. SCARDILLARI (1965).



As no
the crysta
region ca
which rep
The cont
only the
the basis
face geol
numerous

In th
formation
the radic
underlyin
tions hav

i) It
affected
a chiefly
1952; E.

As l
relief of
controlle
faults w
In fact,
dismen
differen

Ste
lateral



COMPLE
(permeab

COMPLE
(imperme

COMPLE
(general
imperme

COMPLE
(permeab

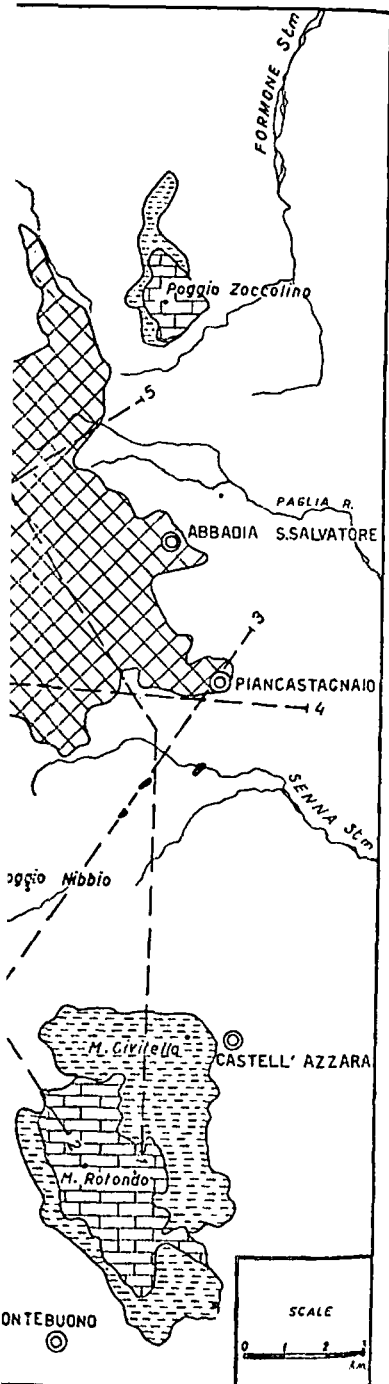
As no sufficient data are available to reconstruct the attitude of the crystalline basement, the deep structural outline of the Amiata region can be given only for the top of the evaporitic formation which represents the most reliable geometrical element of reference. The contour map of it is given in Fig. 7. This map, which represents only the central part of the Amiata region, has been elaborated on the basis of the results of a geoelectrical survey, integrated with surface geological data and calibrated by means of lithologic logs of numerous wells.

In the geological cross-sections (Fig. 8) the permeable Jurassic formations of the Complex IV (from the massive limestones up to the radiolarites and/or « *maiolica* ») have been separated from the underlying calcareous-anhydritic substratum. The traces of these sections have been plotted in Figs. 2 and 7.

i) It is known that the whole region North of Mt. Amiata was affected by a complicated folding tectonics followed, in its turn, by a chiefly distensive tectonics with a set of normal faults (G. MERLA, 1952; E. GIANNINI, R. NARDI, M. TONGIORGI, 1962).

As Figs. 7 and 8 show, in the region of Mt. Amiata too, the relief of the calcareous-anhydritic substratum appears prevalingly controlled by a tension tectonics characterized by a set of normal faults whose throws vary from about ten to some hundred meters. In fact, the top surface of the anhydritic formation appears to be dismembered into a series of unequal blocks, close to each other on different levels like horst-graben combinations.

Step-faults are not unfrequent: they always represent (however) lateral and less sunk portions of the nearest downlifted feature.



← FIG. 2 - Geological schematic map of M. Amiata geothermal region.

COMPLEX (permeable)	I	<table border="0"> <tr> <td></td> <td>quartz-latic ignimbrites, rheoignimbrites, lavas, etc.</td> <td rowspan="2">} Quaternary</td> </tr> <tr> <td></td> <td>selagites</td> </tr> </table>		quartz-latic ignimbrites, rheoignimbrites, lavas, etc.	} Quaternary		selagites
	quartz-latic ignimbrites, rheoignimbrites, lavas, etc.	} Quaternary					
	selagites						
COMPLEX (impermeable)	II	clays, sands and gravels (Neogene); flysch (Cretaceous-Eocene)					
COMPLEX (generally impermeable)	III	polychrome shales, marlstones, lithographic stones and nummulitic limestones (Cretaceous-Eocene)					
COMPLEX (permeable)	IV	dolomitic limestones with anhydritic layers, massive limestones, cherty limestones, radiolarites, etc. (Noric-Tithonian)					

The wideness of each up-faulted block does not exceed $8 \div 10$ sq.km; on the contrary, the negative features are generally rather wider than the positive ones and can even reach 20 sq.km.

The presence of folds in the evaporitic formation and in the overlying sequence of Jurassic formations is not easily recognizable. These folds almost certainly exist, as the data provided by some wells seem to indicate, but it is rather difficult to single out and above all to reconstruct them at depth.

The roughly dome-shaped attitude on the top of many blocks of the evaporitic formation (see Fig. 7) might be considered less as periclinal folds (originated by lateral compression and affecting the whole sedimentary sequence) but rather as a diapiric phenomenon due to the plasticity of the anhydritic layers. A similar explanation was given also for an analogous attitude occurring in the Larderello region, where the diapiric phenomena are in some places clearly evidenced by the complete structural independence between the evaporitic formation and the underlying schistose-quartzitic basement (R. CATALDI, G. STEFANI, M. TONGIORGI, 1963).

Sometimes, this phenomenon originates purely plastic deformations which become more and more moderate upwards within the argillaceous formations of the Complexes II and III. Other times, the diapirism causes also a series of rigid dislocations, real and proper rents in the top of the evaporitic formation, which extend to the whole overlying sequence up to the surface. It is therefore a sort of « piercing tectonics ».

In the writer's opinion, at least part of the fractures and faults which can be singled out in the outcropping blocks of the Complex IV may be attributed to such a type of « piercing tectonics ».

In this respect a typical outcrop appears to be that of Poggio Zocolino where a series of fractures and faults cross each other in such an intricate way that it seems difficult to suppose that they may be the surface expression of an analogous fragmentation in the rigid schistose-quartzitic basement. All the more if one considers that a stratigraphic well (St. Filippo 1) drilled in this area, after about 100 meters of Liassic limestones penetrated through the evaporitic formation for the abnormal thickness of more than 1400 meters, without reaching however the schistose-quartzitic basement.

On the basis of the above mentioned example and other evidence, it is possible to formulate the hypothesis that the structure of the evaporitic formation (and in general of the whole Complex IV) in the

Amiata region
schistose-quartzitic

ii) As regards
it would be
existing and
between each
ever, it is w
from a prac

First of
unities and
particular, (C
Mesozoic bl
thinning-out

Consequen
appear to be
(see Fig. 8).

Almost
also Comple
localized ze
lation of he
able is the

The sa
which cross
under the
face. On th
recognizabl
Complex IV

In some
formations
the faults

The d
certainly d
ing format
underlying

iii) Ap
Amiata re
characteriz

(*) It must
collapse is
Ponsano, Pic

does not exceed 8 ÷ 10
ures are generally rather
reach 20 sq.km.

tic formation and in the
is not easily recognizable.
ta provided by some wells
) single out and above all

he top of many blocks of
be considered less as per-
ession and affecting the
s a diapiric phenomenon
rs. A similar explanation
curing in the Larderello
some places clearly evi-
dence between the evap-
ose-quartzitic basement

; purely plastic deforma-
rate upwards within the
II and III. Other times,
slocations, real and prop-
ion, which extend to the
It is therefore a sort of

the fractures and faults
g blocks of the Complex
ercing tectonics ».

to be that of Poggio Zoc-
cross each other in such
oppose that they may be
gmentation in the rigid
if one considers that a
his area, after about 100
ough the evaporitic for-
ian 1400 meters, without
sement.

uple and other evidence.
at the structure of the
hole Complex IV) in the

Amiata region is very often independent of the structure of the schis-
tose-quartzitic basement.

ii) As regards to the internal structure of Complexes II and III,
it would be out of place in this note to discuss the relationships
existing among the various formations of these complexes, and be-
tween each of them, and the permeable underlying Complex IV. How-
ever, it is worth making a few remarks which seem to be interesting
from a practical point of view.

First of all, it is necessary to stress the remarkable disconti-
nuities and the thickness variability of Complexes II and III. In
particular, Complex III covers and surrounds almost everywhere the
Mesozoic blocks and dies out at a brief distance owing to tectonic
thinning-outs.

Consequently, also the Jurassic formations of Complex IV ap-
pear to be very often wedge-shaped and tectonically reduced blocks
(see Fig. 8).

Almost all the faults which cross the permeable Complex IV cut
also Complex III, determining here an intense brecciation and then
localized zones of permeability which can be favourable for the circu-
lation of hot fluids. The more frequently this occurs, the more remark-
able is the reduction in thickness of Complex III.

The same cannot be said about Complex II. Many deep faults,
which cross the evaporitic formation just where it lies directly
under the flyschoid formations of Complex II, do not reach the sur-
face. On the contrary, several of the faults of Complex II which are
recognizable at the surface show a very reduced throw at the top of
Complex IV.

In some places, the surface faults die out within the cap-rock
formations without reaching the permeable complex. In this last case
the faults have not been recorded on the cross-sections.

The disharmony between surface and deep tectonics is almost
certainly due to plastic adjustments that took place inside the cover-
ing formations during their differential movements with respect to the
underlying Complex IV.

iii) Apart from the main folding, the geological history of the
Amiata region from Oligocene to Upper Tortonian is prevailingly (*)
characterized by a gravitative tectonics with lateral translations in-

(*) It must be said, to this purpose, that in Tuscany also an intermediate phase of
collapse is known in the period from Burdigalian to Upper Tortonian (Manciano,
Ponsano, Pianosa) (E. GIANNINI - M. TONGIORGI, 1957, 1959 and 1962; L. DALLAN, 1964).

volving at least the flyschoid formations and with consequent shearings out and reductions of series. Such reductions and shearing-outs cause therefore a direct overlapping of the flyschoid formations of Complex II (and sometimes with those of Complex III at their base) on any layer of Complex IV. Generally, however, the flyschoid formations of Complex II lie directly over the evaporitic formation.

The following phases of collapse, marine ingression, and final re-emersion of the country, due to normal faults, conclude the geological history of the Amiata region up to the beginning of Quaternary.

iv) In this era another phenomenon occurs: volcano-tectonics, which plays a very important role in the geothermal framework of the region.

The main faults which control the volcanic effusions (see Fig. 7) roughly follow the trends SW-NE and NW-SE which are those prevailing in the Apennine diastrophism.

Apart from the selagites, which represent the initial volcanic phase (G. MARINELLI, 1961) and which all outcrop in a SW-NE belt South of the main mountain, all the extrusion domes recognizable on Mt. Amiata line up according to the same SW-NE trend or to the orthogonal one.

During Quaternary the main volcanic faults must have been not only rather opened (so as to allow the volcanics to rise up) but also active, as the fact proves that almost all the extrusion domes show a bifid subdivision.

During the settlement of the volcanics⁽⁵⁾ at least the central part of the Amiata region was affected by upward pushes, typical of plutonic tectonics. Apart from the upheaval of Pliocenic deposits, which are here a little more than 850 m high a.s.l. (E. TONGIORGI, L. TRIVISAN, 1957), such pushes are evidenced by a sheaf of radial faults converging towards a point located more or less at the center of the volcanic outcrop.

These radial faults are accompanied by a series of orthogonal faults with a roughly concentric trend which rim to a certain extent the volcanic outcrop (see Fig. 7). At approximately the end of the eruptive activity, the partial emptying of the magmatic chamber and

⁽⁵⁾ The settlement of the Mt. Amiata volcanic rocks took place in several phases, each one characterized by different modalities of effusion, petrographic texture and structure, magmatic differentiation and chemical evolution (G. MARINELLI, 1961; R. MAZZUOLI - M. PRATESI, 1963).

the structure
determined the
in the center

The site
shows a wide
rains. Such
pletely over

Hence,
fresh water

v) To (

that it is r

the Amiata

those with

represent t

accompanied

the main f

which were

originated

dera »-type

cluded the

To sur

vious colla

alters the p

THE GEOTHI

In the

Amiata re

1965) with

— to
— to
— to
res
This
in shallow
region, ar
not includ

⁽⁶⁾ Note
survey not
surface of G
of the volca

the structural situation created by the plutonic tectonics have determined the most favourable conditions for a « caldera »-type collapse in the central part of Mt. Amiata.

The situation as it is today, and which is outlined in Fig. 6^(*), shows a wide depression at the top-surface of the impermeable terrains. Such a depression, with irregular bottom and rims, is completely overwhelmed with more or less permeable volcanics.

Hence, the most favourable conditions occur for the storage of fresh water in the permeable volcanic rocks.

v) To conclude this brief tectonic description, it must be added that it is rather difficult to determine the main structural trend of the Amiata region. There exist faults and fractures in all directions: those with NW-SE and SW-NE directions, which further to the North represent the prevailing trends of the Tertiary folding, are here accompanied by other groups of faults and fractures. Almost certainly the main faults of the volcanic effusion joined the previous ones, which were still active during Quaternary; volcanic events, moreover, originated radial and concentric faults of plutonic type; the « caldera »-type collapse of the central part of the volcano finally concluded the tectonic cycle of the Mt. Amiata.

To summarize: the volcanic activity, here determined by the previous collapse phases, prevails during Quaternary and, in its turn, alters the previous structural lines with a peculiar plutonic tectonics.

THE GEOTHERMAL ANOMALY

In the year 1962 a geothermal survey was carried out in the Amiata region (R. BURGASSI, R. CATALDI, J. MOUTON, F. SCANDELLARI, 1965) with the following main purposes:

- to control the existence of a regional geothermal anomaly;
- to determine its extension;
- to find out its minimum values under which the geothermal research is no more profitable for industrial purposes.

This was accomplished by means of temperature measurements in shallow wells statistically distributed in the central part of the region, around the volcanic massif of Mt. Amiata. The survey could not include the area covered by the volcanics owing to their great

(*) *Note added in proof* - According to the preliminary results of a geoelectrical survey not yet completed today, the bottom surface of the volcanics and the top surface of Complex IV are somewhat deeper than those reported in the central part of the volcanic outcrop in Figs. 6 and 7.

permeability and to the presence of a cold water mass. The shallow wells, with an average depth of $25 \div 30$ meters, were therefore all drilled in impermeable terrains (neogenic clays, shaly flysch, « polychromic shales »).

The gradient was determined by means of temperatures measured at depths of $15 \div 25$ m. As a matter of fact, it has been experimentally proved that the superficial yearly thermic excursion is practically reduced to zero at a depth of 10-12 meters below the ground level.

In order to reach a common criterium in the evaluation of the observed gradient data from different terrains and wells, a statistical correction, found on the basis of the electrical logs of all the shallow wells, has been introduced.

The general attitude of the geothermal gradient in the Amiata region, conventionally measured in degrees per 10 meters ($\frac{\Delta t}{10} \text{ } ^\circ\text{C/m}$) and referred to an ideal homogeneous terrain having a resistivity of 10 ohm · m, is shown in Fig. 3.

The « regional anomaly » of the gradient, included in the curve of $1^\circ\text{C}/10$ m, surrounds the volcanic outcrop almost everywhere, but it appears somewhat displaced southwards in comparison with the outcrop itself.

Within the « regional anomaly », that is, within the curve of $1^\circ\text{C}/10$ m, there are various areas where the gradient exceeds $2^\circ\text{C}/10$ m. Such a value has been assumed here to characterize numerically the « local anomalies » that could be of industrial interest. Of the 5 « local anomalies », 3 are particularly accentuated: that of Bagnore and that of Piancastagnaio reach inside values which exceed even $3^\circ\text{C}/10$ m and both of them correspond to producing areas; that of Poggio Nibbio, which presents values not exceeding $2.5^\circ\text{C}/10$ m, is at present under exploration.

The other two « local anomalies » are located North of Abbadia S. Salvatore and near Roccalbegna. Both have already been explored by a first test-drilling: the first anomaly, of a very limited extension, does not seem to be interesting for industrial purposes; the second one, on the contrary, has revealed favourable conditions for the research of geothermal energy.

The anomalies of Roccalbegna, Bagnore and Abbadia S. Salvatore are almost perfectly aligned along the most important of the main faults controlling the volcanic effusion; on such an alignment the regional gravimetric survey has recorded an appreciable mass deficit.

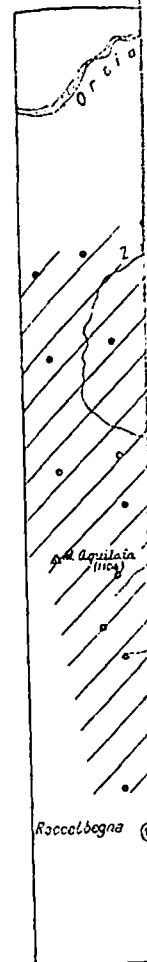


FIG. 3

Also
and the c
with a tre

water mass. The shallow meters, were therefore all layers, shaly flysch, « poly-

of temperatures measured it has been experimentally excursion is practically low the ground level.

in the evaluation of the is and wells, a statistical al logs of all the shallow

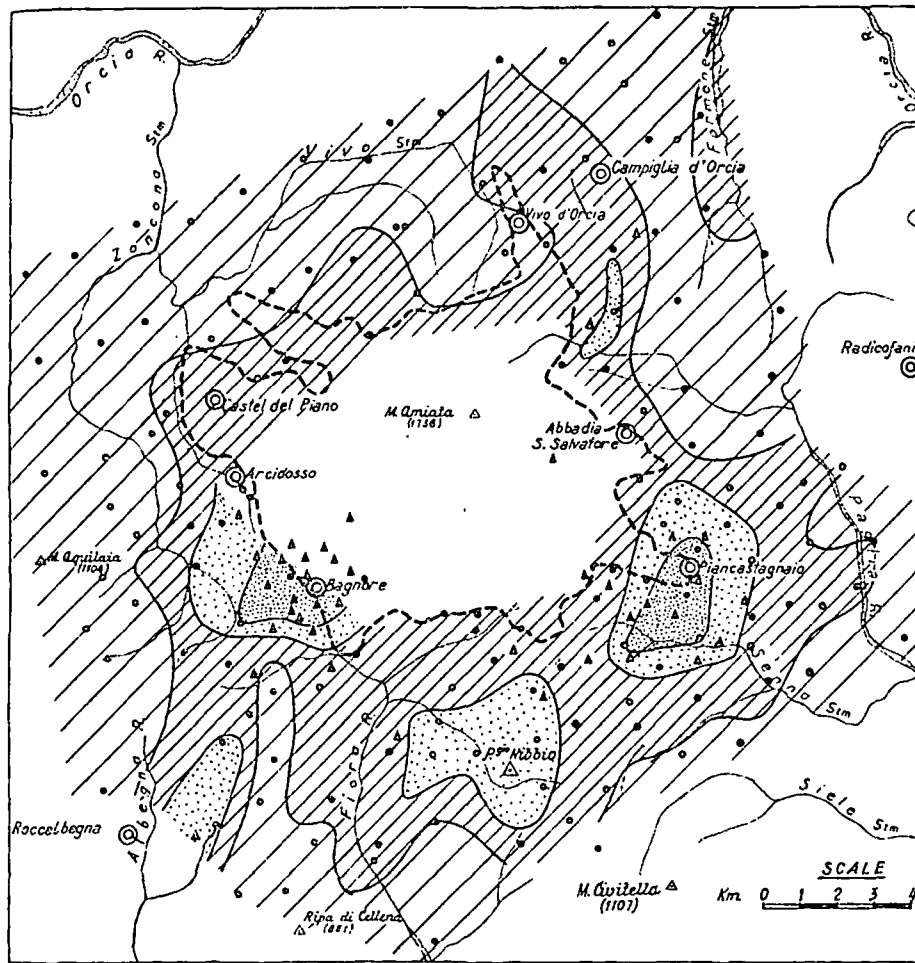
gradient in the Amiata er 10 meters ($\frac{\Delta t}{10} \text{ } ^\circ\text{C/m}$) ain having a resistivity

t, included in the curve rop almost everywhere, rds in comparison with

s, within the curve of gradient exceeds $2^\circ\text{C}/10$ characterize numerically strial interest. Of the 5 uated: that of Bagnore- ues which exceed even roducing areas; that of ceeding $2.5^\circ\text{C}/10$ m, is

ated North of Abbadia already been explored very limited extension. l purposes; the second conditions for the re-

d Abbadia S. Salvatore mportant of the main uch an alignment the preciable mass deficit.



SYMBOLS

- Scale of thermal gradient.
- Thermometric shallow wells.
- ▲ Deep wells.
- - - Boundary of the volcanic rocks.

FIG. 3 - Temperature gradient map in the Mt. Amiata geothermal region.

Also the local anomalies of Poggio Nibbio and Piancastagnaio and the eastern prolongation of the « regional anomaly » are aligned with a trend parallel to the previous one.

Such an alignment corresponds to a belt, along which there appear a series of selagite outcrops and the volcanic dome of Radicofani⁽⁷⁾. Finally it should be pointed out that all the anomalies correspond to structural highs of Complex IV: this fact leads to the hypothesis that each one of the « local anomalies » does not represent anything else but the trace at the surface of an important convection cell for the hot fluids circulating within the permeable Complex IV.

REMARKS ON THE WATER SUPPLY TO THE GEOTHERMAL AREAS

Analyses concerning the ratio O^{18}/O^{16} , carried out by the Laboratory of Nuclear Geology of Pisa, have shown that also in the Amiata region the water issued from the geothermal wells has a meteoric origin (R. GONFIANTINI, E. TONGIORGI: personal communication).

Granting this assumption, it is possible to state the problem of the hydrologic balance of steam producing areas by comparing the total capacity of the water drawn out of the wells with that absorbed⁽⁸⁾ at the surface by the permeable terrains of Complex IV. To this purpose, as the minor outcrops of Complex IV may be considered at present as omissible from the point of view of water supply at depth (owing to their limited extension, tectonic situation and distance from the exploitation areas), only the outcrop of Mt. Rotondo⁽⁹⁾ will be taken into consideration.

The water falling on this outcrop is about 14×10^6 cubic meters/year. From the comparison of this value with the total yearly output of the Mt. Amiata wells (*i.e.* about 6×10^6 cubic m/year⁽¹⁰⁾) it ensues that the water falling yearly on the Mt. Rotondo permeable Mesozoic outcrop would be sufficient to guarantee the necessary water supply to the wells, provided that at least 40 ÷ 45 % of it penetrates underground and feeds the deep circulation.

⁽⁷⁾ It is a small volcanic outcrop located about 13 km East of Mt. Amiata. Its volcanism, genetically analogous to that of the selagites outcropping in the Senna stream valley, belongs to the initial volcanic activity of the Mt. Amiata. The interested reader can see the note of G. MARINELLI, 1961.

⁽⁸⁾ As the map published in 1957 by the Italian Hydrological Survey shows, the average rainfall values for the Amiata region in a period of 30 years (1921-'50) ranges from 1,100 and 1,300 mm/year.

⁽⁹⁾ The outcrop cover an extension of 11 sq. km, with an average height of 800 m. and a distance from the « fields » of Bagnore and Piancastagnaio of 13 ÷ 14 and 10 ÷ 12 km, respectively.

⁽¹⁰⁾ This value, recorded in December 1965, might be actually higher: because, while the Bagnore « field » is now almost stabilized on its maximum « water-production » capacity, the exploration in the Piancastagnaio « field » is still going on.

As i
almost
transpir



Fig. 4

appeal
carcov
B
in the
joins

belt, along which there are volcanic dome of Radico. that all the anomalies cor- IV: this fact leads to the anomalies » does not re- pe surface of an important ating within the permeable

As in the Mt. Rotondo area, the seasonal rainfall distribution is almost uniform, and the vegetation is scanty and therefore evapo- transpiration is rather limited, an absorption coefficient of $40 \div 50 \%$

OTHERMAL AREAS

carried out by the Labo- own that also in the Amiata rmal wells has a meteoric onal communication). le to state the problem of g areas by comparing the the wells with that absorb- rrains of Complex IV. To Complex IV may be con- int of view of water supply tectonic situation and dis- the outcrop of Mt. Ro-

out 14×10^6 cubic meters/ ith the total yearly output cubic m/year⁽¹⁰⁾ it ensues ondo permeable Mesozoic re necessary water supply % of it penetrates under-

13 km East of Mt. Amiata. Its sites outcropping in the Senna the Mt. Amiata. The interested

Hydrological Survey shows, the od of 30 years (1921-50) ranges ith an average height of 800 m. astagnaio of $13 \div 14$ and $10 \div 12$

actually higher: because, while maximum « water-production » is still going on.

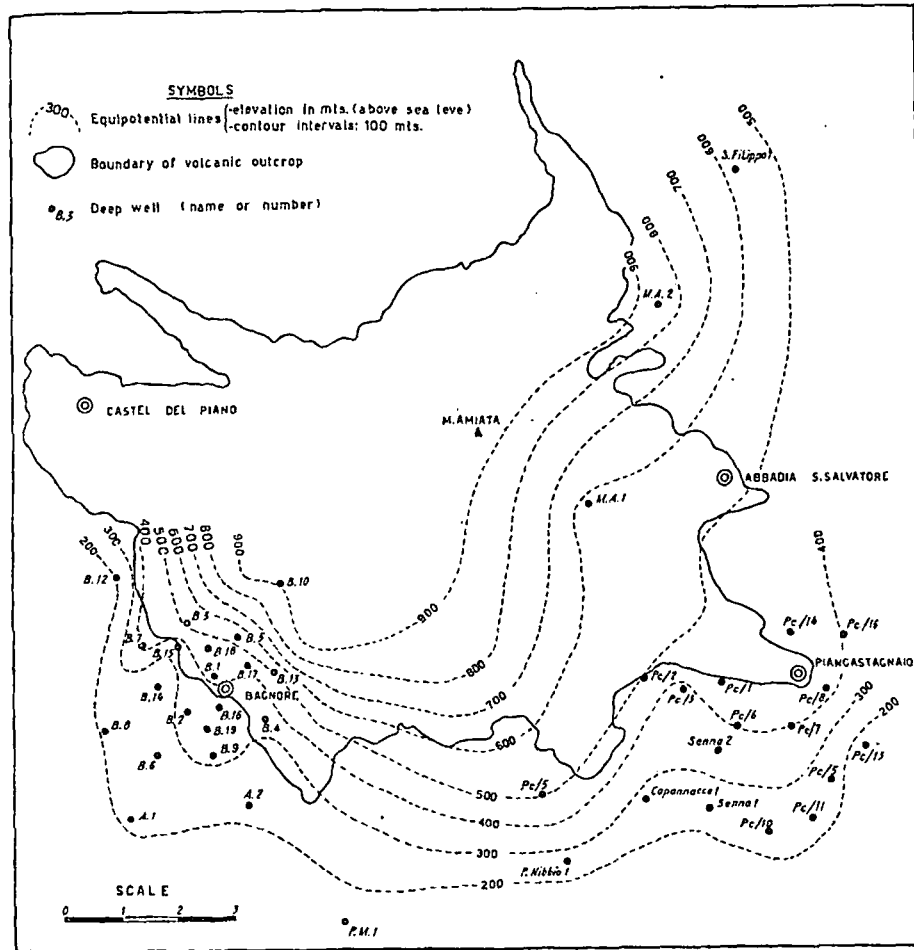


Fig. 4 - Hydrostatic levels in the wells of the Mt. Amiata geothermal region (values observed at completion of each well).

appears to be consistent with the typically karst nature of the calcareous rocks of this outcrop.

But all this could lead to an hydrologic balance at depth only in the case that the water absorbed by the Mt. Rotondo outcrop joins the deep circulation of Piancastagnaio and Bagnore « fields »

without any other leakage. Such an hypothesis does not appear sustainable. In fact, the structure of the permeable Mesozoic core of Mt. Rotondo, the number, the output and the distribution of its springs lead to the conclusion that only about a quarter of the water infiltrated at Mt. Rotondo can flow underground into the area North of the outcrop, towards the « fields » of Bagnore and Piancastagnaio.

The question arises, therefore, if other outcrops of permeable terrains do not contribute to the water supply of the deep reservoir. The data and information presently available are not sufficient to make this point clear. However, it is possible to point out that also the volcanic outcrop of Mt. Amiata represents an absorbing area of meteoric water.

The large reservoir existing in the permeable volcanic rocks could be connected with the deep reservoir of the Complex IV through extrusion chimney and faults which cross in several places the whole sedimentary sequence (see Figs. 6 and 8).

An indirect confirmation of such a possibility is given by the hydrostatic levels measured in the wells of Mt. Amiata (see Fig. 4). The attitude of the equipotential curves shows, in fact, a general rising of the hydrostatic levels toward the volcanic outcrop, *i.e.* toward the supposed absorbing area.

The Producing Areas

« Field » of Bagnore

The drilling, started in August 1958, was ended in November 1962. 21 wells were completed, subdivided as follows:

— producing wells	no. 8 = 38 %
— non-commercial wells	no. 6 = 29 %
— sterile wells	no. 7 = 33 %
	<hr/>
Total	no. 21 = 100 %

The producing area, which has an extension of 4÷5 sq.km, occupies more or less the central part of the explored zone (15 sq.km) and corresponds to a positive feature of the permeable Complex IV. The geothermal fluids, issued from depths of 500÷600 m, have

physic
the pe
whole
steam
Fig
vision
record
values.
fluids,
after th
Fr
—
well. S
of the
terval
—
the pro
pressur
—
—
In
(R, per
comme
discove
existing
to sub
disting
i).
of the
shut-in
the co
ii)
therefo
curves
the no
ratio o
these c
curves

s does not appear sus-
able Mesozoic core of
he distribution of its
a quarter of the water
nd into the area North
re and Piancastagnaio.
outcrops of permeable
of the deep reservoir.
e are not sufficient to
to point out that also
s an absorbing area of

le volcanic rocks could
Complex IV through
veral places the whole

ibility is given by the
Mt. Amiata (see Fig. 4).
ws, in fact, a general
volcanic outcrop, i.e.

as ended in November
follows:

- o. 8 = 38 %
- o. 6 = 29 %
- o. 7 = 33 %

- o. 21 = 100 %

ension of 4÷5 sq.km.
xplored zone (15 sq.km)
permeable Complex IV.
of 500÷600 m, have

physical characteristics which vary from the central part towards the periphery of the producing area; in fact, in this direction the whole range of the physical state of the fluids, from superheated steam to hot water, can be observed.

Figure 7 shows the structural outline, the location and the subdivision of the wells into producing, non-commercial and sterile. Table 1 records the technical characteristic of the wells and their average values. Table 2 shows the physical characteristics of the exploited fluids, with reference to the measurements taken within 6 months after the explosion and to those of June 1965.

From Table 2 it is possible to point out:

— a substantial decrease in the total output of fluid in each well. Such a decrease is very strong in the first years of exploitation of the « field », but then gradually diminishes the more the time interval increases from the explosion of the well Bg. 1;

— the stabilization of the temperature of the fluid obtained from the producing wells around values of $140 \div 150^{\circ}\text{C}$ at the exploitation pressure;

— an evolution of the gas/steam ratio;

— a rapid stabilization of the shut-in pressures.

In Fig. 5 the initial shut-in pressure (P) and the gas/steam ratio (R , percentage in weight) of the various positive (producing and non-commercial) wells are graphically shown in their evolution from the discovery up to 1965. These diagrams clearly indicate the relation existing between the P curve and the R curve and make it possible to subdivide the history of the Bagnore « field » into two clearly distinct periods:

i) the first, a little more than two years long, represents the phase of the initial rapid decline of the physical characteristics (such as shut-in pressure, gas/steam ratio, output, etc.). It ended in 1961 after the completion of the well Bg. 9;

ii) the second is characterized by more stabilized conditions and, therefore, by a more or less asymptotic attitude of the P and R curves. This fact is confirmed by the average values of the SIP of the non-commercial wells and by the average values of the gas/steam ratio of the producing wells. The two dashed curves representing these data (see Fig. 5) perfectly correspond, in fact, with the relative curves of P and R .

TABLE 1 - Mount Amiata geothermal area

Productive area of Bagnore.

Wells	Date of completion	G.L. elevation (m)	Tubing at well head (Ø")	Hole-size at bottom well (Ø")	Final depth from G.L. (m)	Top of reservoir (m a.s.l.)	Distance from the nearest well (m)	Result
Bg 1	13-4-'59	825	9 ³ / ₈	8 ⁵ / ₈	551	447	475	Producing
Bg 2	25-8-'59	825	13 ³ / ₈	8 ³ / ₄	346	350	500	Producing
Bg 3	15-11-'59	875	13 ³ / ₈	8 ⁵ / ₈	873	187	500	Not commercial
Bg 4	18-11-'59	760	13 ³ / ₈	8 ³ / ₄	730	160	625	Not commercial
Bg 5	23-4-'60	825	13 ³ / ₈	12 ¹ / ₄	470	376	475	Producing
B 7	9-7-'60	835	13 ³ / ₈	12.—	689	446	550	Producing
Bg 6	21-9-'60	850	13 ³ / ₈	5 ⁵ / ₈	1025	80	875	No production
Anteic 1	8-11-'60	825	13 ³ / ₈	8 ³ / ₄	1331	375	1350	No production
Bg 9	9-11-'60	730	13 ³ / ₈	12.—	586	229	600	Producing
Anteic 2	25-1-'61	640	9 ⁵ / ₈	5 ⁵ / ₈	877	— 5	950	Not commercial
Bg 2 bis	7-6-'61	825	13 ³ / ₈	12.—	346	350	500	Producing
Bg 12	22-6-'61	715	13 ³ / ₈	12.—	846	121	1350	No production
Bg 8	15-7-'61	810	13 ³ / ₈	12.—	1475	89	975	No production
Bg 10	17-8-'61	1080	13 ³ / ₈	12.—	1144	— 48	1425	No production
Bg 13	24-9-'61	840	17 ¹ / ₄	16 ¹ / ₈	686	189	475	No production
Bg 14	15-11-'61	835	13 ³ / ₈	12 ¹ / ₄	694	188	700	No production
Bg 16	7-12-'61	740	13 ³ / ₈	12 ¹ / ₄	605	300	525	Not commercial
Bg 19	18-3-'62	750	13 ³ / ₈	12.—	429	340	500	Producing
Bg 17	2-5-'62	825	9 ⁵ / ₈	8 ³ / ₄	636	265	470	Not commercial
Bg 15	25-9-'62	805	13 ³ / ₈	8 ⁵ / ₈	1105	325	550	Not commercial
Bg 18	16-11-'62	875	13 ³ / ₈	8 ³ / ₄	625	411	475	Producing
Average of 21 wells	—	814	(9 ⁵ / ₈ ÷ 17 ¹ / ₄) 13 ³ / ₈	(5 ⁵ / ₈ ÷ 16 ¹ / ₈) 12	765	246	≈ 700	Producing: n. 8 Not comm: n. 6 No produc: n. 7

Technic

Wells

Senna 1

Senna 2

Capannacce

Pc/4

Pc/3

Pc/7

Pc/5

Pc/2

Pc/6

Pc/10

Pc/11

Pc/8

Pc/1

Pc/13

Pc/16

Pc/14

Average of 16 wells

Mount Amiata geothermal area

— Technical characteristics of the wells.

Productive area of Piancastagnaio

Top of reservoir (m a.s.l.)	Distance from the nearest well (m)	Result	Wells	Date of completion	G.L. elevation (m)	Tubing at well head (Ø")	Hole size at bottom well (Ø")	Final depth from G.L. (m)	Top of reservoir (m a.s.l.)	Distance from the nearest well (m)	Result
447	475	Producing	Senna 1	27- 8-'61	525	9 ^{5/8}	8 ^{3/4}	421	- 105	790	Not commercial
350	500	Producing	Senna 2	1-12-'61	575	13 ^{3/8}	12 ^{1/4}	662	- 77	510	Producing
187	500	Not commercial	Capannacce 1	8- 7-'62	690	13 ^{3/8}	8 ^{3/4}	972	- 75	1050	Not commercial
160	625	Not commercial	Pc/4	17-10-'62	625	13 ^{3/8}	12 ^{1/4}	686	171	510	Producing
376	475	Producing	Pc/3	27-11-'62	780	9 ^{5/8}	8 ^{3/8}	923	- 50	625	Not commercial
446	550	Producing	Pc/7	15- 5-'63	600	13 ^{3/8}	12 ^{1/4}	542	- 150	820	Producing
80	875	No production	Pc/5	29- 7-'63	900	13 ^{3/8}	12 ^{1/4}	1059	- 169	1700	Not commercial
375	1350	No production	Pc/2	24- 9-'63	955	13 ^{3/8}	12 ^{1/4}	1102	- 139	625	No production
229	600	Producing	Pc/6	21-12-'63	446	13 ^{3/8}	12 ^{1/4}	647	- 24	720	Not commercial
- 5	950	Not commercial	Pc/10	30-11-'64	585	13 ^{3/8}	12 ^{1/4}	734	- 15	790	Not commercial
350	500	Producing	Pc/11	30-11-'64	435	13 ^{3/8}	12 ^{1/4}	561	- 32	720	Not commercial
121	1350	No production	Pc/8	16- 2-'65	685	13 ^{3/8}	12 ^{1/4}	591	165	820	Producing
89	975	No production	Pc/1	29- 3-'65	730	13 ^{3/8}	12 ^{1/4}	725	155	725	Not commercial
- 48	1425	No production	Pc/13	16- 5-'65	520	13 ^{3/8}	12 ^{1/4}	651	15	920	Producing
189	475	No production	Pc/16	19- 7-'65	645	13 ^{3/8}	12 ^{1/4}	744	- 90	830	Producing
188	700	No production	Pc/14	23- 9-'65	705	13 ^{3/8}	12 ^{1/4}	751	- 40	830	Producing
300	525	Not commercial									
340	500	Producing									
265	470	Not commercial									
325	550	Not commercial									
411	475	Producing									
146	~ 700	Producing: n. 8 Not comm: n. 6 No produc: n. 7	Average of 16 wells	—	650	13 ^{3/8}	12 ^{1/4}	736	0	~ 810	Producing: n. 7 Not comm: n. 8 No produc: n. 1

TABLE 2 - Mount Amiata geothermal areas
Productive area of Bagriore

Wells and date of completion	Within 6 months after completion				On June, 1965				Remarks
	G Ton/h	T °C	R %	P Ata.	G Ton/h	T °C	R %	P Ata.	
Bg 1 (13- 4-'59)	173.6	148	81.—	21.5	24.5	144	7.2	—	Producing
Bg 2 (25- 8-'59)	214.—	143	75.—	20.—	The well died on April, 1961 owing to mechanical failure			5.4	Replaced by Bg2 bis
Bg 3 (15-11-'59)	29.—(1)	134	62.5	12.5	Only gas since Dec., 1963			7.8	Not commercial
Bg 4 (18-11-'59)	9.—(2)	138	65.—	12.5	Died on 1961			—	—
Bg 5 (23- 4-'60)	78.—	135	64.3	11.4	19.6	142	8.1	—	Producing
Bg 7 (9- 7-'60)	144.—	130	82.9	10.5	Put out of steam on Jan., 1963 due to increasing output of water			6.4	—
Bg 9 (9-11-'60)	61.—	138	36.3	8.6	15.4	151	9.3	—	Producing
Anteina 2 (25-1-'61)	~10.—(3)	—	—	—	Died a few days after completion			—	—
Bg 2 bis (7-6-'61)	50.3	150	8.—	8.—	23.2	150	7.2	—	Producing (replaces Bg 2)
Bg 16 (7-12-'61)	6.3(4)	144	7.—	7.4	Closed			5.7	—
Bg 19 (18- 3-'62)	68.6	150	10.7	7.—	33.3	154	11.5	—	Producing
Bg 17 (2- 5-'62)	about 15 ton/h of water, steam and gas			6.5	Closed			5.6	—
Bg 15 (25- 9-'62)	about 15 ton/h of water, steam and gas			6.7	Closed			5.8	—
Bg 18 (16-11-'62)	13.5	150	15.5	6.5	13.—	142	12.4	—	Producing

- (1) flowing with water at pressures less than 12 Ata
- (2) flowing with water at pressures less than 10 Ata
- (3) flowing with about 90 ton/h of water
- (4) flowing with about 0.2 ton/h of water

G = output at a pressure-interval of 4±5 Ata
T = temperature at a pressure-interval of 4±5At

Thermody

Wells and da
f completi

enna 1 (27-8-

enna 2 (1-12-

Capannacce 1
17-'62)

Pe 4 (17-10-'6

Pe 3 (27-11-'6

Pe 7 (15- 5-'6

Pe 5 (29- 7-'6

Pe 6 (21-12-'6

Pe 10 (30-11-'

Pe 11 (30-11-'

Pe 8 (16- 2-

Pe 1 (29- 3-

Pe 13 (16- 5-

Pe 16 (19- 7-

Pe 14 (23- 8-

(1) flowing

(2) flowing

(3) flowing

(4) flowing

R = gas

P = shot

unt Amiata geothermal areas

Thermodynamic characteristics of the exploited fluids.

Productive area of Piancastagnaio

1965	R %	P Ata	Remarks	Wells and date of completion	Within 6 months after completion				On June, 1965				Remarks	
					G Ton/h	T °C	R %	P Ata	G Ton/h	T °C	R %	P Ata		
	7.2	—	Producing	Begna 1 (27-8-'61)	63.—	154	91.—	28.1	Closed				24.2	Not commercial
ed on ing to lure		5.4	Replaced by Bg2 bis	Begna 2 (1-12-'61)	128.—	130	40.5	37.—	Open flow of about 3 tons/h at 21 Ata				—	Out of stream since Febr., 1965
Dec.,		7.8	Not commercial	Capannacce 1 (7-'62)	~10.—(1)	—	—	31.5	Open flow of about 160 tons/h of water, steam and gas				—	Not commercial
		—	—	Bc 4 (17-10-'62)	86.—	145	46.—	40.5	15.—(2)	—	—	—	Producing	
	8.1	—	Producing	Bc 3 (27-11-'62)	13.—	122	80.—	27.8	Died				—	—
eam on to in- put of		6.4	—	Bc 7 (15- 5-'63)	100.—	160	43.—	40.8	66.—(3)	187	41.7	—	Producing	
				Bc 5 (29- 7-'63)	about 25 ton/h of water, gas and steam				Closed				20.2	Not commercial
	9.3	—	Producing	Bc 6 (21-12-'63)	about 25 ton/h of water, gas and steam				Closed				34.—	Not commercial
vs after		—	—	Bc 10 (30-11-'64)	A few ton/h of water, gas and steam				Closed				28.2	Not commercial
	7.2	—	Producing (replaces Bg 2)	Bc 11 (30-11-'64)	57.5	100	92.—	31.4	Closed				33.5	Not commercial
d		5.7	—	Bc 8 (16- 2-'65)	310.—	177	33.8	36.—	Closed				36.—	Producing since Sept., 1965
	11.5	—	Producing	Bc 1 (29- 3-'65)	A few ton/h of steam, gas and water				Closed				32.—	Not commercial
d		5.6	—	Bc 13 (16- 5-'65)	24.1 (4)	132	56.8	34.5	Closed				34.5	Future produc.
d		5.8	—	Bc 16 (19- 7-'65)	~47.—	168	36.5	36.5	—				—	Future produc.
	12.4	—	Producing	Bc 14 (23- 8-'65)	44.—	138	45.—	38.—	—				—	Future produc.

1) flowing with about 70 ton/h of water
 2) flowing on stream at a well-head pressure of 29.3 Ata
 3) flowing on stream at a well-head pressure of 9.4 Ata
 4) flowing with about 5 ton/h of water
 R = gas/steam ratio (percentage in weight)
 P = shut-in pressure

pressure-interval of 4÷5 Ata
 at a pressure-interval of 4÷5At

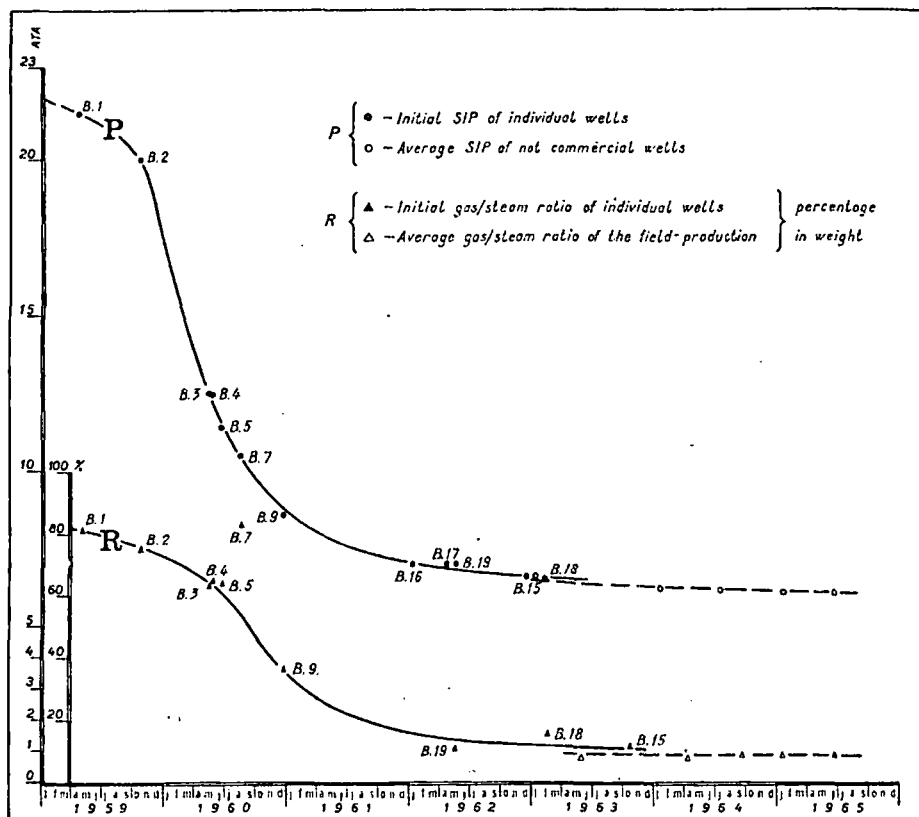


FIG. 5 - Gas/steam ratio (R) and shut-in pressure (P) in the Bagnore « steam-field » from 1959 to 1965.

In a few words, the more or less stabilized values of the parameters determining the industrial capacity of the Bagnore « steam-field » are:

- G (total output of fluid utilizable for the production of electric power) 125 tonn/h
- p (operating pressure) 4 ÷ 5 Ata
- T (temperature at the operating pressure) 145 ÷ 150°C
- R (gas/steam ratio, percentage in weight) 8 ÷ 10 %
- P (shut-in pressure) 6 Ata

« Field » of

The in
is still goin
they are su

The d
sq.km, 6 c
The a
whole area
of it.

As Fig
responde
main tech
and the pl
The f
well as th
acteristic
gradually
the produ

The r
stagnatio
stagnatio
sures sinc
tion quick

As fa
the progr
is not cle

Actua
peripheri
initial va
cludes th

This
the perip

« Field » of Piancastagnaio

The industrial exploitation of this area, started in August 1961, is still going on. Up to September 1965, 16 wells had been drilled; they are subdivided as follows:

— producing wells	no. 7 = 44 %
— non-commercial wells	no. 8 = 50 %
— sterile wells	no. 1 = 6 %
<hr/>	
Total	no. 16 = 100 %

The drilling has covered up to now an extension of about 16 sq.km, 6 of which correspond to the producing area.

The average spacing, therefore, is of 1 well per sq.km out of the whole area and of 1.1 well per sq.km for the producing central part of it.

As Fig. 7 shows, also the Piancastagnaio « field » is located in correspondence of a positive feature in the permeable Complex IV. The main technical characteristics of the wells are recorded on Table 1 and the physical characteristics of the fluids in Table 2.

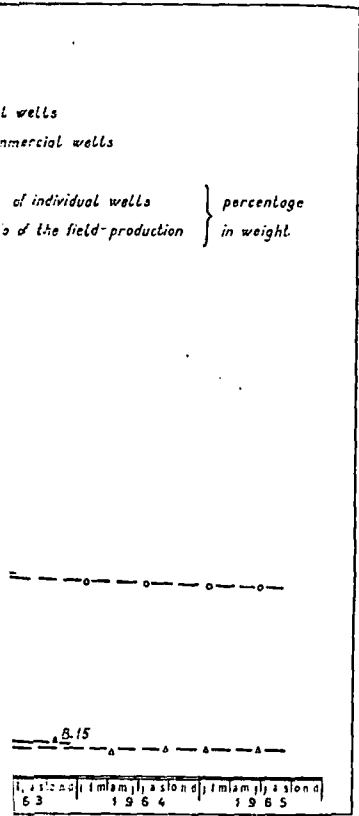
The fluids drawn from the various wells of Piancastagnaio, as well as those of Bagnore, show a succession of thermodynamic characteristics (steam percentage temperature, shut-in pressures, etc.) gradually improving from the periphery towards the central part of the producing area.

The mean steam temperature of the producing wells at Piancastagnaio is higher than that of Bagnore. As a matter of fact, Piancastagnaio recorded somewhat higher temperatures at the shut-in pressures since its discovery; in this « field », moreover a thermic evolution quicker than that of Bagnore appears possible.

As far as gas/steam ratio (*R*) is concerned, the phenomenon of the progressive gas reservoir drainage determined by the first wells is not clearly recognizable.

Actually there are two areas with different characteristics: in the peripheric area (which includes the non-commercial wells) *R* reaches initial values of about 90 %, whereas in the central one (which includes the producing wells) these values are around 35-40 %.

This fact is not likely to depend on the gas drainage caused by the peripheric wells, both because most of them have been drilled



in the Bagnore « steam-field »

ized values of the param-
of the Bagnore « steam-
or the

.	125 tonn/h
.	4 ÷ 5 Ata
sure)	145 ÷ 150°C
ght)	8 ÷ 10 %
.	6 Ata

after the central ones and because they have been kept constantly closed. On the other hand also the wells on stream (Senna 2, Pc 4 and Pc 7), after about a two years' yielding, show only a very limited decrease in the gas/steam ratio. A similar limited decrease is recorded for the production rates of the total output.

As regards the shut-in pressures, the main points are:

— the existence of initial values ($30 \div 40$ Ata) remarkably higher than those at Bagnore;

— a good agreement between the pressure distribution and the hydrostatic levels measured in the wells;

— a very slight decrease even in wells which have been operating for many months.

To conclude: the Piancastagnaio « field » is in phase of advanced development, but up to September 1965 only the fluid found in the central-western portion of the producing area was utilized (wells: Senna 2, Pc 4 and Pc 7) for electric power production. Therefore, it has not been possible to follow in details, as for Bagnore, the behaviour of the various wells, their possible mutual interferences, and the evolution trend of the physical parameters of the fluids drawn out; in other words, it has not yet been possible to state the present evolutive stage of the « field ». However, on the basis of the data gathered up to now, the Piancastagnaio field may be assumed to have at least a double capacity in comparison with that of Bagnore.

Reference Notes

The geological interest for the Mt. Amiata region is evidenced by a large bibliographical contribution.

A summary, however brief, of the purely geological literature would involve such an extent of space and time as to exceed the scope of this report, which intends to give only a preliminary contribution to the knowledge of the geothermal phenomenology of the region. The writer, therefore, limits himself to mention here only those works considered as the more appropriate to the character of this report and he refers the interested reader to the relevant bibliography.

For geological questions concerning general characters of the geology of the Apennines and of the Amiata region, the following studies are to be quoted: G. MERLA (1952 and 1959), E. TONGIORGI, L. TREVISAN (1957) and E. GIANNINI, R. NARDI, M. TONGIORGI (1962).

The wo
specifically
nuclei outc

Among
of the regio
and R. MAZ

The r
CONTINI (19
metalliferoi

On the
thermal pr

For qu
of the Mt.

NANI (1962

As reg
research in

of the firs
J. MOUTON

a geotherm

The v
of the Nu

Technical
their crit

BOZZA G.,
steam.

ference
BURGASSI, B

geoterm
Roma.

CATALDI, R.
contrib

ogy in
CONTINI, L.
cinabri

The works by P. ELTER (1955) and U. LOSACCO (1959) deal instead specifically with the stratigraphy and the tectonics of the Mesozoic nuclei outcropping in the Amiata region.

Among the studies which deal with the volcanological problems of the region, those by A. DE BENEDETTI (1958), G. MARINELLI (1961) and R. MAZZUOLI, M. PRATESI (1963) deserve a special mention.

The reports by C. DE CASTRO (1914), O. MARINELLI (1919), E. CONTINI (1950), F. ELTER (1955) are particularly concerned with the metalliferous mineralizations.

On the contrary, the works up to now published about the geothermal problems of the Amiata region are quite few.

For questions of general character, involving also the situation of the Mt. Amiata geothermal « fields », the notes by G. FACCA, F. TONANI (1962) and by G. MARINELLI (1963) are worth mentioning.

As regards specific works on various aspects of the geothermal research in the Mt. Amiata region, N. GENNAI (1960) gives the results of the first wells drilled at Bagnore, while R. BURGASSI, R. CATALDI, J. MOUTON, F. SCANDELLARI (1965) present and discuss the results of a geothermal survey carried out in the region.

Acknowledgements

The writer expresses his gratitude to Prof. E. TONGIORGI, Director of the Nuclear Geology Laboratory of Pisa and to Dr. M. MARCHETTI, Technical Director of the Centro Studi Geotermici of the C.N.R. for their criticism and helpful suggestions.


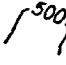



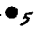
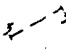
References

- BOZZA G., 1961 - *On the origin of thermality in underground waters and endogenous steam*. Privately printed by Larderello S.p.A. and presented to the O.N.U. Conference on New Sources of Energy, Roma.
- BURGASSI, R., CATALDI R., MOUTON J. e SCANDELLARI F., 1965 - *Prospezione delle anomalie geotermiche e sua applicazione alla regione amiatina*. L'Industria Mineraria, Roma.
- CATALDI, R., STEFANI, G. e TONGIORGI M., 1963 - *Geology of Larderello region (Tuscany): contribution to the study of geothermal basins*. Spoleto Meeting on Nuclear Geology in Geothermal Areas. Laboratorio di Geologia Nucleare, Pisa.
- CONTINI, E., 1950 - *La geochimica della mineralizzazione del mercurio. Il giacimento cinabrifero di Abbadia S. Salvatore*. L'Industria Mineraria, Roma.

- DALLAN L., 1964 - *I foraminiferi miocenici dell'isola di Pianosa*. Boll. Soc. Geol. Ital., Vol. LXXXIII.
- DE BENEDETTI A., 1958 - *Sulle cosiddette « rocce ofiolitiche » della valle della Senna - Mt. Amiata*. Soc. Mineral. It., Rendiconti, Vol. XIV.
- , 1959 - *Altre notizie sulle selagiti della regione del Mt. Amiata*. Soc. Mineral. It., Rendiconti, Vol. XV.
- DE CASTRO, C., 1914 - *Le miniere di mercurio del Mt. Amiata*. Mem. Descritt. Carta Geol. Ital., Vol. XVI, Roma.
- ELTER F., 1955 - *Note sulla localizzazione e la genesi dei giacimenti cinabritici del Mt. Amiata*. L'Industria Mineraria, Roma.
- ELTER P., 1955 - *Geologia della regione di Castell'Azzara a Sud del Monte Amiata*. Boll. Soc. Geol. Ital., Vol. LXXIV, Fasc. II.
- FACCA, G. e TONANI, F. 1962 - *Geologia e geochimica del vapore naturale*. L'Industria Mineraria, Roma.
- , 1964 - *Theory and technology of a geothermal field*. Bull. Volcanologique, Tome XXVII.
- FERRARA, G. C., GONFIANTINI, R. e PANICHI, C., 1965 - *La composizione isotopica del vapore di alcuni soffioni di Larderello e dell'acqua di alcune sorgenti e mofete della Toscana*. Atti Soc. Tosc. Sc. Nat., Serie A, Vol. LXXII.
- GENNAI, N., 1960 - *Résultat de forages effectués à Bagnore (Monte Amiata, Italie)*. Bull. Volcanologique, Serie II, Tome XXIII.
- GHERARDI, S., 1964 - *Sui caratteri diagnostici del processo di sostituzione in posto*. Memor. Soc. Geol. Ital., Vol. IV, n. 1.
- GIANNINI, E., 1957 - *I fossili dell'arenaria di Manciano (Grosseto)*. Palaeontographia Italica, LI (n. ser. XXI).
- GIANNINI, E., NARDI, R. e TONGIORGI, M., 1962 - *Osservazioni sul problema della falda toscana*. Boll. Soc. Geol. Ital., Vol. LXXXI.
- GIANNINI, E. e TONGIORGI, M., 1959 - *Stratigrafia neogenica toscana - I - L'arenaria elveziana di Ponsano (Volterra)*. Boll. Soc. Geol. Ital., Vol. LXXVIII.
- , 1962 - *Les phases tectoniques néogènes de l'orogénèse alpine dans l'Apennin septentrional*. Bull. Soc. Geol. de France, 7e série, t. IV.
- LOSACCO, U., 1958 - *Osservazioni geologiche sulle arenarie della Toscana meridionale*. Boll. Soc. Geol. Ital., Vol. LXXVII.
- , 1959 - *Ricerche geologiche nella Toscana meridionale - I - Stratigrafia e tettonica del gruppo Mt. Civitella-Mt. Elmo (Grosseto)*. Boll. Soc. Geol. Ital., Vol. LXXVIII.
- , 1959 - *Ricerche geologiche nella Toscana meridionale - III - Stratigrafia e tettonica del Poggio Zoccolino (Mt. Amiata)*. Boll. Soc. Geol. Ital., Vol. LXXVIII.
- LOTTI, B., 1878 - *Il Monte Amiata*. Boll. R. Com. Geol. It.
- , 1910 - *Geologia della Toscana*. Mem. Desc. Carta Geol. d'Italia, Vol. XIII.
- MARINELLI, G., 1961 - *Les anomalies thermiques et les champs géothermiques dans le cadre des intrusions récentes en Toscane*. O.N.U. Conference on New Sources of Energy, Roma.
- , 1961 - *Genesi e classificazione delle vulcaniti recenti toscane*. Atti Soc. Tosc. Sc. Nat., Vol. LXVIII, Ser. A.
- , 1963 - *L'énergie géothermique en Toscane*. Ann. Soc. Géolog. de Belgique, T. 85, 1961-1962, Bull. n. 10.

DO NOT WRITE ABOVE THIS LINE - FOR LIBRARIAN'S USE ONLY!
XEROX ORDER FORM

SYMBOLS

-  Boundary of the volcanic outcrop
-  Contour lines {
 - elevations in mts.
 - datum plane: sea level
 - contour intervals: 100 mts.
-  Volcanic chimneys
-  Boundary of the internal depression
-  "Threshold" of the internal depression
-  Deep well (number or name)
-  Traces of the geological cross-sections

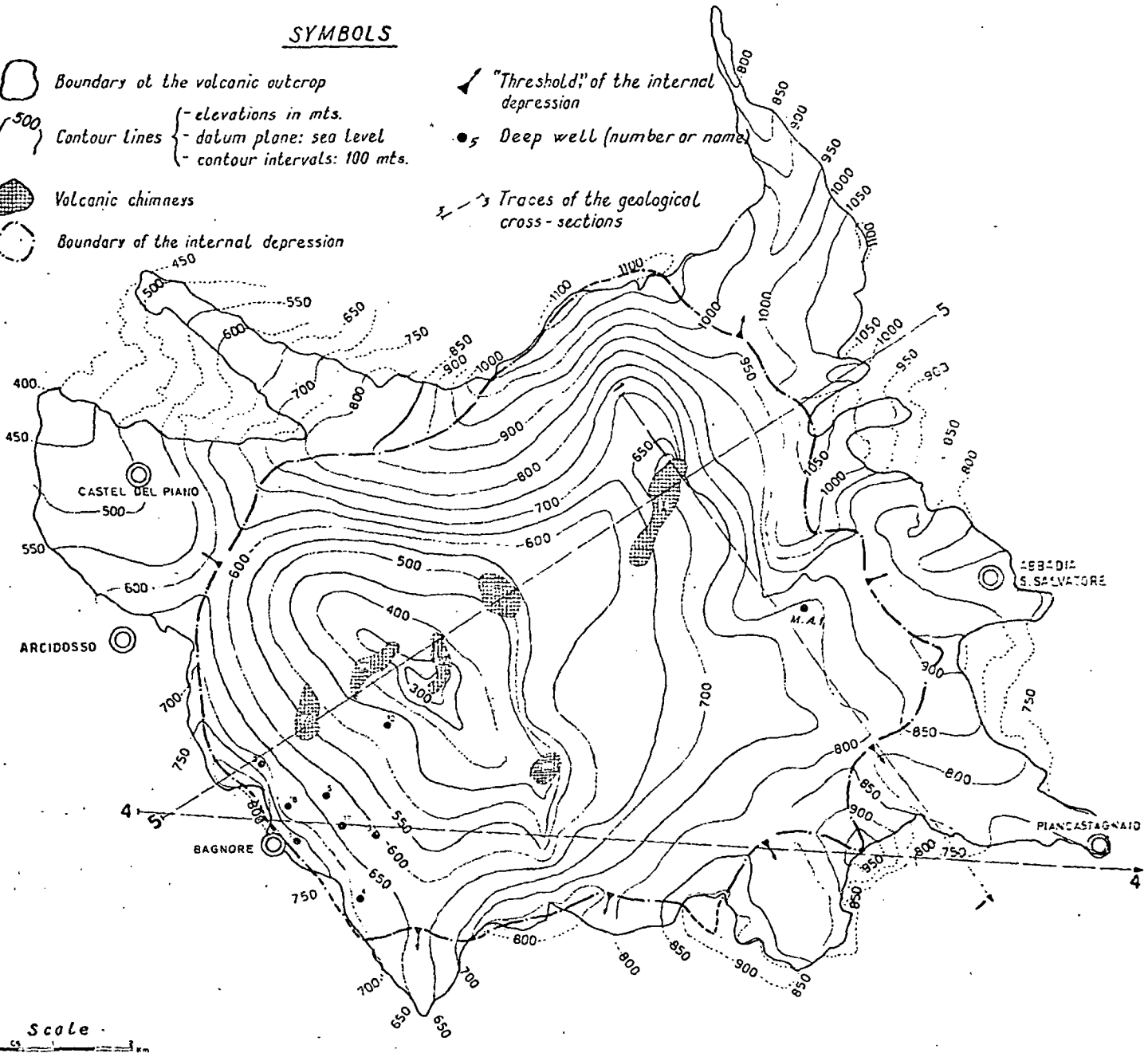


Fig. 6 - Contour map of the substratum of the volcanic rocks of the Mt. Amiata geothermal region.

- MARINELLI, O., 1919 - *La Regione del Monte Amiata*. Mem. Geog. Suppl. a Riv. Geog. Ital. n. 39, Roma.
- MAZZUOLI, R. e PRATESI M., 1963 - *Rilevamento e studio chimico-petrografico delle rocce vulcaniche del Monte Amiata*. Atti Soc. Tosc. Sc. Nat., Vol. LXX, Ser. A, Fasc. II.
- MERLA, G., 1952 - *Geologia dell'Appennino settentrionale*. Boll. Soc. Geol. Ital., Vol. LXX, n. 1.
- , 1959 - *Essay on the geology of the Northern Apennines. Meeting on the gas fields of Western Europe*, Vol. II, Acc. Naz. dei Lincei.
- RODOLICO, F., 1935 - *Ricerche sulle rocce eruttive recenti della Toscana - III - Le rocce del Monte Amiata*. Atti Soc. Tosc. Sc. Nat., Vol. XLV.
- SCHIEFFER V., 1963 - *Questioni regionali geofisiche riguardanti la geologia dell'Appennino*. Boll. Soc. Geol. Ital., Vol. LXXXII.
- SERVIZIO IDROGRAFICO ITALIANO, 1957 - *Precipitazioni medie mensili ed annue e numero dei giorni piovosi per il trentennio 1921-1950*. Pubbl. n. 24, Fasc. IV, Roma.
- TONGIORGI, E. e TREVISAN L., 1957 - *I movimenti tettonici quaternari in Toscana e nel Lazio Settentrionale*. Proc. of the 5th Intern. Cong. INQUA, Madrid.
- TRABUCCO, G., 1921 - *Le sorgenti del Mt. Amiata*. Mondo Sotterraneo, Vol. XVII.

Some Considerations on the Flow-rate/Pressure Curve of the Steam Wells of Larderello

O. RUMI *

AREA
IT
Lard
Gthm

ABSTRACT

The flow-rate/pressure relation for the wells of the Larderello area is considered.

After an examination of the experimental results recorded in many years, and after the discussion of the experimental flow-rate/pressure curve, an attempt is made to find the theoretic link between pressure and flow-rate at the mouth of the borehole. The results of the experimental and theoretical approach are then compared, and a best fit curve is proposed.

Moreover, the flow-rate/well bottom pressure curve as the true characteristic of the whole system of flow is suggested.

The flow-rate/well-head pressure curve

It is very useful to know the relation between the flow-rate and the well-head pressure: this enables one to understand the phenomena of vapour flow and gives all the necessary indications for the determination of the best conditions of exploitation. Unfortunately it is not possible to have the experimental characteristic curves for all the wells because this would involve a great waste of energy. It is thus of interest to consider whether the definition of a theoretical or experimental curve can be made when only few data are available. e.g. flow-rate and exit pressure in working conditions and shut-down pressure, or flow rate and pressure in two different conditions.

EXPERIMENTAL RESULTS

The experimental characteristic curve giving the connection between the flow-rate and the well-head pressure is usually determined by measuring the flow-rate at different exit pressures, following the method described by NENCETTI (1961).

As the whole system of vapour generation and flow has a slow response, it is necessary to wait rather a long time (the period required for stabilization) before the true readings of flow-rate and pressure can be taken.

For a better understanding of this fact, the readings taken during stabilization ⁽¹⁾ and the actual final values, are shown in Figure 1.

From all the experimental data obtained from the wells of superheated vapour at Larderello it has been

* Istituto di Fisica Tecnica. Politecnico di Milano. Now with A. T. Kearney S.p.A. Management Consultants, via Durini 18, Milano, Italy.

Work supported by Istituto Internazionale per le Ricerche Geotermiche del C.N.R. under the research program for the exploitation of the geothermal energy sources.

shown that the relation between flow-rate and well-head pressure is always of the form

$$\left(\frac{Q}{Q_M}\right)^n + \left(\frac{p}{p_0}\right)^n = 1 \quad (1)$$

where p_0 is the well head shut-down pressure (pressure when $Q = 0$) and $Q_M = \lim_{p \rightarrow 0} Q$ is the maximum theo-

retical flow-rate that can be obtained from the system under consideration.

n is an exponent generally different for different wells, depending fundamentally on the geometrical shape of the fractures conveying the vapour at the bottom of the well and on the type of flow in these fractures; the observed value always ranges between 1.4 and 2 (in Figure 1, $n = 1.5$).

In the Figures 2 to 5 the experimental data from four different wells in the Larderello area are reported. To account for the influence of the exponent n on the shape of the curve, in addition to the one with $n = 1.7$ (mean value between 1.4 and 2 ⁽²⁾), the curves with exponent 1.4, 1.5, 1.6, 1.8, 1.9 are drawn.

Q_M in equation (1), cannot be determined by experiment. Even if the value obtained with an exhaust pressure of 2-4 bars is fairly close to the actual value, a better approximation is obtained by extrapolation of the experimental curve to the point $p = 0$ (this method has been followed for the curves of Figures 1 to 5): it should be pointed out that this approximation no longer holds when the curve is very steep in the region of higher flow-rates.

⁽¹⁾ The need to wait for stabilization before a reading means that some days are needed for the determination of the complete curve. If, in addition, we consider the time needed to provide the well with the instruments and the facilities necessary, it is easy to understand that the non-producing time of the well is quite long, and the loss of energy is important.

For this main reason the curve is determined experimentally for only a few wells. In consideration of this situation it is thus very useful to be able to draw a flow-rate/pressure curve, even if approximate, when only one point and shut-down pressure or when two points (even if fairly close) are known.

⁽²⁾ It has been said before that a different value of n can be determined for every well. As this from a general point of view would make the calculation very cumbersome and almost impossible, a mean value of 1.7 will be assumed for all the wells. This of course will imply a slight error: but it is better to have this error instead of determining a further experimental point of the curve. Afterwards the errors resulting from this approximation will be evaluated and discussed.

A39A

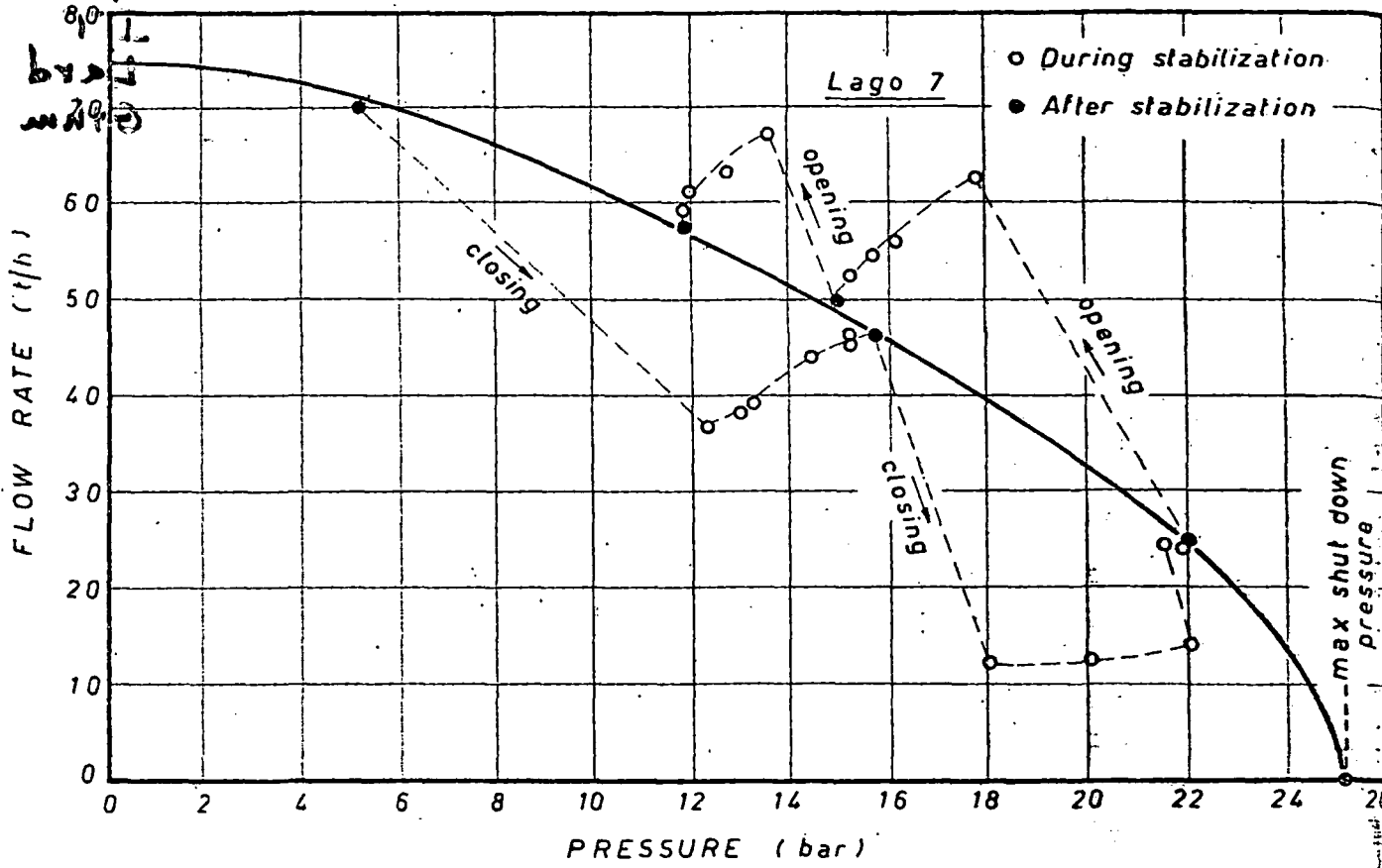


FIG. 1. — Variations of pressure and flow-rate readings during the opening and closing phase of a vapour well.

If equation (1) is assumed as the law governing the phenomenon, we can draw the characteristic curve when only two experimental points (i.e. pressure and flow rate in two different conditions of flow) or one point and the shut-down pressure are known (3).

From Eq. (1)

$$Q_M = \frac{Q}{\left[1 - \left(\frac{p}{p_0}\right)^n\right]^{1/n}} \quad (2)$$

or

$$p_0 = \frac{p}{\left[1 - \left(\frac{Q}{Q_M}\right)^n\right]^{1/n}} \quad (3)$$

In the first situation (two points available) Eq. (2) and (3) are solved together, while when one point and p_0 are known, only Eq. (2) is used.

Output records taken on the wells of the Larderello field for many years show very interesting results. It is for instance noted (and this fact has always been confirmed) that for a well discharging at constant exhaust pressure, the flow-rate and the shut-down pressure decrease with time.

(3) See paragraph Discussion of the theoretical flow-rate/exhaust pressure curve... etc. for a discussion of the accuracy of results obtained in these two cases.

As an example in Figure 5 the experimental data taken on the well « La Selvaccia » at an interval of six years are reported.

As we can see, the drop both in maximum flow rate and shut-down pressure is considerable: but the

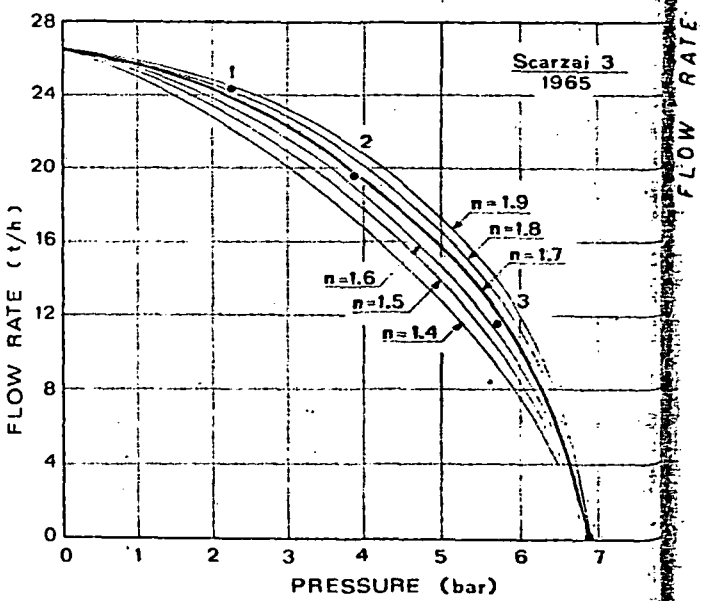


FIG. 2. — Actual recorded values for well Scarzai 3 and interpolating curves obtained applying Eq. (1) with different values of the exponent n.

ne
of
gro
the
inter
of fl
vari
losses
time b
the bo
the exp
Th
tion of
wells the
istic of t
140
130
120
110
100
90
80
70
60
50
40
30
20
10
0

new characteristic is of the same family as the curves of Eq. (1).

This is perfectly correct because if in the underground flow area no collapses nor anything changing the structure of the rock occurred during the time interval between the two recordings, the physical system of flow is always the same.

The exponent « n » generally undergoes a slight variation: this depends mainly on the greater friction losses of the steam. These losses are increasing with time because the path followed by the vapour to reach the bottom of the well becomes longer and longer as the exploitation goes on.

The flow-rate/pressure curve depends on the position of the borehole: when a well is far from other wells the curve can be considered as the true characteristic of the whole system of flow.

If, on the contrary, the underground flow area of a well is in communication with the flow area of the nearby wells, the curve obtained will be affected by these communications: in this case the shut-down pressure of a single borehole, if measured with the influencing wells discharging at a certain rate, is different from the pressure obtained when all the interdependent wells are closed. The reason lies in the fact that a true static situation exists only in the second case. Of course the difference between the true static and the « dynamic » shut-down pressure will increase with increasing underground communication of the wells.

However, for a system not isolated the flow-rate-exhaust pressure relation is of the same form of Eq. (1); in this case even if the determination of the true absolute value of the shut-down pressure is generally impossible, the curve is always of great help, as it allows the determination of the best conditions of exploitation.

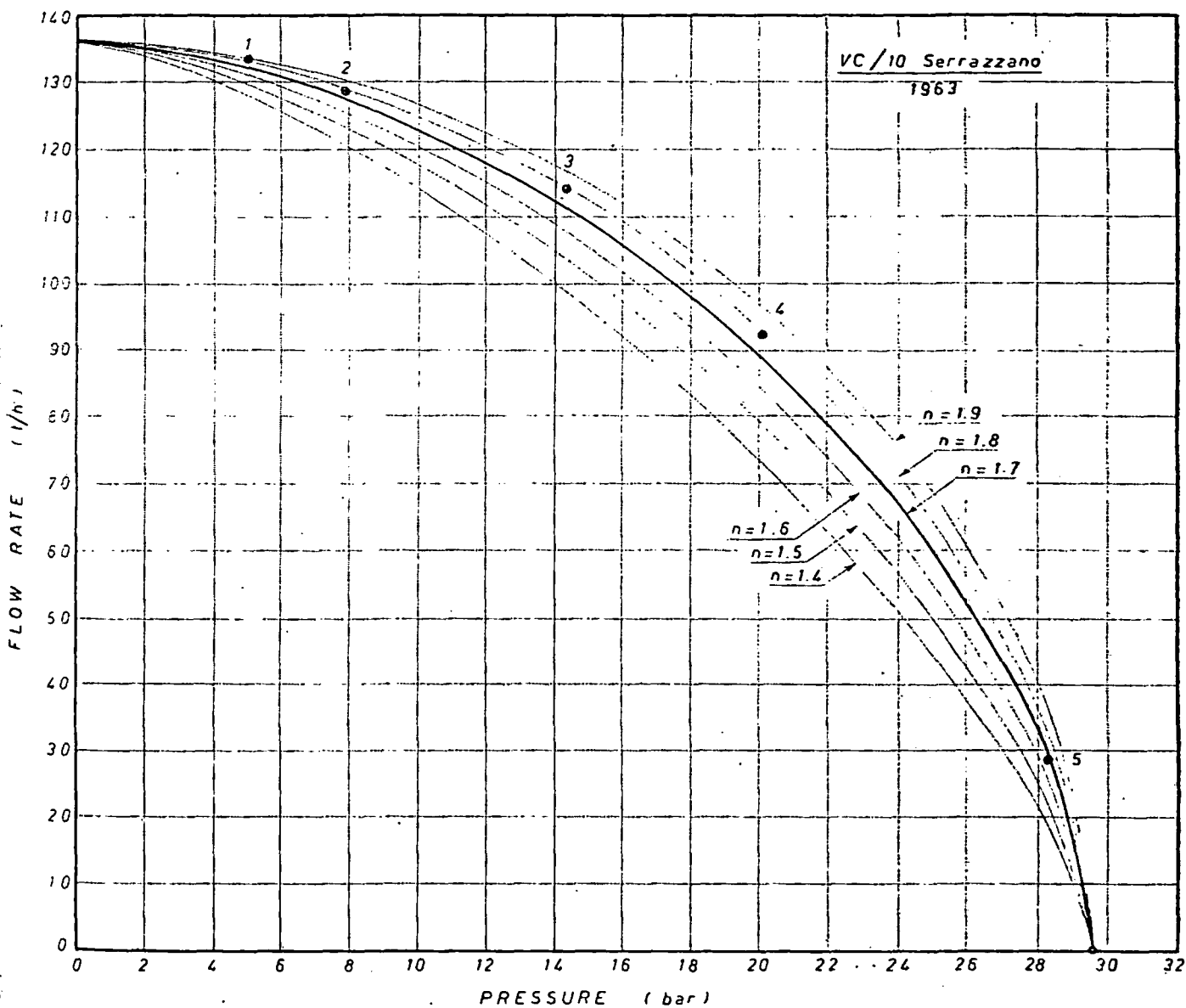


Fig. 3. — Actual recorded values for well VC/10 and interpolating curves obtained applying Eq. (1) with different values of the exponent n .

DETERMINATION OF THE THEORETIC FLOW-RATE/EXHAUST PRESSURE CURVE

Nomenclature:

- C_p specific heat at constant pressure
- D hydraulic diameter of the vapour duct, equals 4 times the cross section divided by total wetted perimeter
- G mass velocity
- G_M maximum mass velocity (exhaust pressure = 0)
- h enthalpy of unit mass
- k ratio of the specific heats, C_p/C_v
- l length of duct, positive in the direction of flow and measured from the beginning of duct
- L_T total equivalent length of duct
- n a constant
- p pressure
- p_o well-bottom shut-down pressure ($G = 0$), equal to saturation pressure
- q heat flux entering the duct
- Q flow rate
- Q_M maximum flow rate (exhaust pressure = 0)
- R steam constant in the equation of perfect gases
- Re Reynolds' number

- R_{vs} friction force per unit surface of the wall of the duct
- s entropy of unit mass
- T absolute temperature of the fluid
- T_o absolute saturation temperature at p_o pressure
- u internal energy of unit mass
- v specific volume
- w mean velocity of the vapour in the section under consideration
- ϵ surface roughness of the duct
- λ coefficient of friction, dimensionless
- ρ density
- Ω cross section area of the flow.

For the sake of simplicity let us consider an isolated borehole, i.e. without any communication with the nearby wells. Making the suitable assumptions and introducing some simplifications, we want to find the theoretical relation between the flow-rate and the exhaust pressure. In this investigation the system is considered in a steady state and the water is assumed to evaporate at an unknown distance from the bottom of the well. The vapour on the way from the generating site to the bottom of the well flows through a fracture

limiting all the fractures. It is another a numerical coefficient. A changing think the temperature are held the bottom and length also unknown means of the well. With exhaust p set up.

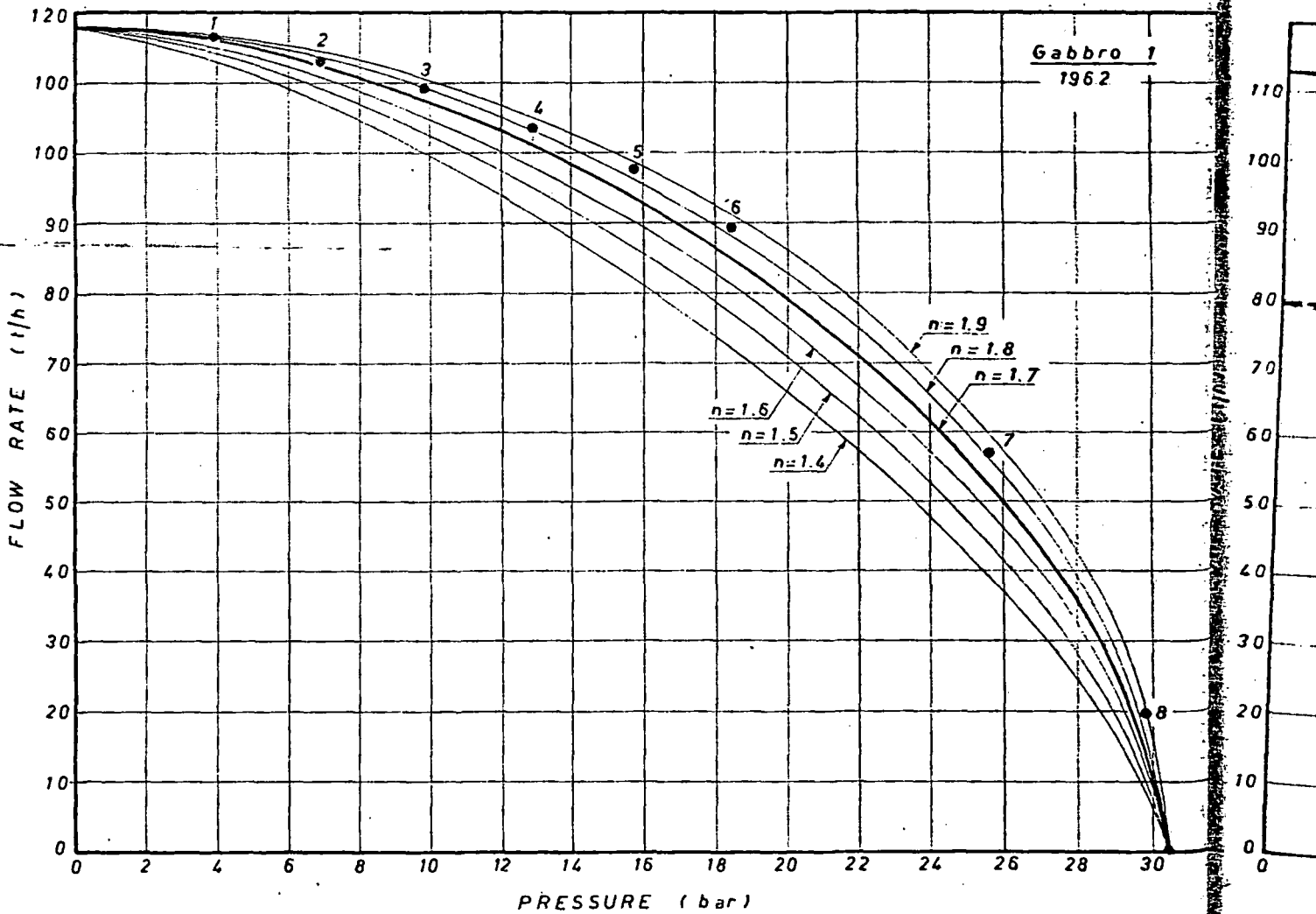


FIG. 4. — Actual recorded values for well Gabbro 1 and interpolating curves obtained applying Eq. (1) with different values of exponent n . FIG. 5. — Actual recorded values for well Gabbro 1 and interpolating curves obtained applying Eq. (1) with different values of exponent n .

all the vapour follows the low resistance paths of the fractures.

It is then possible to substitute for the actual system another simplified system consisting of the well and of a number of ducts having length, cross section and coefficient of friction which are unknown.

A further simplification can be introduced without changing the initial and final conditions: we can always think that the vapour flows from a tank in which the temperature T_0 and the pressure p_0 (saturation values) are held constant. From this tank the vapor flows to the bottom of the well through a duct of diameter D and length L_r not known; λ is the coefficient of friction, also unknown, related to the frictional resistance by means of the equation

$$R_{vs} = \frac{\lambda}{8} \rho \cdot w^2$$

With a system of this kind, for every value of exhaust pressure, a definite value of flow-rate will be set up.

In addition the equation of state of perfect gases is assumed for the vapour.

Let us consider an infinitesimal element dl of the hypothetical duct connecting the generating tank to the bottom of the well; neglecting the inclination of this duct (the effect of this inclination is actually very small) and assuming that a heat flux q is entering in the duct, we write (*) (BOZZA 1967; SHAPIRO 1953):

(*) Equations (4) to (8) and (4a) to (7a) are written for the underground path of the vapour to the bottom of the well; to find the exact relation between flow-rate and « exhaust » pressure it would be necessary to write the same equations for the adiabatic flow in the well: these equations are completely similar, the only difference being the term $q = 0$ in Eq. (4) and the term $(+gd)$ entering in Eq. (4) and (5) to account for the effect of gravity. The following integration can be performed in two steps: from the generating site to the bottom of the well and from the bottom to the head of the well. For the sake of simplicity it has been examined in detail only the first step: however, from the results obtained at the bottom, the determination of the flow-rate/exhaust pressure curve is extremely easy, and the equation of the exhaust curve is of the same type of that of the bottom. For this reason in the following pages we will speak often of exhaust curve, even when the right definition would be bottom curve.

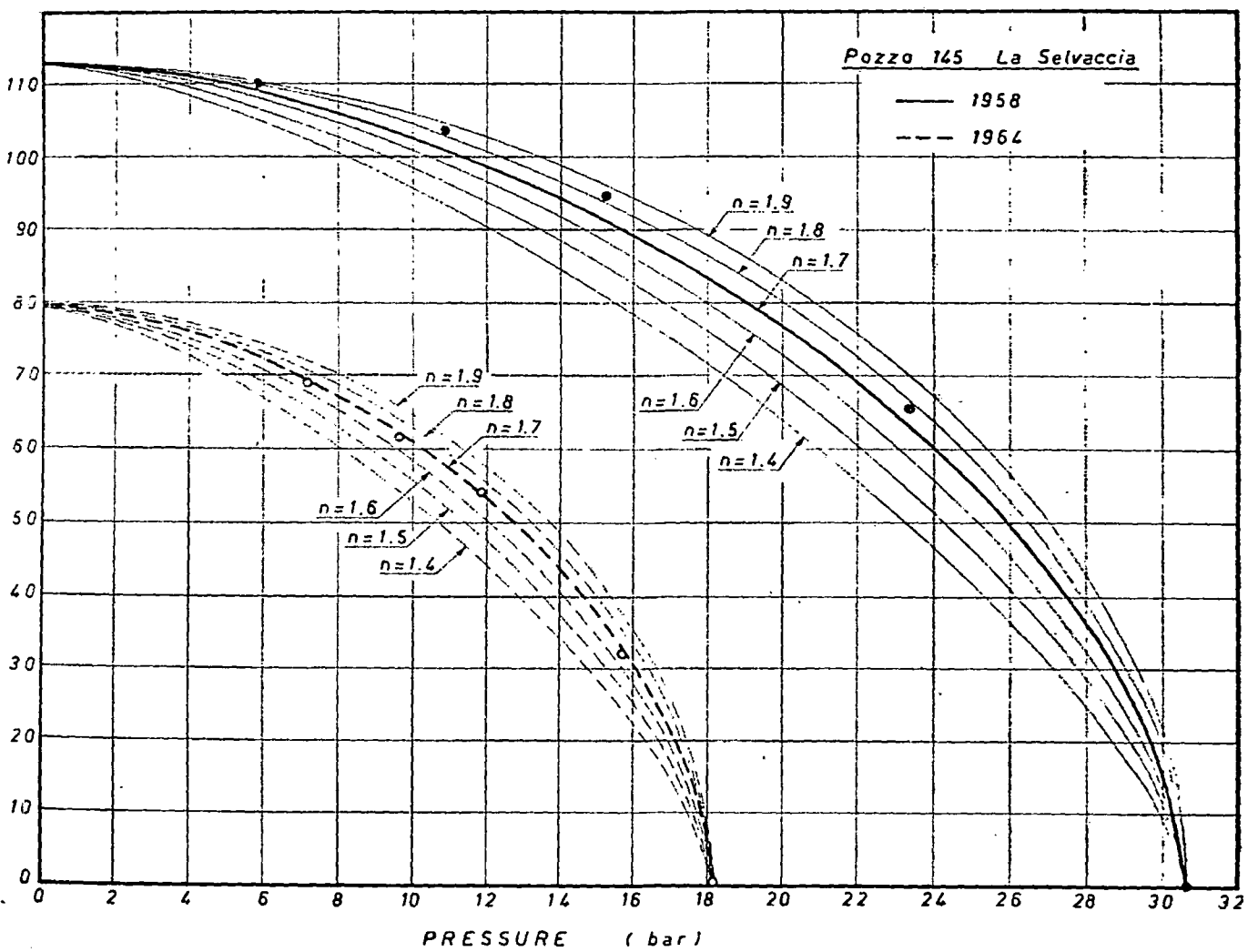


Fig. 5. — Actual recorded values for well 145 La Selvaccia and interpolating curves obtained applying Eq. (1) with different values of the exponent n.

$$w dw + dh - q \frac{\pi D}{\Omega_0 w} dl = 0 \text{ Eq. of energy (4)}$$

$$w dw + \frac{dp}{\rho} + \frac{\lambda}{2} \frac{G^2}{\rho^2} \frac{1}{D} dl = 0 \text{ Eq. of momentum (5)}$$

$$ds = \frac{du}{T} + \frac{p dv}{T} \text{ Eq. of production of entropy (6)}$$

$$\frac{dp}{\rho} = \frac{dq}{\rho} + \frac{dT}{T} \text{ Eq. of state of perfect gases (7)}$$

$$\frac{dG}{G} = \frac{dq}{\rho} + \frac{dw}{w} \text{ Eq. of continuity (8)}$$

Introducing Eq. (8) in the preceding equations and observing that the total variation of entropy in the element dl can be expressed by

$$ds = d_i s + d_e s$$

where $d_i s$ is the internal and $d_e s$ the external change of entropy, if $d_i s$ is due only to the friction losses it follows:

$$-\frac{G^2}{\rho^2} dq + C_p dT - q \frac{4}{DG} dl = 0 \text{ (4a)}$$

$$-\frac{G^2}{\rho} dq + \rho dp + \frac{\lambda}{2} G^2 \frac{1}{D} dl = 0 \text{ (5a)}$$

$$\frac{1}{C_p T} \left(\frac{\lambda}{2} \frac{G^2}{\rho^2} \frac{1}{D} + q \frac{4}{DG} \right) dl + \frac{k-1}{k} \frac{dp}{\rho} - \frac{dT}{T} = 0 \text{ (6a)}$$

$$\frac{dp}{\rho} - \frac{dq}{\rho} - \frac{dT}{T} = 0 \text{ (7a)}$$

The above system is homogeneous, the unknowns being $d\rho$, dT , dp dl . The solution can be obtained easily by means of the usual mathematical methods. As the subsequent integration of the above differential forms is very difficult in the general case, it is practically impossible to find a simple relation between pressure and flow-rate. However this relation can be obtained if some simple assumptions are introduced.

Considering, for instance, an isothermal flow the integration is quite easy and leads to the equation

$$\left(\ln \frac{p_0}{p} + \frac{\lambda}{2D} L_T \right) G^2 + \frac{1}{2} \frac{p_0^2}{RT_0} \left[\left(\frac{p}{p_0} \right)^2 - 1 \right] = 0 \text{ (9)}$$

As generally $\ln p_0/p \ll \frac{\lambda}{2D} L_T$, equation (9) becomes

$$\left(\frac{G}{G_M} \right)^2 + \left(\frac{p}{p_0} \right)^2 = 1 \text{ (10)}$$

In this equation (9)

$$G_M = \sqrt{\frac{p_0^2}{R \cdot T_0} \frac{D}{\lambda L_T}} \text{ (10a)}$$

As we can see Eq. (10) is very like Eq. (1) when $n = 2$, the only difference being G_M , that is no more

constant; this means that the simplifications introduced do not change the actual system. Furthermore we can observe that the more the exponent n approaches 2, the more closely the flow approaches the isothermal flow.

An approximate relation between flow-rate (or mass velocity) and exit pressure, holding for every possible thermodynamic transformation of the vapour in the duct, is obtained in the following way.

Let us consider the equation of momentum (5a)

$$-\frac{G^2}{\rho} dq + \rho dp + \frac{\lambda}{2} G^2 \frac{1}{D} dl = 0$$

Together with this equation we can use the relation defining the type of thermodynamic transformation. Without loss of generality this can be assumed to be of the type

$$p v^n = \text{constant} \text{ (11)}$$

where n is an exponent constant along the entire path followed by the vapour (6).

For a reversible process, equation (11) would represent a polytropic transformation.

Even if a constant value of n along an irreversible process, as the one considered, does not allow us to define Eq. (11) as polytropic (i.e. with constant specific heat) it is always possible to think of Eq. (11) as of a relation linking all the states of the system during its evolution.

This relation is only useful in determining the changes of internal energy, enthalpy, entropy and of other parameters; in addition, with this assumption it is sufficient to know only the initial and final states of the system. Solving the system of equations (5a) and (11), we have

$$G^2 \left(\frac{1}{n} \ln \frac{p_0}{p} + \frac{\lambda}{2} \frac{1}{D} L_T \right) + \frac{n}{n+1} \frac{p_0^n}{RT_0} \left[\left(\frac{p}{p_0} \right)^{\frac{n+1}{n}} - 1 \right] = 0 \text{ (12)}$$

Introducing the value $n = 1$ in this equation (isothermal flow) Eq. (9) is obtained; this confirms the general validity of the equation found.

In this case, as $\frac{1}{n} \ln p_0/p \ll \frac{\lambda}{2} \frac{1}{D} L_T$ and setting $m = \frac{n+1}{n}$, we can write

$$\left(\frac{G}{G_M} \right)^2 + \left(\frac{p}{p_0} \right)^m = 1$$

(5) Equation (10) is the bottom equation when Eq. (10a) accounts only for the underground path and is the well-head equation when in Eq. (10a) λ and L_T account also for the flow in the vertical well.

(6) In the actual case the exponent n is not constant along the transformation and is surely different in the underground flow and in the well because the first part of flow is diabatic and the flow in the well can be considered adiabatic.

Since it does not very much affect the accuracy of the results, a single mean value of n is assumed for simplicity.

where

$$G_M = \sqrt{\frac{1}{m} \frac{2D}{\lambda L_T} \frac{p_0^2}{RT_0}} = \sqrt{\frac{1}{m} \frac{1}{K_F} \frac{p_0^2}{RT_0}} \quad (14)$$

For $p \rightarrow 0$, G_M is the maximum specific flow-rate of the system under consideration (⁷).

The exponent n is not known *a priori*: but as for n varying from 1 to 2, m ranges between 2 and 1.5, we can adopt in all the cases a constant value of $m = 1.7$ (⁸).

In equation (12) and (14) the term $\frac{\lambda}{2D} L_T = K_F$

relates the coefficient of friction to the geometric characteristics of the system; being dimensionless it can be considered as a characteristic coefficient of the system of flow of the vapour.

Starting from the experimental data of some wells, K_F has been calculated, with $m = 1.7$ from the equation

$$K_F = \frac{1}{G^2} \frac{1}{m} \frac{p_0}{RT_0} \left[1 - \left(\frac{p}{p_0} \right)^m \right] \quad (15)$$

As we can see in Figure 6, K_F decreases with decreasing exhaust pressure (i.e. with increasing flow rate (⁹)). This decrease of K_F is probably due to two main reasons: the coefficient λ as one can verify from tables or from empirical correlations like the one of Colebrook (¹⁰), increases with decreasing Reynolds' number and the increase is important if at very low flow-rates, somewhere in the flow path the critical Reynolds' number is reached; more probably, however, the increase in K_F with decreasing flow-rate comes from the fact that at very low flow-rates (i.e. high bottom pressures), not all the fractures keep conveying the vapour, thus modifying the term $\frac{L_T}{D}$.

DISCUSSION OF THE THEORETICAL FLOW-RATE/EXHAUST PRESSURE CURVE AND OF ITS APPLICATION TO THE ACTUAL CASES

G_M in equation (13) is known when the curve of K_F is available; since this is not possible in the majority of cases, let us consider equation (13) with $G'_M = \text{constant} = \lim_{p \rightarrow 0} G$.

The right value of G'_M could be obtained by extrapolating the curves of the type reported in Figure

(⁷) see note no. 5 on page 18.

(⁸) see note no. 2 on page 13.

(⁹) That K_F decreases with increasing flow-rate does not mean that the pressure loss too decreases. This is confirmed by the pressure loss relation, that for the system considered can be written $\Delta p = \frac{\lambda}{2D} L_T \frac{G^2}{\rho} = K_F \frac{G^2}{\rho}$, being ρ the mean density; K_F decreases with increase in G , but as a whole Δp is always increasing with G .

(¹⁰) $\frac{1}{\sqrt{\lambda}} = -2 \log \left[\frac{2.5}{Re\sqrt{\lambda}} + \frac{1}{3.7} \frac{\epsilon}{D} \right]$ where $\frac{\epsilon}{D}$ is the relative roughness.

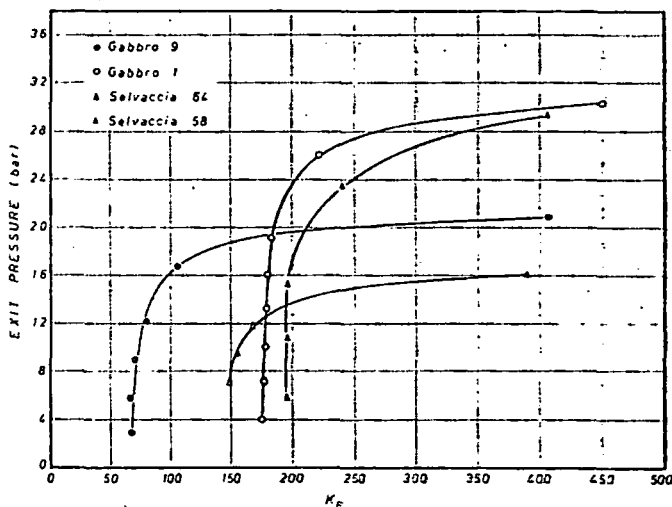


FIG. 6. — Variation of the characteristic coefficient of flow at varying exit pressures.

6, but as these are not available an alternative solution is to be followed.

As we can see in Figure 6 and as it has been verified in other cases not reported here, the error made in assuming at $p = 0$, the value K_F calculated at the maximum flow-rate or at the working flow-rate (i.e. with discharge at the pressure of the manifold) is negligible.

For the above mentioned reasons we can easily draw the flow-rate pressure curve by means of Eq. (13), assuming a constant value of m , after G_M considered constant ($= G'_M$) has been determined by introducing in the same equation (13) the working, or better the maximum, recorded value of flow-rate and pressure.

The curves reported in Figures 7 to 10 have been obtained by this method. In drawing these curves together with the point defining the maximum recorded values of flow-rate and pressure, the shut-down pressure was known.

To show the influence of the exponent m , in addition to the mean value 1.7, the values 1.5, 1.6, 1.8 and 1.9 have been considered.

Looking at these curves we see that they are less affected by a variation of the exponent than the curves obtained considering Eq. (1): it follows that with Eq. (13) the error due to the assumption of a constant exponent is lower.

In Table 1 are listed the errors obtained when taking the values calculated by means of Eq. (1) with a constant exponent 1.6 and 1.7 respectively and by means of Eq. (13) with exponent $m = 1.7$.

The error e is given by the absolute value of the expression $\frac{V_M - V_C}{V_M}$, where V_M and V_C are the measured and calculated value respectively.

From the table we see that neglecting the last point of the curves (condition of minimum flow-rate) the error is always low: it never exceeds 1% in the region

of highest flow-rates (the region of practical interest for exploitation) when we consider the theoretical curve.

With the same curve the error in the region of higher pressures seldom exceeds 5%.

For all the wells listed in the table we find a rather high value of the error at the point of minimum flow-rate. This probably depends on the conditions of the experimental recording, and, as explained in the following, on the change of G_M at low flow-rates.

In fact the flow-rate is affected by a certain systematic error because, due to the nature of the pheno-

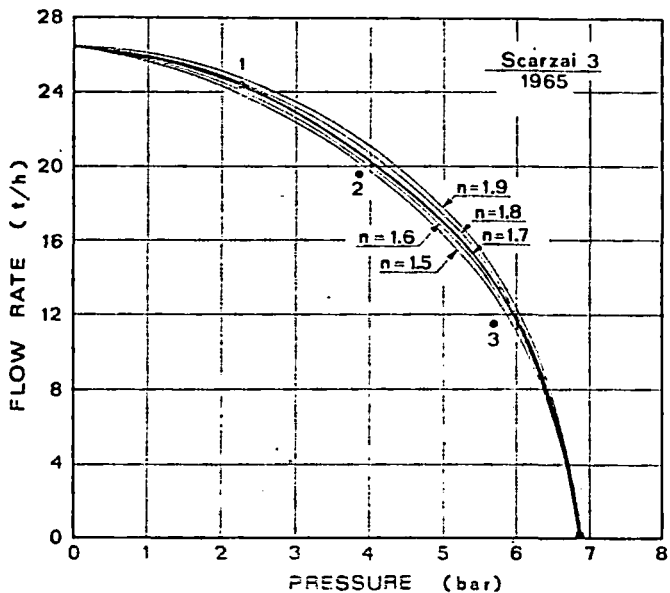


FIG. 7. — Actual recorded values for well Scarzai 3 and interpolating curves obtained applying Eq. (13) with different values of the exponent m .

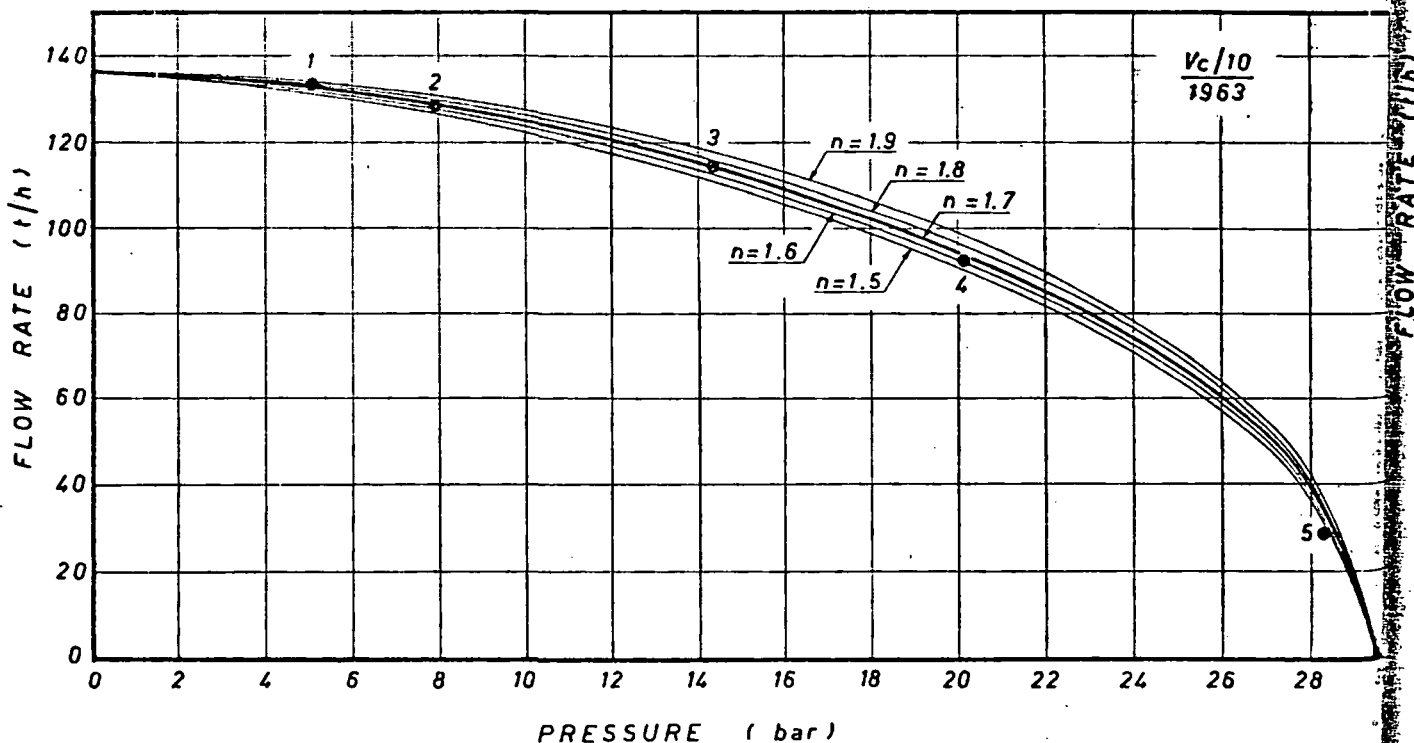


FIG. 8. — Actual recorded values for well VC/10 and interpolating curves obtained applying Eq. (13) with different value of exponent m .

TABLE I. — Errors (%) obtained applying both experimental and theoretical curves to actual values.

Well	Experimental points	Experimental curve		Theoretical curve $m = 1.7$
		$n = 1.6$	$n = 1.7$	
Selvaccia 1958	1	3.5	1.14	0.75
	2	5.0	2.91	0.57
	3	6.4	3.68	0.76
	4	9.25	4.55	5.44
	5	20	9.47	13
Selvaccia 1964	1	1.45	0.72	0.53
	2	3.18	0.81	1.25
	3	5.5	0.50	2.39
	4	7.8	0.50	11
Gabbro 1	1	1.7	0.86	0.11
	2	1.77	0.62	0.36
	3	3.21	1.38	0.21
	4	4.84	2.61	0.22
	5	7.18	4.1	0.41
	6	9.55	5.04	0.40
	7	14	7.9	4.37
	8	30	30	9.52
VC/10	1	1.89	1.13	0.49
	2	2.33	0.80	0.30
	3	5.75	2.64	0.64
	4	8.7	4.12	2.45
	5	12.5	12.3	29.56
Scarzai 3	1	4.1	0.82	0.35
	2	2.6	1.07	6.15
	3	0.5	6.45	18.84

menon, it cannot be measured in the best conditions and with more suitable instruments.

The error, insignificant for high flow-rates, is not negligible when the flow-rate is very low. In addition it must be pointed out that the system tends to become unstable when the pressure is close to the shut-down pressure.

The accuracy of Eq. (13) is not so very good when the shut-down pressure is not known. This can be understood if we think of the way we draw the curve: when the shut-down pressure is known together with a value of pressure and flow-rate (possibly high, to be in a field of $K_F = \text{constant}$), these two points, being at the opposite ends, define a curve that interpolates quite well the experimental results and changes very little with the exponent m (see Figures).

When we have two close points, the curve we obtain applying Eq. (13) interpolates with sufficient accuracy the region of high flow-rate, where $K_F = \text{constant}$, but it gives not acceptable results in the region of low flow-rates (variable K_F) and for the shut-down pressure itself. This because a slight error in the experimental points of in the exponent adopted, while giving as said before, an acceptable interpolation at high flow rates, shifts the curve very much at low flow rates.

This fact can be better understood if we consider Eq. (13). In this equation the term G_M actually is variable with the pressure (it depends on K_F).

When we know the shut-down pressure, even if we

put a constant value of K_F (at high flow-rate), the interpolation is very good, except at very low flow-rate (see Table 1), but even at low pressure, being p_o fixed, the change in G_M does not introduce a very great error.

If instead we know two working points and knowing these we determine p_o and G_M , p_o is not more constant but it depends on K_F . This increases the above mentioned shifting. Because, as we have seen, the experimental curve of Eq. (1) is more affected by a variability of the exponent, and gives errors greater than those obtained with the theoretical curve, we suggest the assumption of Eq. (13) as the equation governing the phenomenon of vapor flow in Lardèrlo.

Moreover, as we have observed the small influence of the exponent, and as all the experimental recordings give a mean exponent $m = 1.7$, we believe that the equation

$$\left(\frac{Q}{Q_M}\right)^2 + \left(\frac{p}{p_o}\right)^{1.7} = 1 \quad (16)$$

holds in all the cases with a very good accuracy ⁽¹¹⁾.

⁽¹¹⁾ Within the limits before mentioned.

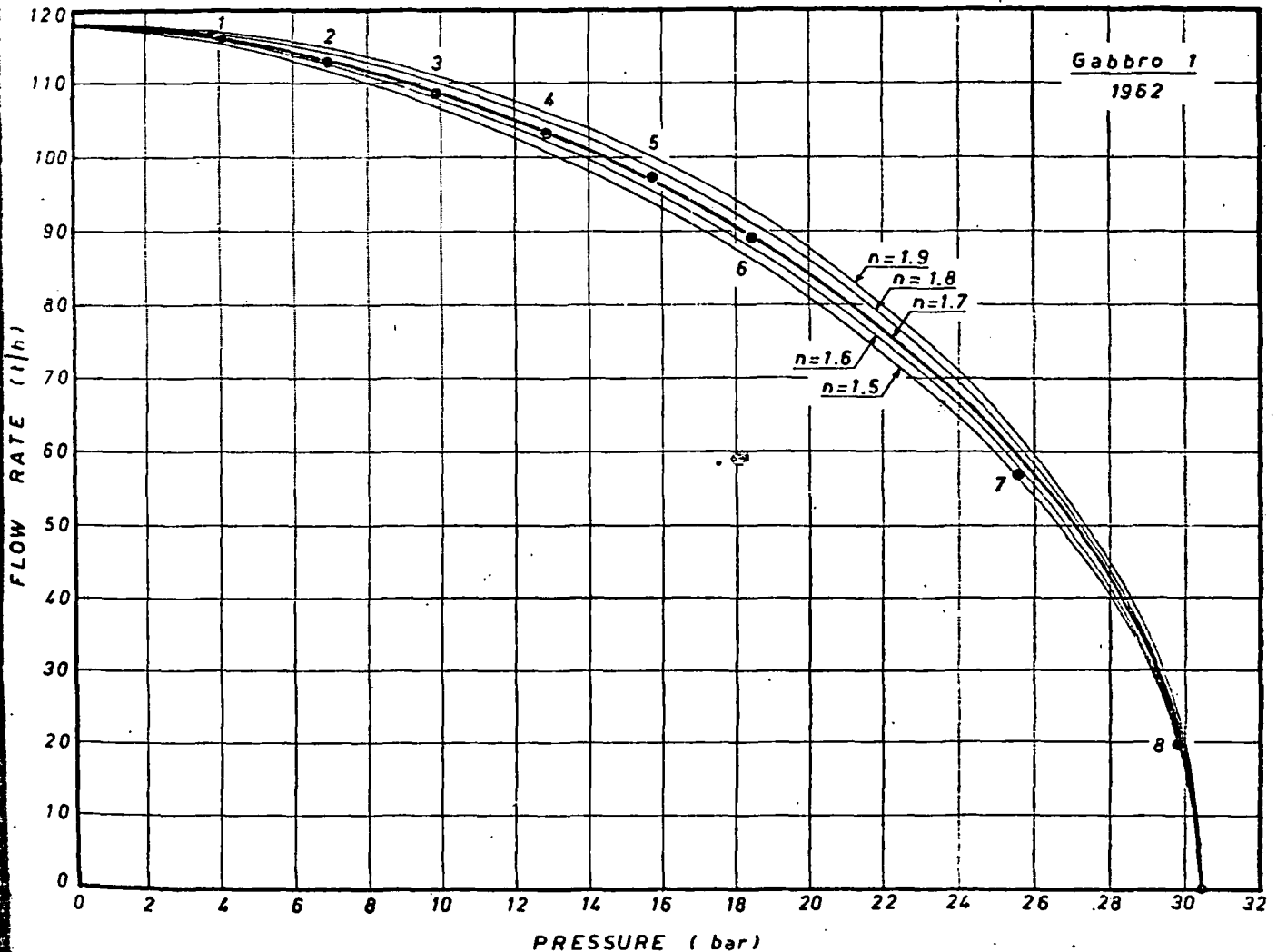


Fig. 9. — Actual recorded values for well Gabbro 1 and interpolating curves obtained applying Eq. (13) with different value of the exponent m .

The flow-rate/well bottom pressure curve.

We have so far studied the flow-rate/pressure curve at the head of the well, having considered the vertical casing pipe as part of the system of flow. It is, however, advisable not to take into consideration this part.

The reason lies in the fact that the fractures acting as conveying ducts depend only on the underground structure and nothing can be done to modify their shape; on the contrary, the casing pipe is the only element of the whole system not strictly predetermined, because the diameter, fixed according to considerations of drilling and of anticipated flow-rate, can be chosen within certain limits.

Thus, if we define a flow-rate/pressure curve at the bottom of the well, we have the limiting working conditions of the borehole under examination. And because it is impossible to modify these conditions (unless underground modification changes the structure of the conveying fractures) we can verify, after a calculation of the pressure loss, how good the vertical discharge tube is.

It is not difficult to draw the well bottom curve: starting from the values of pressure and temperatures

measured at the well-head by means of one of the methods outlined by RUMI (1967) it is possible to find the condition at the bottom ⁽¹²⁾.

The well bottom curve is, as said before, of the same family of curves of Eq. (13) and the exponent m can be considered the same.

This allows the drawing of an approximated well bottom curve when the shut-down pressure and the values of flow-rate and exit pressure in working conditions are known ⁽¹³⁾. In this case too a mean exponent $m = 1.7$ should be adopted.

The method is the same of that employed in the drawing of the well-head curve.

In Figures 11 and 12 are reported the bottom

⁽¹²⁾ From the experimental data at the head the flow rate/bottom temperature curves for different wells have been calculated. The results are not reported in this paper because the discussion about the shape of the curves obtained would imply come considerations on the superheating of the vapor and this would take too long a time. This subject will be widely discussed in another paper.

⁽¹³⁾ Whenever the shut-down pressures are not available another value of flow-rate and pressure must be known; the curve obtained in this case does not hold, as explained before at low flow-rates.

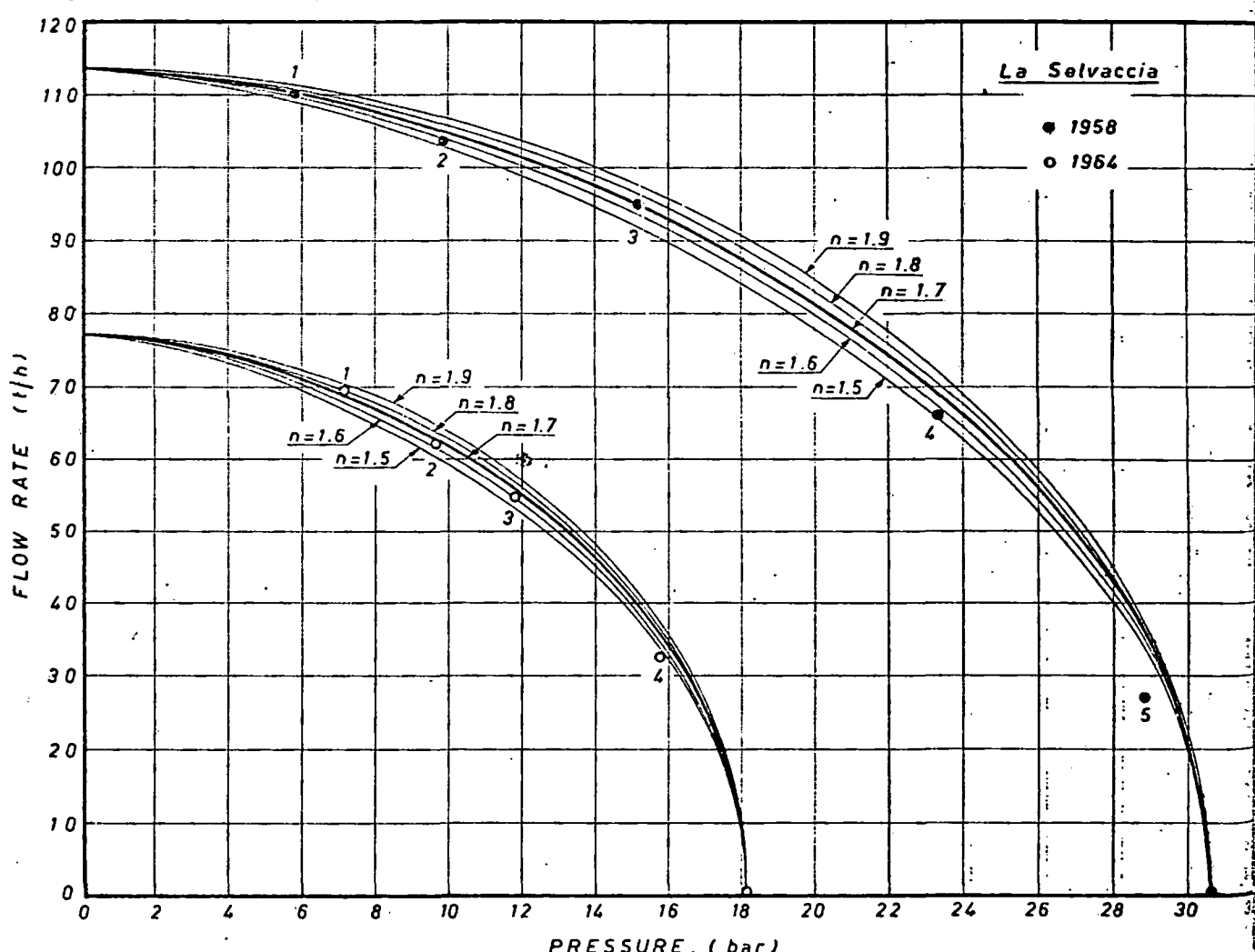


FIG. 10. — Actual recorded values for well La Selvaccia and interpolating curves obtained applying Eq. (13) with different values of the exponent m .

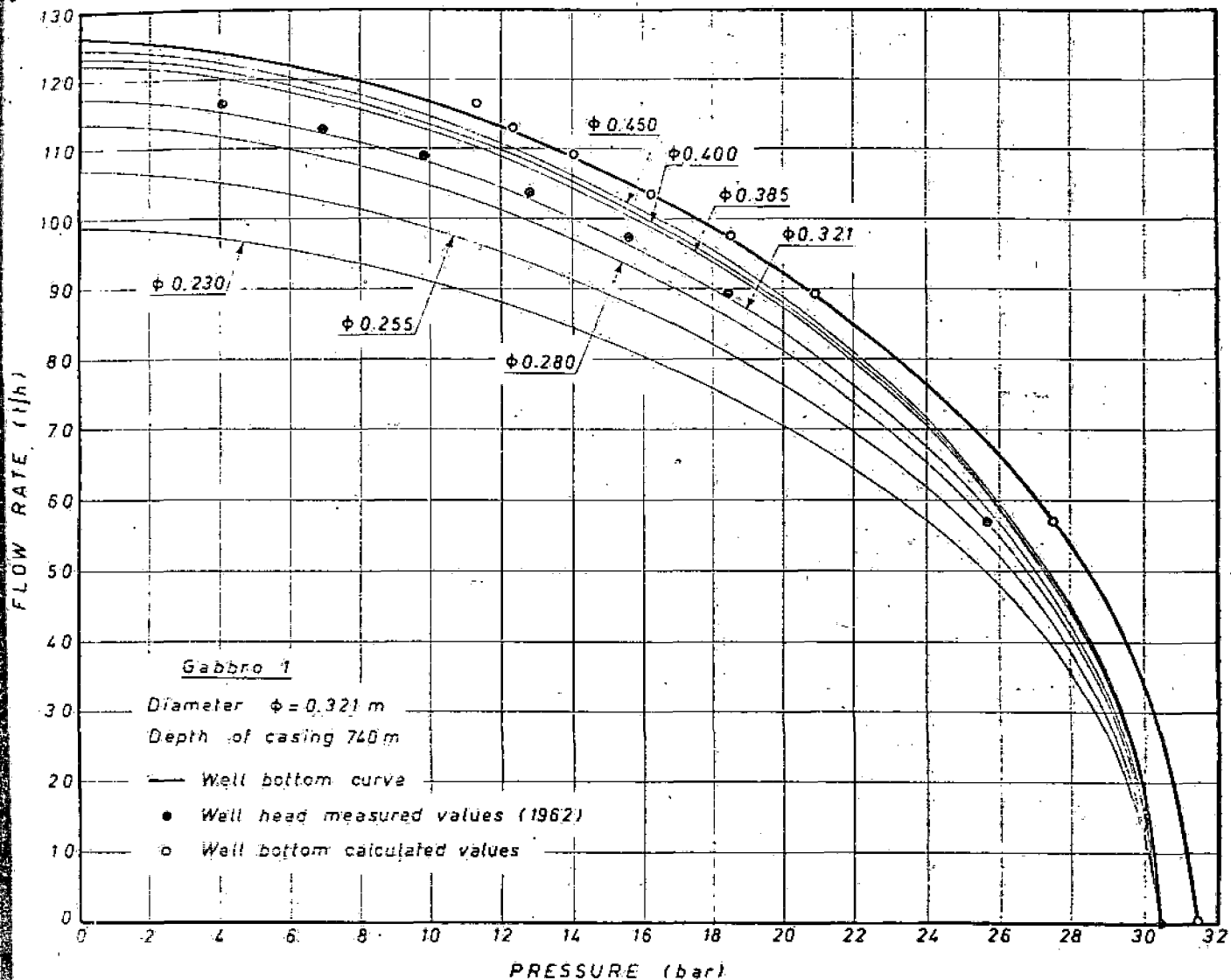


FIG. 11. — Bottom curves for the well Gabbro 1 and corresponding well-head curves for different well diameters.

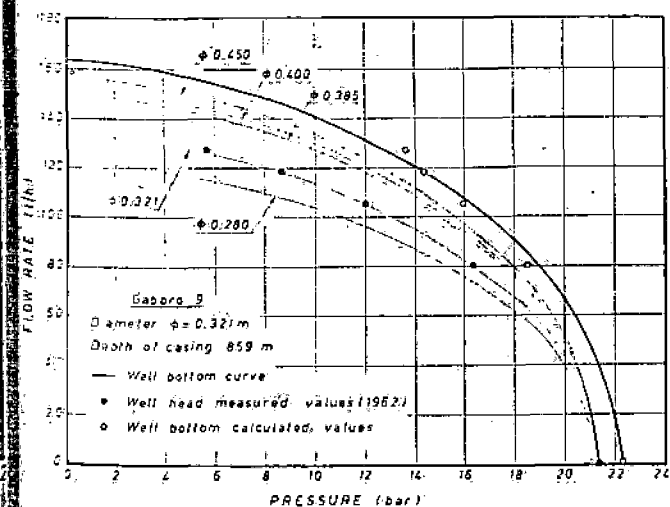


FIG. 12. — Bottom curves for the well Gabbro 9 and corresponding well-head curves for different well diameters.

curves of the wells Gabbro 1 and Gabbro 9. Starting from these, the characteristic curves at the well-head have been calculated considering different values of the diameter of the well.

It is very interesting to observe how the increase in the diameter of the vertical pipe is promising only under certain value. Surely it is not worth-while to go above these limits, because the higher cost of the borehole and of the casing is not compensated by the gain in the amount of energy obtained.

RÉFÉRENCES

- BOZZA G. 1967 — Alcune relazioni per il calcolo delle condotte di gas e vapori. *La Termotecnica*, 4.
- NENCETTI R. 1961 — Methods et dispositifs de mesure en tête des puits employée au champ géothermique de Larderello après eruption d'un sondage. *U.N. Conference on New Sources of Energy, Roma*.
- RUMI O. 1967 — Determination of the thermodynamic state of water vapor in steady adiabatic flow along a vertical pipe (well). *La Termotecnica*, 8.
- SHAPIRO A. H. 1933 — The dynamics and thermodynamics of compressible fluids flow. Vol. 1, New York, The Ronald Press. Co.

AREA
Italy
Abano

Determination of the sources and circulation paths of thermal fluids: the Abano region, northern Italy

D. NORTON

Department of Geosciences, University of Arizona, Tucson, AZ 85721, U.S.A.

and

C. PANICHI

CNR, Istituto Internazionale per le Ricerche Geotermiche, Pisa, Italy

(Received 21 March 1977; accepted in revised form 13 April 1978)

Abstract—Water samples from natural springs and artesian wells in the Abano region of northern Italy are characterized by anomalous temperatures and compositions. Concentrations of major components and oxygen isotopes in samples of these fluids have been interpreted in the context of the regional geologic environment, circulation of groundwaters, and reactions between rocks and circulating groundwaters. These considerations define source regions and pathlines of the groundwaters.

Circulation of fluids in the Abano region is interpreted to be the result of meteoric water infiltration into outcrops of Permian and Mesozoic aquifers in the pre-Alps, which lie north of the Abano region. These aquifers have southerly dips and, therefore, extend under the Abano region at depths between 0.5 and 2.5 km. This aquifer geometry is conducive to forced convection both of aqueous ions derived from the evaporite, limestone and dolomite bearing formations, and of thermal energy along flow paths which extend from the outcrops in the source regions to depths of 2 km below the Abano region and upward along high angle faults to thermal springs. Local variation in compositions of water samples is consistent with the mixing of local meteoric waters and formation fluids that were ultimately derived from Alpine sources.

INTRODUCTION

THE ABANO region in northern Italy contains numerous occurrences of saline thermal waters which are utilized in the local termes. These thermal waters flow from springs and artesian wells located around the Berici and Euganei hills and in the valley separating these hills. The Abano thermal area lies at the northern edge of the Po River Valley and at the southern edge of the pre-Alps. Calcareous mudstones of Cretaceous age, pyroclastic volcanic rocks of Tertiary age, and alluvium outcrop in the area.

The presence of a hydrothermal system in the subsurface rocks beneath the Abano region has been hypothesized by PICCOLI *et al.* (1973). On the basis of positive correlations between salinity and temperature of spring samples, they postulated a regional circulation system and further concluded that the systematic variation in salinity and correlations between major dissolved components were the result of subsurface fluids flowing along different circulation paths. In particular, they noted that samples with relatively large concentrations of chloride are also characterized by high temperatures. These samples were inferred to represent fluids derived from evaporite bearing formations at depths below the region.

Oxygen isotope data on samples from the region indicate that these fluids were originally of meteoric origin (PANICHI *et al.*, 1967). However, they observed that some of the samples are depleted in ^{18}O with respect to the local meteoric waters and are more

representative of precipitation which falls at high elevation, such as occurs to the north of Abano in the pre-Alps. Variations in the ^{18}O content of samples were, therefore, attributed to mixing of meteoric waters from the pre-Alps with local meteoric waters. The correlation between high salinity and low $\delta^{18}\text{O}$ values was also observed, and this Panichi *et al.* suggested to be evidence for a deep circulation path through the subsurface rocks, as hypothesized by PICCOLI *et al.* (1973). However, Panichi *et al.* pointed out that these waters were probably meteoric in origin and were derived from the pre-Alps. Calculation of mixing ratios conformed this hypothesis for many of the samples (PANICHI *et al.*, 1976).

Fluid-rock reactions along fluid circulation paths occur in response to changes in temperature, pressure, and composition of the environment through which the fluids flow. As a single fluid packet flows from a source region along its pathline, the rate of change in concentration of aqueous ions and isotopes in the fluid phase is the result of both equilibrium and non-equilibrium mass transfer between fluid and minerals (NORTON, to be published). Therefore, associated with the flow path of a particular fluid packet is a complex reaction path that affects the fluid's composition. These reaction paths can be represented by equilibrium diagrams which include the composition of the aqueous phase (HELGESON *et al.*, 1970). When fluid compositions along the reaction paths coincide with mineral stability fields, a reasonable hypothesis is that local equilibrium occurs between the mineral and the

fluid. Extrapolation of these reaction paths further suggests the mineralogical composition of environments which occur 'upstream' from the observation point. On the basis of this premise, a sample of the aqueous fluid at some point along its flow path should have a composition characteristic of the product mineral phases present at that point. Furthermore, a sequence of samples along the flow path should define a reaction path which passes through the stability fields of the product minerals and trends toward overall equilibrium between the solution and initial reactant phases along the flow path.

Since the composition of fluid along a circulation path is the result of reactions which occurred further 'upstream', the chemical and mineralogical composition of the upstream environment should be evident from the fluid composition. Obviously, for very complex flow paths, or in systems characterized by flow rates which are small relative to reaction rates, this may be practically impossible. However, if independent data are available which define the original fluid source and the geologic environment between the source and sample site, the reliability of the interpretation is enhanced.

Samples from the Abano region are well suited for this type of analysis since the original fluid sources are defined by oxygen isotope data, the possible fluid pathlines are defined by the regional circulation pat-

terns of groundwaters, and the rock compositions along the pathlines are known from geologic mapping. The purpose of this communication is to reinterpret the Abano data on the basis of the concept that fluid compositions are diagnostic of the geologic environment which occurs upstream along the flow paths.

DATA

Water samples from the Abano region were collected from artesian wells and springs (Fig. 1), and have been analyzed for their major element and oxygen isotope content by PANICHI *et al.* (1976) (see Table 1). Samples of spring waters were collected during dry (September) and rainy (January-June) seasons to ascertain the effect of seasonal variations (Table 2). Replicate analyses were also made to ascertain the reliability of both oxygen isotope and major element determinations. The precision is $\pm 0.1\%$ for oxygen isotope determinations and $\pm 5\%$ for major element determinations.

Geologic data on the surface and subsurface environments was taken from the summary discussion and geologic sections in PICCOLI *et al.* (1973). The true ionic strength of the samples ranges between 0.01 and 0.2 molal. The electrical balance for water analyses was found to be < 0.005 meq/kg. Mineral stability data for equilibrium diagrams were taken from HELGESON (1969). From approx 225 of these samples, 88, for which the analytical data were complete and most reliable, were selected.

The activities of ions and aqueous complexes were computed from the major component concentrations and temperatures of each sample, using program DIST (KNIGHT,

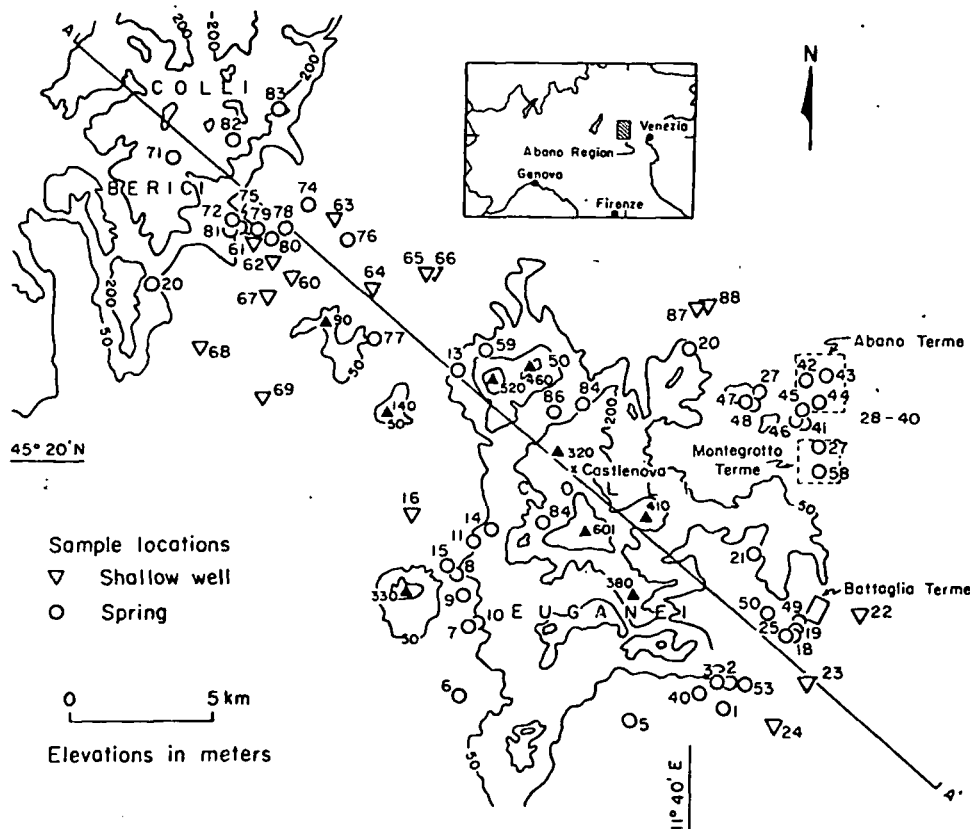


Fig. 1. Topographic and sample location map for the Abano region, northern Italy.

Table 1. Analytical data on Abano region samples*

Sample no.	Temp.	$\delta^{18}O$	Al+++	K+	Na+	Ca++	Mg++	H ₄ SiO ₄	SO ₄ ⁻⁻	CO ₃ ⁻⁻	Cl ⁻	
8-9	6.66	17.6	-9.5	0.03	9.2	53	104	18.2	11.3	133	249	34
10-9	6.85	30.3	-10.0	0.1	16.0	116	90	31.5	21.4	77	113	177
60-1	7.05	18.4	-10.2	0.2	11.1	70	100	42.0	15.6	11.0	64	59
61-9	7.05	30.0	-10.3	0.03	2.6	100	104	51.1	13.8	329	219	145
62-9	6.95	28.5	-10.3	0.1	18.2	91	108	55.9	15.5	401	143	126
63-9	7.10	34.5	-9.9	0.1	17.0	97	16	49.5	15.1	275	244	125
72-9	6.90	16.5	-8.8	0.06	9.0	27	110	15.2	6.6	80.7	328	36
73-1	7.05	17.0	-8.9	0.04	2.5	11.0	91	6.2	11.0	56.0	43	14
74-9	7.05	25.8	-9.6	0.07	15.0	56	126	46.8	14.3	363	200	73
78-9	7.10	25.2	-9.8	0.1	17.2	83	37	49.5	15.6	386	212	103
79-9	6.95	28.5	-9.8	0.09	16.2	94	112	46.2	13.0	200	273	126
80-9	7.10	26.5	-9.8	0.1	14.7	75	25	46.4	15.0	362	222	95
61-9	7.00	28.8	-11.5	0.02	17.9	123	108	46.2	15.0	289	244	174
4-9	6.75	17.3	-7.9		1.8	10	103	7.0	9.8	10.0	340	13
5-9	6.60	14.9	-8.1		1.3	8	106	5.6	6.0	14.8	337	9
6-9	7.00	36.0	-9.4		20.1	116	85	29.0	21.0	179	212	175
9-9	6.80	21.2	-9.3		10.7	64	95	21.1	15.1	112	270	109
11-6	7.10	12.0	-9.1		7.9	20	29	2.1	12.6	30.6	67.6	20
12-6	6.10	11.5	-9.2		1.4	4	3	0.70	6.3	.01	19.2	4
13-6	7.50	12.0	-9.4		1.7	7	7	1.7	16.5	7.5	31.9	6
14-6	7.00	13.5	-9.1		2.1	10	7	2.0	11.4	.01	46.6	8
15-6	6.75	15.2	-8.5		3.4	20	112	8.7	8.0	36.1	351	22
16-9	6.55	15.0	-8.5		8.3	52	115	51.3	17.5	2.9	733	51
19-9	7.20	48.9	-11.0		54.1	638	150	35.1	20.6	334	273	980
22-6	7.10	14.0	-8.9		85.7	85	152	48.7	7.0	120	801	60
23-6	7.00	16.5	-8.0		68.6	67	115	32.1	13.5	87.6	624	29
24-9	6.80	17.8	-8.4		28.8	78	150	31.9	10.0	152	567	59
26-1	6.95	17.6	-9.2		14.2	121	102	21.1	17.3	17.4	219	181
28	6.82	75.0			93.9	1840	352	71.0	44.4	25.8	18.6	2070
29	6.82	75.0			86.6	1180	360	64.8	43.8	865	18.6	3000
30	7.10	52.0			60.0	872	336	71.7	33.8	801	849	1420
31	7.00	70.0			69.0	820	367	82.2	36.3	835	181	1400
32	7.10	74.0			116	1330	400	59.0	45.7	896	195	2250
33	7.34	75.0			81.2	NA	397	63.2	53.2	781	176	2400
34	7.50	72.0			95.6	1070	400	81.1	41.3	798	192	1770
35	7.40	80.0			85.0	1500	452	88.0	46.9	830	168	2620
36	7.20	67.0			100	1430	352	60.0	56.3	876	180	2300
37	7.40	76.0			113	1520	394	73.4	43.2	899	168	2510
39	7.30	81.0			80.0	1280	377	59.0	39.4	830	180	2160
40	7.20	70.0			110	1340	376	75.0	46.3	847	168	2470
41-6	6.90	73.0	-10.3		72.0	1010	333	65.4	36.9	778	205	1720
42-6	7.00	82.0	-10.6		170	1130	391	88.9	52.5	865	175	2060
43-6	6.60	86.0	-11.0		94.3	1480	405	70.7	53.5	861	34.8	2630
44-6	6.90	74.0	-10.7		80.5	1470	392	58.6	38.3	830	129	2520
45-6	6.70	74.5	-10.5		68.6	1090	332	68.0	43.3	784	209	1850
46-6	7.20	70.0	-10.6		107	1400	380	64.0	40.7	887	190	2350
47-6	6.70	70.0	-10.0		67.9	787	332	65.4	49.0	865	134	1520
48-6	6.80	77.0	-10.4		76.0	785	349	66.0	49.4	672	190	1340
49-6	6.85	72.0	-11.4		61.0	612	150	33.0	41.0	316	147	1010
50-6	7.10	67.0	-11.5		68.0	602	162	36.0	50.0	316	166	1020
51-9			-11.7		62.0	575	159	30.6	46.0	320	143	1010
53-9	7.05	43.0	-11.6		36.0	262	113	47.0	35.0	358	114	0440
54-9	6.85	72.0	-11.5		65.0	589	148	36.0	44.0	359	133	1020
55-9	7.40	67.0	NA		22.0	300	190	21.0	35.0	320	113	1240
56-9	7.35	70.0	NA		02.0	500	161	22.0	11.0	222	122	1240
57-9	7.30	69.0	NA		90.0	613	159	32.0	52.0	330	182	999
58-9	6.90	72.0	NA		78.4	970	308	79.7	43.8	770	192	1660
59-6	7.60	12.0	-8.9		1.6	6	5	1.3	11.7	.01	31.8	5
64-6	6.75	12.0	-7.8		133	76	174	75.3	12.3	197	837	126
65-9	6.75	15.5	-7.6		10.7	68	84	65.0	16.6	25.1	577	124
66-9	7.05	16.5	-7.9		10.4	49	89	50.4	13.1	33.3	516	83
67-6	7.30	14.5	-7.9		24.2	43	195	51.4	7.9	168	677	57
68-9	6.65	16.8	-7.8		1.9	13	126	35.7	13.3	21.6	525	29
69-6	6.80	14.0	-7.7		0.70	7	137	28.9	6.6	66.1	474	11
71-9	7.00	12.4	-8.7		0.40	2	109	1.7	.01	2.0	333	4
75-9	6.90	19.5	-9.5		13.0	5	117	27.9	10.8	162	294	80
76-1	7.10	24.6	-10.3		13.2	96	74	47.0	14.0	260	200	117
77-9	7.25	24.0	-10.1		15.8	115	64	45.7	15.0	244	155	165
83-1	7.05	6.0	-9.4		.01	2	106	2.1	4.0	21.0	297	4
87-9	6.65	15.3	-8.0		1.9	11	120	33.5	5.4	37.7	517	10
88-9	6.75	16.0	-7.5		25.8	33	141	56.5	11.8	111	611	57

* Temperature, °C. $\delta^{18}O$, ‰ concentrations in ppm.

† Sample numbers and month of collection, e.g. 8-9; sample 8 was collected 9th month of the year.

compositions
ologic map-
is to reinter-
concept that
geologic en-
ng the flow

were collected
nd have been
n isotope con-
) Samples of
ptember) and
e effect of sea-
ses were also
xygen isotope
precision is
and ±5% for

face environ-
on and geolo-
ionic strength
2 molal. The
found to be
quilibrium dia-
From approx
tical data were

axes were com-
IST (KNIGHT.

erme

Terme

Table 2. Analytical data on Abano region replicate samples*

Sample No.	pH	Temp	$\delta^{18}\text{O}$	Al^{+++}	K^+	Na^+	Ca^{++}	Mg^{++}	H_4SiO_4	SO_4^{--}	CO_3^{--}	Cl^-
4-1	6.85	17.0	-8.2	-	1.70	8	93	5.4	28.9	12	301	13
5-1	6.85	14.8	-8.3	-	1.1	8	110	5.6	27.9	14.6	347	10
6-1	7.05	33.8	-10.2	trace	0.1	113	80	32.5	42.9	163	104	171
9-1	6.75	15.4	-9.2	-	4.1	9	92.3	5.5	17.4	42	264	13
10-1	6.95	29.6	-9.9	0.1	13.5	96	82	33.0	41.9	161	222	153
15-1	6.65	13.6	-8.8	-	2.6	6	107	5.2	12.6	41	305	9.2
61-12	6.85	38.5	-11.0	0.08	17.4	180	103	49.9	24.6	338.1	167	153
61-1	7.05	27.4	-11.0	trace	16.0	97	113	44.7	17.7	320.0	100	146
63-2	7.25	25.0	-10.0	trace	14.0	94	84	47.2	20.0	270.0	209	122
63-2	7.10	32.6	-10.0	0.10	14.0	92	80	44.6	21.0	277.4	197	121
63-2	7.75	34.5	-10.0	trace	15.2	91	90	45.4	24.0	278.0	193	126
71-1	7.30	9.8	-9.1	-	1.0	2	96.4	2.0	5.9	5.0	299	4
72-12	6.60	17.5	-9.1	0.08	8.9	32	96	17.2	15.7	109.7	251	52
72-1	7.00	12.8	-8.8	trace	5.7	14	82	9.0	17.6	50.0	243	11
74-12	6.80	24.0	-9.5	0.07	14.9	50	115	36.3	23.6	296.0	212	62
74-1	6.90	23.2	-9.3	trace	9.0	33	97	31.7	18.8	196.0	236	40
75-1	7.00	19.6	-9.7	-	10.1	56	107	30.5	17.1	178.0	280	76
77-1	7.05	20.8	-10.0	trace	10.2	68	78	27.0	19.5	162.0	190	99
78-12	7.00	28.5	-10.2	0.11	16.4	75	130	51.4	25.3	405.0	173	112
78-1	7.05	27.8	-10.5	trace	15.4	76	132	46.9	23.0	390.0	186	107
79-12	6.65	28.5	-10.8	0.09	16.6	91	103	49.0	20.5	298.7	211	140
79-1	7.00	27.6	-10.5	trace	14.2	87	88	48.0	22.4	266.0	168	123
80-12	7.00	25.3	-10.5	0.11	14.6	71	117	46.4	27.8	361.0	170	101
80-1	7.05	25.6	-10.3	trace	13.9	71	108	42.5	24.3	362.0	131	94
81-12	6.95	29.0	-11.5	0.02	17.0	116	57	47.0	27.7	296.6	179	100
81-1	7.05	28.5	-11.4	trace	15.8	113	85	45.7	26.7	297.0	136	175

* Temperature, °C. $\delta^{18}\text{O}$, ‰ concentrations in ppm.

† Sample numbers and month of collection, e.g. 6-1; sample 6 was collected 1st month of the year.

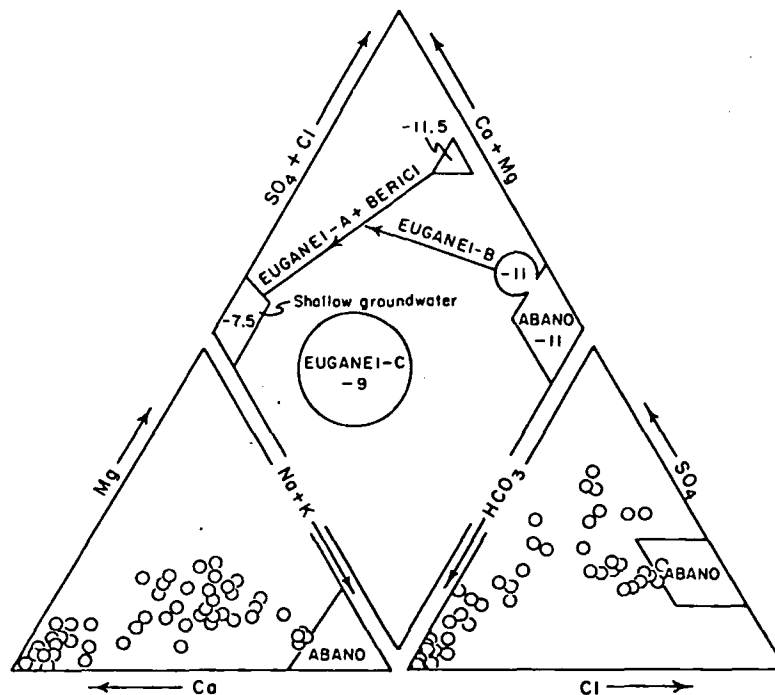


Fig. 2. Composition diagram showing relative amounts of major anions and cations in samples. Sample compositions, small open circles, in relative milliequivalents, are depicted in ternary plots of cations (lower left) and anions (lower right). Points from ternary plots are projected into central diamond where points represent meq% of both anion and cation concentration, generalized from PANICHI (1976). All Abano samples project into the very small labeled region on the diagram, whereas the samples from Berici and Euganei-A-B clearly have a range in bulk composition, as indicated by the circle and triangle and mixing lines connected to other samples. Euganei-C samples all project into large region outlined by circle.

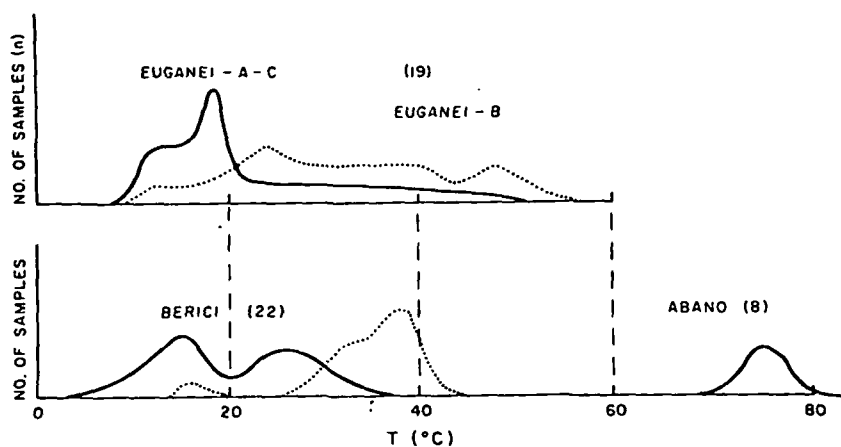


Fig. 3. Temperature histogram for samples from the Abano region showing number of samples vs temperature at which samples were collected, solid line, and temperature predicted by assuming quartz saturation for each sample, dotted line. Total sample numbers for each group in parentheses.

1976). These computations were based on equilibrium stability constants for aqueous complexes, taken from HELGESON (1969), and on a modified Debye-Hückel expression, taken from HELGESON and JAMES (1968).

BULK CHEMICAL COMPOSITION OF SAMPLES

The concentration of major components in the water samples indicates that there are five principal types of spring waters in the region. These are referred to as Abano, Euganei-A, Euganei-B, Euganei-C, Ber-

ici, and shallow groundwater, and they are distinctly different in their bulk composition, temperature, and isotopic composition (Figs. 2, 3 and 4). The relative composition diagram for these waters indicates the Abano samples are relatively concentrated in Na + K and SO₄ + Cl relative to the other cations and anions (Fig. 2). These same samples represent fluids which have an average temperature of 75°C (Fig. 3), and which are used in the Abano, Battaglia, and Montegrotto termes. They also have larger ionic strengths (~0.2 molal) than the other samples. Euganei-B

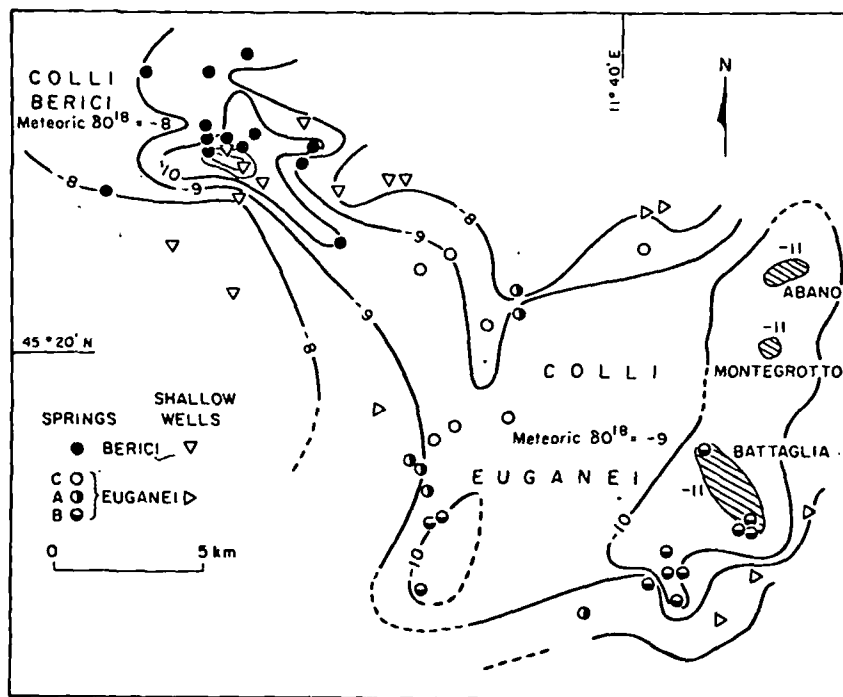


Fig. 4. Oxygen isotope map of the Abano region. $\delta^{18}\text{O}$ values in ‰ are contoured for both artesian well and spring samples. Sample points are also accordingly coded to bulk composition groups, as defined in Fig. 2. $\delta^{18}\text{O}$ values for meteoric waters in the Euganei and Berici hills and for the terme wells are also indicated.

samples have similar compositions, but trend toward relatively higher Ca + Mg and $\text{SO}_4 + \text{Cl}$, and their temperatures range from 50°C down to $\sim 20^\circ\text{C}$. They also have correspondingly lower ionic strength, $\sim 0.15\text{--}0.1$ molal. Several samples from springs which occur in the valley at the base of the Berici Hills are similar to the Abano and Euganei-B groups of samples, with respect to their relatively high $\text{SO}_4 + \text{Cl}$ and moderately anomalous temperatures. They also tend to contain relatively larger amounts of Ca (Fig. 2). These three groups of samples have anomalous temperature and bulk composition with respect to other samples in the Abano region.

Extremes in bulk compositions are represented by sample groups: Euganei-A, Euganei-C and local groundwaters (Figs. 2 and 3). Relatively concentrated in HCO_3^- and total calcium (Fig. 2), these samples come from springs along the base of Euganei Hills, in the valley between the Euganei and Berici hills, and in the Berici Hills (Fig. 1).

Oxygen isotope compositions of the samples in this region vary from -11.8 to -7.5 ‰ (Fig. 4). The very low values are typical of samples from Berici and Abano, Montegrotto and Battaglia termes, whereas the slightly more positive values, -10 ‰ are in samples which come from an area which extends into the Euganei region adjacent to the south end of the Euganei Hills. Samples from the valley between the Euganei and Berici hills contain the highest $\delta^{18}\text{O}$ values, -7.5 ‰, whereas samples containing the lowest $\delta^{18}\text{O}$ values are from springs or artesian wells which occur along bedrock fracture zones. The high $\delta^{18}\text{O}$ samples also tend to have relatively high $\text{SO}_4 + \text{Cl}$ and Ca + Mg concentrations (Fig. 2).

Linear correlations between the oxygen isotopic composition and salinity have been defined for different sample groups by PANICHI *et al.* (1976) (Figs. 5 and 6). These trends suggest that the Euganei, Berici and Abano waters are a result of mixing between low ^{18}O -content high salinity waters and lower salinity high ^{18}O waters. The isotopic values obtained by extrapolation of these functions to zero salinity might be expected to coincide with isotopic values of local meteoric waters. In the case of Berici and Euganei-A samples, there is reasonable agreement between the local meteoric and ground-water values with the zero salinity value, $\delta^{18}\text{O} \sim 7.2$ ‰ (Fig. 6) whereas the Euganei-B and Abano functions extrapolate to a $\delta^{18}\text{O}$, ≤ -9 ‰ (Fig. 5). All three of the sample groups have similar $\delta^{18}\text{O}$ maximum values, approx -11 ‰, which suggests that fluid circulation of these different types of water may originate in the same source region and that their different bulk chemical characteristics are related to differences in the reservoir rocks through which they flowed. The $\delta^{18}\text{O}$ value for local meteoric waters in the Berici area is -8 ‰ and in the Euganei area is -9 ‰ (Fig. 4). These values are somewhat lighter, but generally agree with extrapolated values for local meteoric waters, as derived in Figs. 5 and 6. Isotopic values which lie between the extremes of local meteoric water values and the -11 ‰ water values derived from springs are apparently the result of mixing of meteoric or shallow groundwater and subsurface waters.

The seasonal variations in composition of the water samples further substantiate the observation that local meteoric waters are mixing with waters from another source. Spring waters from the two regions

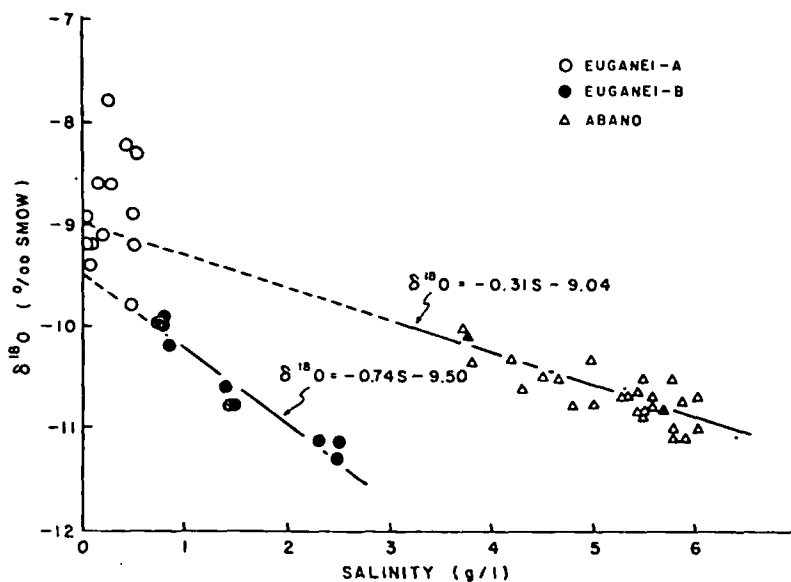


Fig. 5. Oxygen isotope variations, expressed as $\delta^{18}\text{O}$, ‰, as a function of salinity, generalized from PANICHI *et al.* (1976). Systematic increases in $\delta^{18}\text{O}$ values noted for Abano, Euganei-A and Euganei-B sample groups are expressed as linear functions, as computed from least squares analysis of data.

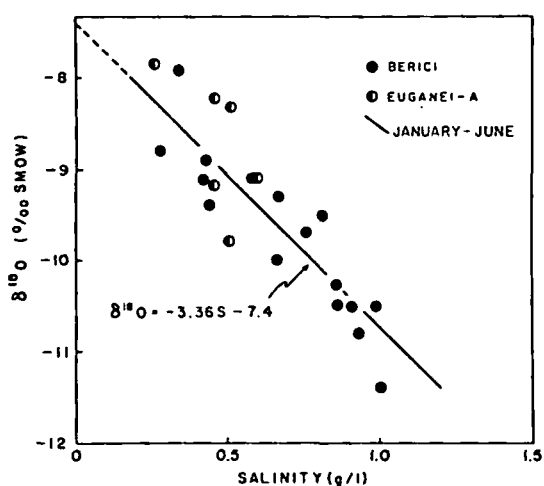


Fig. 6. Oxygen isotope variations, expressed as $\delta^{18}\text{O}$, ‰, as a function of salinity, generalized from PANICHI *et al.* (1976). Systematic increases in $\delta^{18}\text{O}$ values noted for Berici and Euganei-A sample groups are expressed as linear functions, as computed from least squares analysis of data.

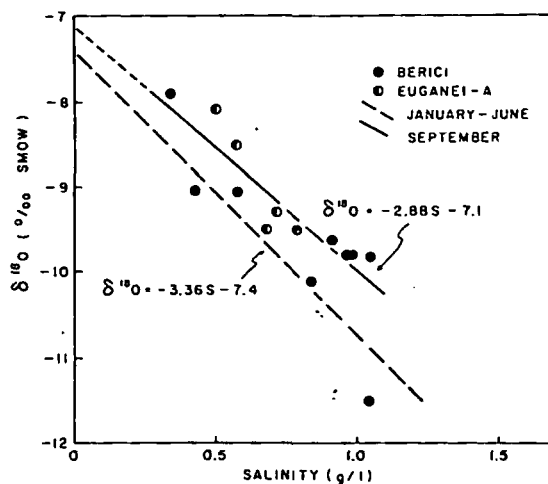


Fig. 7. Season variation of $\delta^{18}\text{O}$ values in Berici and Euganei-A samples represented in $\delta^{18}\text{O}$ vs salinity plot. Note January-June trend derived from sample points in Fig. 6.

each show linear correlations between the oxygen isotopic composition and total salinity, but in each case values on samples collected in September extrapolate to $\delta^{18}\text{O}$ values at zero salinity, which are notably more positive than those obtained from January to June (Figs. 7 and 8). During this same period the salinity values are higher, thus confirming the hypothesis that there is a smaller contribution to the mixtures from the surface waters, with very low salinity and relatively higher ^{18}O contents. This is particularly clear for the Berici area and Euganei-A families whose seasonal variations in salinity are about 10% for all the samples, with isotopic variations of 0.3%.

The chemical characteristics of the water from

some boreholes in the low elevation plain lying between the Berici and Euganei hills indicate that none of the samples in this group has a high chloride content. There are some waters whose chemical composition is identical to the Berici samples, whether they be sulfate or carbonate types, and to the Euganei-C samples. Therefore, these appear to be wells that draw, at shallow depths, from very shallow circulation waters characterized by the bicarbonate ion and by a varying percentage of the Ca and Na + K ions, depending on the amount of volcanic rock present.

The source region for the waters characterized by -11‰ $\delta^{18}\text{O}$ values must be aquifer recharge areas at much higher elevations, such as realized to the

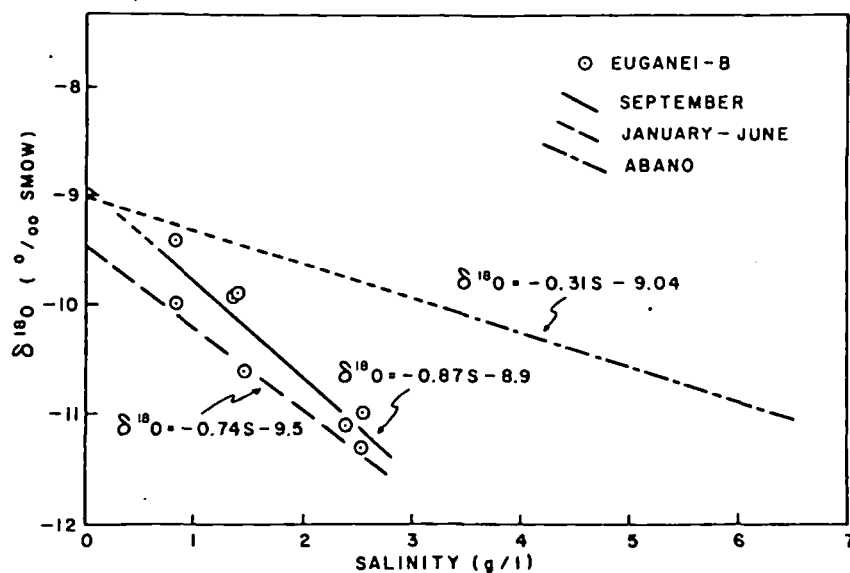


Fig. 8. Season variation of $\delta^{18}\text{O}$ values in Abano and Euganei-B samples represented in $\delta^{18}\text{O}$ vs salinity plot. Note January-June trend derived from sample in Fig. 6.

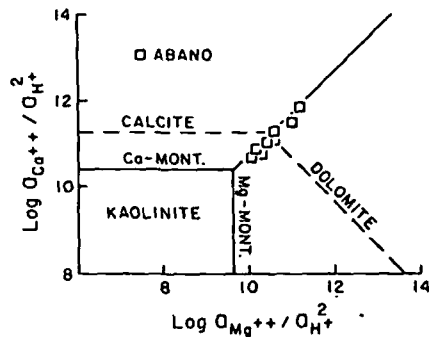


Fig. 9. Theoretical activity diagram for the system $\text{CaO-MgO-Al}_2\text{O}_3\text{-SiO}_2\text{-CO}_2\text{-H}_2\text{SO}_4\text{-HCl-H}_2\text{O}$ in the presence of an aqueous phase at 75°C, 1 bar, and unit activity of H_2O and of the mineral phases, $\log a_{\text{H}_2\text{SiO}_4} = -0.34$. Dashed lines represent saturation surfaces of calcite and dolomite at $P_{\text{CO}_2} = 10^{-2}$ bar. Compositions of samples from the Abano Terme are projected onto the equilibrium diagram.

north in the Alpine region. Isotopic gradients measured under similar climatic conditions in Tuscany are 0.22‰ per 100 m elevation change, Panichi, unpublished data; therefore, the 3.5‰ difference would require a 1.6 km elevation change. Isotopic values on local river waters, Adige (-17.4‰), Brenta (-10.0‰) and Piave (-9.9‰), at elevations of 1.6, 1.3 and 1.3 km, respectively, lend further support to this observation. Further evidence for a meteoric origin of these waters is provided by the δD and $\delta^{18}\text{O}$ values, determined on thermal and cold water springs in the Venice plain. BORTOLAMI *et al.* (1973) observed that the values for the cold springs range from $\delta\text{D} = -42$ to -53 ‰, and, furthermore, that the values are coincident with the meteoric water line, defined by $\delta\text{D} = 8\delta^{18}\text{O} + 15$.

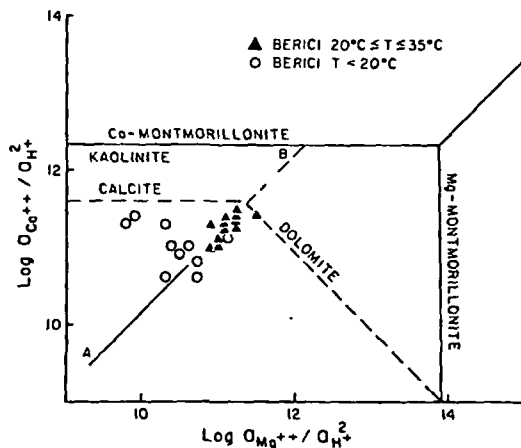


Fig. 10. Theoretical activity diagram for the system $\text{CaO-MgO-Al}_2\text{O}_3\text{-SiO}_2\text{-CO}_2\text{-H}_2\text{SO}_4\text{-HCl-H}_2\text{O}$ in the presence of an aqueous phase at 25°C, 1 bar, and unit activity of H_2O and of the mineral phases $\log a_{\text{H}_2\text{SiO}_4} = -4.0$. Dashed lines represent saturation surfaces of calcite and dolomite at $P_{\text{CO}_2} = 10^{-2}$ bar. Compositions of samples from the Berici area are projected onto diagrams in two groups.

Reaction between fluids and rocks along the flow path might also contribute to the isotopic shifts. These reactions might include exchange between waters and CO_2 gas at low temperatures, such as observed by FERRARA *et al.* (1965); however, Abano region waters are all low in CO_2 . Mineral water exchange reactions in subsurface environments would cause shifts toward more positive $\delta^{18}\text{O}$ values.

Representation of the sample compositions on mineral equilibrium diagrams depicts the relationship between the natural waters and the stability of common rock forming minerals, as well as reaction paths between the fluids and minerals (Figs. 9-11). Although aluminum was not determined on most of the samples, the solution compositions project on to kaolinite and montmorillonite stability fields, suggesting local equilibrium between solution and these types of phases. The nature of the reaction paths, implied by the composition of the waters in activity-activity coordinates and the minerals which were locally in equilibrium with the fluids, permits interpretation of the mineralogy of the subsurface environment through which the fluids have circulated.

Abano sample compositions plot along the Ca-montmorillonite-Mg-montmorillonite saturated solution phase boundary in close proximity to the calcite-dolomite saturation surface for $P_{\text{CO}_2} = 10^{-2}$ (Fig. 9), whereas the Berici and Euganei sample compositions (Figs. 10 and 11) plot entirely within the kaolinite-solution field and close to the calcite and dolomite saturation surface at $P_{\text{CO}_2} = 10^{-2}$, but clearly on the undersaturated side of this surface. The sample compositions generally plot along a line whose slope is equivalent to the cation charge ratios on the activity-activity diagrams. These types of compositional trends have been recognized in other groups of natural waters (NORTON, 1974; PAČES, 1972; GAR-

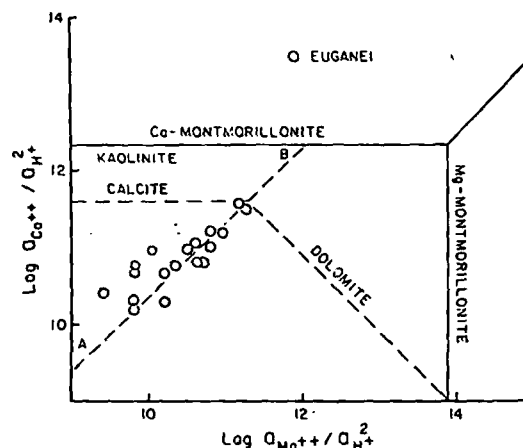


Fig. 11. Theoretical activity diagram for the system $\text{CaO-MgO-Al}_2\text{O}_3\text{-SiO}_2\text{-CO}_2\text{-H}_2\text{SO}_4\text{-HCl-H}_2\text{O}$ in the presence of an aqueous phase at 25°C, 1 bar, and unit activity of H_2O and of the mineral phases $\log a_{\text{H}_2\text{SiO}_4} = -4.0$. Dashed lines represent saturation surfaces of calcite and dolomite at $P_{\text{CO}_2} = 10^{-2}$ bar. Compositions Euganei samples are projected onto diagram.

RELS :
nume
reacti
HELG
irreve
in wh
of hys
towar
reacta
be lo
produ
fields
versit
ations
tion |
temp
gress
along
W
The
slight
T > 2
from

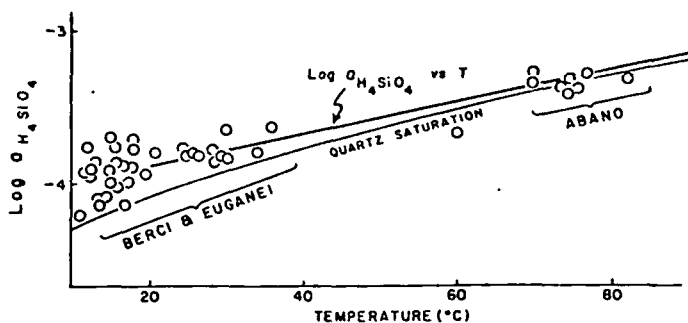


Fig. 12. Theoretical activity-temperature diagram for $\text{SiO}_2\text{-H}_2\text{O}$ system relating the saturation surface to the aqueous phase at $P = 1$ bar. $a_{\text{H}_4\text{SiO}_4}$ for all samples shows slight supersaturation with respect to quartz at low temperatures. $\text{Log } a_{\text{H}_4\text{SiO}_4}$ vs T line approximates values of $\text{log } a_{\text{H}_4\text{SiO}_4}$ in samples.

REL and MACKENZIE, 1967) and are consistent with numerical simulations of irreversible solution-rock reactions (HELGESON, 1968; HELGESON *et al.*, 1969; HELGESON, 1970). They are a consequence of overall irreversible reactions between minerals and solutions in which there is a simple consumption or production of hydrogen ions as the solution composition evolves toward equilibrium with the bulk mineralogy of the reactant mineral assemblage. Reaction paths tend to be locally discontinuous functions which trend from product phase stability fields toward the stability fields of the phases which are causing the overall irreversible reaction. Because of the temperature variations between the samples and with depth, the reaction paths are examined in composition as well as temperature coordinates. Variation in reaction progress with temperature is related to the distance, W , along reaction paths in activity-activity diagrams by

$$W = [(\text{log } a_{\text{Ca}^{2+}} / a_{\text{H}^+}^2)^2 + (\text{log } a_{\text{Mg}^{2+}} / a_{\text{H}^+}^2)^2]^{0.5}$$

The samples all appear to be saturated or only slightly supersaturated with quartz, collected at $T > 20^\circ\text{C}$, but samples collected at $T \leq 20^\circ\text{C}$ range from quartz saturation to supersaturation with chal-

cedony. This feature is not normally observed in low temperature waters. Samples from both Euganei and Berici groups might have been saturated with quartz at temperatures higher than collection temperatures, and the supersaturation effect would then be the result of cooling from the higher temperature. Based on this hypothesis, their predicted saturation temperatures range from 10 to 30°C higher than the temperatures at the collection point (Fig. 3) except for Abano samples, which are saturated with quartz at their collection temperatures. Subsequent diagrams are constructed using $\text{log } a_{\text{H}_4\text{SiO}_4} = f(T)$, as defined by the heavy line in Fig. 12.

The relationship between the stability fields for alumina silicate minerals and the solution compositions indicates that the Abano solutions are in equilibrium with montmorillonite and kaolinite (Fig. 13), whereas the other samples are equilibrated with only kaolinite; and a few Berici and Euganei samples suggest a temperature-concentration trend toward the montmorillonite-kaolinite phase boundaries, line A-B (Fig. 13). Temperatures that were predicted on the basis of the quartz saturation surface and $a_{\text{H}_4\text{SiO}_4}$ in the samples would shift all these samples closer

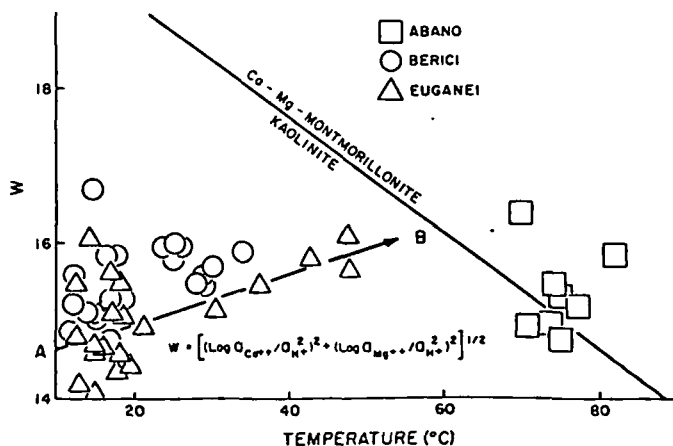


Fig. 13. Temperature-composition projection for the theoretical activity diagrams, Figs. 6-8, in the $\text{CaO-MgO-Al}_2\text{O}_3\text{-SiO}_2\text{-HCl-H}_2\text{SO}_4\text{-CO}_2\text{-H}_2\text{O}$ system at $\text{log } a_{\text{H}_4\text{SiO}_4} = -10^{-2} T - 4.2$, 1 bar, and unit activity of H_2O and the mineral phases. Compositions of samples were collected. Line A-B represents temperature reaction path suggested from data.

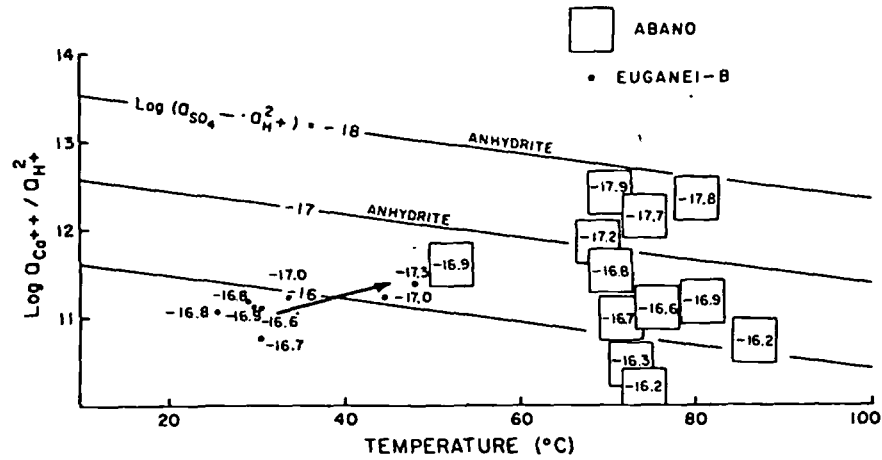


Fig. 14. Theoretical temperature-activity diagram for CaO-H₂SO₄-HCl-H₂O system at 1 bar in the presence of an aqueous phase at 1 bar and unit activity of H₂O and the mineral phases. The saturation surface for anhydrite at $\log(a_{\text{SO}_3^{2-}} \cdot a_{\text{H}^+}^2) = -18, -17$ and -16 is shown, and the composition of samples which are close to saturation with anhydrite are represented by squares with their respective $\log(a_{\text{SO}_3^{2-}} \cdot a_{\text{H}^+}^2)$ values. Euganei samples suggest reaction path depicted by arrow.

to the phase boundary. Seven of the ten Abano samples are saturated with respect to anhydrite, two are undersaturated with respect to anhydrite, and the other two are undersaturated with respect to anhydrite by only 15–20°C (Fig. 14). These same two samples are also supersaturated, by about 10°C, with respect to quartz. The Euganei samples, with temperatures in the 30–50°C range, are slightly undersaturated, but their distribution on the diagram is suggestive of a trend toward the anhydrite saturation surface. All the Berici and Euganei sample compositions have $\log(a_{\text{SO}_3^{2-}} \cdot a_{\text{H}^+}^2)$ values one to two

log units less than the value necessary for anhydrite saturation at the respective temperatures and $\log a_{\text{Ca}^{2+}} / a_{\text{H}^+}^2$ values. Only a few samples from each of the groups is close to or saturated with respect to calcite and dolomite (Fig. 15) because of the relatively low P_{CO_2} values in the majority of the samples. The reaction-paths in composition and temperature coordinates all suggest many of the solutions were in equilibrium with anhydrite, calcite or dolomite, at slightly higher temperatures, and that these phases occur along their flow paths 'upstream' from the collection point.

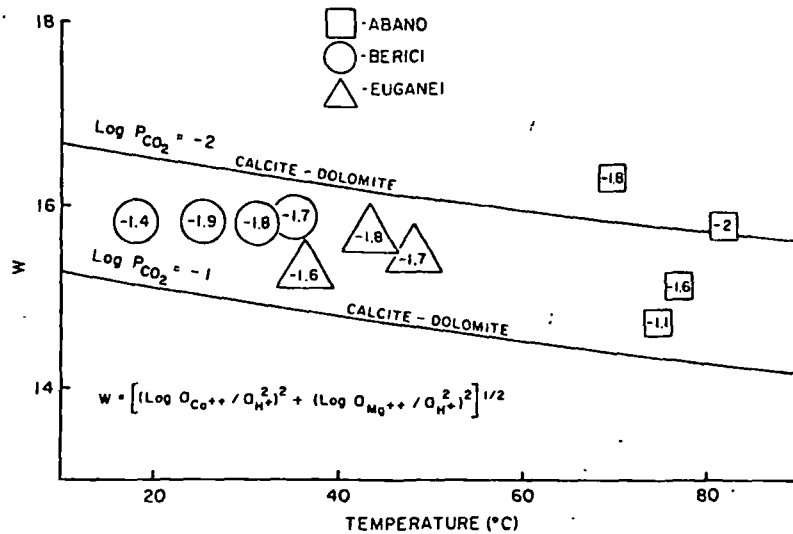


Fig. 15. Temperature-composition projection for the theoretical activity diagrams. Figs. 6–8, in the CaO-MgO-Al₂O₃-SiO₂-HCl-H₂SO₄-CO₂-H₂O system at $\log a_{\text{H}_2\text{SiO}_4} = -10^{-2} T - 4.2$, 1 bar, and unit activity of H₂O and the mineral phases. Compositions of samples which are saturated or nearly saturated with respect to calcite and dolomite are represented by respective paths. The $\log P_{\text{CO}_2}$ value for each sample appears in the point for comparison with the saturation surfaces for calcite and dolomite at $\log P_{\text{CO}_2} = -2$ and -1 . Other samples are at least 1 log unit undersaturated in their activity products and are not represented on this projection.

CONCLUSIONS

The combined isotopic and major component data suggest the waters in the general region have been derived from both local meteoric and groundwater sources. Systematic shifts in compositions of these waters can clearly be attributed to fluid-rock reactions along pathlines at depth and to mixing with waters in shallow and deep aquifers. Major element compositions of the waters indicate the mineralogic composition of the subsurface aquifers through which the waters flowed, and isotopic compositions indicate the ultimate sources of the water.

Low $\delta^{18}\text{O}$, -11‰ values of the Abano and some of the Berici and Euganei-A samples require that these waters were ultimately derived from meteoric waters at ~ 1.5 km elevations. These elevations are realized in the pre-Alps, northwest of the region, and, therefore, are probably the source region for these waters (Fig. 16, large circle Ab). In the event that isotope values of deeply circulating fluid were affected by mineral-fluid exchange reaction, these waters would have had sources at even higher elevations. Since exchange reactions between fluids and the subsurface rocks would tend to shift the oxygen values to more positive than -11‰ local sources, in either the Berici or Euganei hills, for the samples with intermediate $\delta^{18}\text{O}$ values, ca -9.5 to -8‰ , and in the intervening valley for samples with the lowest $\delta^{18}\text{O}$ values, -7.5‰ , are also possible (Fig. 16).

Fluid pathlines from the source regions to the spring or well locations are constrained by the mineral-fluid reaction paths and the mineral-fluid equilibrium relationships depicted in Figs. 6-12. These relationships

require that certain mineral assemblages were encountered along the pathlines as the water circulated from the source regions to the sample site. Samples from the Abano thermal wells are saturated with respect to anhydrite and Ca-Mg-montmorillonite and are supersaturated with respect to calcite and dolomite at temperatures between 50 and 90°C. This feature suggests that at some point along their circulation paths aquifers containing anhydrite, clay minerals, calcite, and dolomite were encountered (Fig. 16). Rocks of this composition, Permian evaporites which extend northward into the source regions of the meteoric water, occur at 2 km depths below the region. The fact that the Abano waters are supersaturated with the carbonates probably reflects internal solution disequilibrium as a result of circulation from low P_{CO_2} environments below the surface to higher P_{CO_2} surface environments. Samples from Euganei-B and Berici springs are saturated with respect to calcite and dolomite, but are undersaturated with anhydrite. These Berici and Euganei-B waters are also relatively concentrated in SO_4 , Cl, Ca and Mg. These characteristics require that flow paths through limestones and dolomites contain pore fluids relatively concentrated in SO_4 and Cl, or that these latter components result from mixing with Abano type waters. The Mesozoic stratigraphic section beneath the region consists of a 1.5 km thick sequence of limestones and dolomites, which accounts for these characteristics. The Berici and Euganei-B samples, which tend to have lower SO_4 and Cl but high Ca, probably flowed through the Tertiary marine limestones and volcanics that comprise the Berici and Euganei hills (Fig. 16). Euganei-C and local groundwaters tend to be satu-

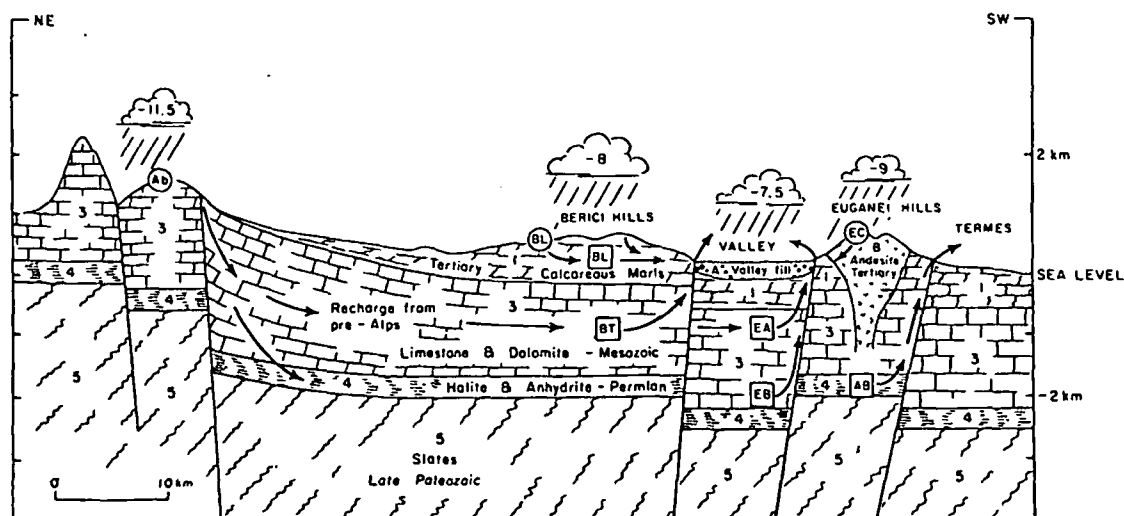


Fig. 16. Schematic geologic cross-section of Abano region from NE to SW relating geologic units and fluid circulation paths deduced from this study. Source regions of various sample groups are indicated by large circles with group names: Abano = Ab, Euganei-C = EC, and Berici low temperature samples = BL. Pathlines of fluids are depicted by lines with arrows and large squares with sample group letters as above, plus Euganei-A = EA, Euganei-B = EB, Berici high temperature = BT, and Berici low temperature samples = BL. Note subsurface mixing, particularly of Berici and Euganei-A and Euganei-B samples.

rated with kaolinite, montmorillonite and quartz, but are undersaturated with respect to calcite, dolomite and anhydrite, suggesting flow paths through the alluvium or volcanic rocks or shale beds.

The circulation paths for waters which occur in the Abano area are from sources in the pre-Alps, at an elevation of ~1.5 km, as evidenced by the ^{18}O data. This meteoric water then circulates into subsurface aquifers which contain anhydrite, halite, calcite, and dolomite. The Permian evaporites and Mesozoic carbonates near the basement contact (Fig. 16) are the aquifers through which these fluids flowed. The fluid paths through the evaporites intersect the surface, primarily in the termes, whereas those paths through the Mesozoic carbonates form springs near the base of the Berici and Euganei hills. Mixing of shallow groundwaters with those from the deeper aquifers is clearly indicated by the oxygen isotope values which vary as a function of salinity with the season. The dilution effects between local meteoric waters and groundwater appear less for the more saline (e.g. deeper) groundwaters, further substantiating the predicted fluid pathline. The time duration of fluid circulation from the source regions in the Alps is unknown except that tritium data on two Abano samples require that they are greater than 20 yr old.

The anomalous thermal energy content of the Abano waters apparently results from a forced convection system caused by groundwater recharge at high elevations into confined aquifers. The circulating fluid transports thermal energy from 1 to 2 km depth below the Abano region upward, along faults which transect the confined aquifers, to the surface. A moderate geothermal gradient of 25°C/km and exothermic reactions between anhydrite and meteoric waters are sufficient to account for the 75°C temperatures of the terme waters. The local volcanic rocks are apparently not the source of thermal energy in these waters. Because of their Tertiary age, they have long ago cooled to ambient conditions.

Acknowledgements—This research was supported by funds from NSF-EAR74-03515-AO1 to Norton. We thank the Istituto Internazionale per la Ricerca Geotermica, Pisa for sponsoring the original study and making the data available for analyses, and we express our thanks to the Istituto staff for their assistance in this study. We are also grateful to R. KNAPP, J. KNIGHT and R. CAPUANO for

assisting with the calculations, and to LYNN MCLEAN for editorial improvements and numerous rough drafts of the manuscript.

REFERENCES

- BORTOLAMI G., FONTES J. C. and PANICHI C. (1973) Isotopes du milieu et circulations dans les aquifères du sous-sol vénétien. *Earth Planet. Sci. Lett.* **19**, 154-167.
- FERRARA G. C., GONFIANTINI R. and PANICHI C. (1965) La composizione isotopica del vapore di alcuni soffioni di larderello e dell'acqua di alcune sorgenti e mofete delle Toscana. *Soc. Tosc. Sc. Nat. Serie A* **72**, 1-19.
- GARRELS R. M. and MACKENZIE F. T. (1967) Origin of the chemical composition of some springs and lakes. In *Equilibrium Concepts in Natural Water Systems, Advances in Chemistry Series* **67**, pp. 222-242. Am. Chem. Soc.
- HELGESON H. C. (1969) Thermodynamics of hydrothermal systems at elevated temperatures and pressures. *Am. J. Sci.* **267**, 729-804.
- HELGESON H. C., GARRELS R. M. and MACKENZIE F. T. (1969) Evaluation of irreversible reactions in geochemical processes involving minerals and aqueous solutions—II. Applications. *Geochim. Cosmochim. Acta* **33**, 455-481.
- HELGESON H. C. and JAMES W. R. (1968) Activity coefficients in concentrated electrolyte solutions at elevated temperatures (abs.). Abstr. of Papers, 155th Natl. Mtg., Am. Chem. Soc., April, 1968, San Francisco, Cal., S-130.
- HELGESON H. C., BROWN T. A., NIGRINI, A. and JONES T. A. (1970) Calculation of mass transfer in geochemical processes involving aqueous solutions. *Geochim. Cosmochim. Acta* **34**, 569-592.
- KNIGHT J. (1976) DIST—computer program to distribute solution composition. Dept. of Geosciences, Univ. Arizona, Tucson.
- NORTON D. (1974) Chemical mass transfer in the Rio Tanama system, west-central Puerto Rico. *Geochim. Cosmochim. Acta* **38**, 267-277.
- NORTON D. (1978) Source regions, source lines and pathlines for fluids in hydrothermal systems related to cooling plutons. *Econ. Geol.* **73**, 21-28.
- PAÇES T. (1972) Chemical characteristics and equilibration in natural water-felsic rock-CO₂ systems: *Geochim. Cosmochim. Acta* **36**, 217-240.
- PANICHI C., TONGIORI E., BALDI P., FERRARA G. C., CHEZZI G., MARCHETTI M. (1967) Geochimica delle acque termali euganeo-beriche. In *Il Sistema Idrotermale Euganeo-berico E La Geologia Dei Colli*. Mem. Ist. Geol., Mineral., Università de Padova, Vol. 30, pp. 113-141.
- PICCOLI G., DALPRA A., SEDEA R., BELLATI R., DI LALLO E., CATALDI R., BALDI P. and FERRARA G. C. (1973) Contributo alla conoscenza del sistema idrotermale euganeo-berico. *Atti Acc. Naz. Lincei, Memorie Classe Sc. Fis. Mat. Nat.*, VIII, Vol. 11, pp. 103-133.

~~O. Christensen~~ 6/14

~~W. St. H. ...~~

~~02/120~~
~~W. St. H. ...~~

AREA
IT

APPLICATION OF ELECTRICAL PROSPECTING METHODS TO
TECTONICS IN THE SEARCH FOR NATURAL STEAM AT
LARDERELLO, ITALY*

J. J. BREUSSE† AND J. P. MATHIEZ†

ABSTRACT

In this paper are examined briefly the conditions which seem necessary for the presence of natural steam exploited industrially. These conditions are fulfilled in the Larderello field. The geological features of the soffioni region are summarized.

The use of the well known technique of electrical sounding were aimed at determining the structural features, outlining the horsts, and tracing the main faults. Later on reconnaissance wells were located on the horsts near these major thrusts.

The electrical characteristics of the various geological horizons are illustrated by some examples of typical electrical soundings. The results of this tectonical investigation are summarized in a contour map of the productive layer and this was the first structural map of the great horst Larderello-Castelnuovo.

An interesting application of electrical prospecting is also mentioned: the determination of warm zones corresponding to a local lowering of the resistivity of the overburden through the rise of temperature caused by the heat given out by steam. This is a striking example of direct prospecting in case of natural steam. A resistivity map of the lower layers of the overburden shows clearly this phenomenon and to our knowledge this is one of its first practical utilizations.

Finally a chart of the first wells drilled on the results of the electrical survey brings forth an estimation of its accuracy.

A zone of boraciferous soffioni covers an area of approximately 200 sq km in the upper Maremma in Tuscany, Italy from Volterra in the north to the Massa Maritima mining center in the south. The largest emanations are grouped around the following eight places: Larderello, Castelnuovo Val di Cecina, Sasso Pisano, Monterotondo, Lago, Lagoni Rossi, Serrazzano, and Travade.

In 1818, the Larderello Company created a veritable mining industry by first working natural soffioni, then artificial soffioni obtained from wells and shallow drillings. Steam was first utilized in 1913 as a source of thermal energy and seven electric power houses of an overall installed power of 258,000 kilowatts now consume 2,900 tons of natural steam per hour, the temperature of which varies according to the borings from 140° to 290° C and the pressure from 3 to 6 atmospheres under production conditions.

The topography of the area is quite rough with elevations varying from 200 to 1,000 m. From the geological point of view, the basement consists of several horsts of autochthonous Primary and Secondary formations. They are covered by an allochthonous overburden of "scagliose" clays which include formations from the upper Cretaceous to the Eocene.

We shall limit ourselves to the Larderello-Castelnuovo area, which alone is the

* Read at the Algiers Geological Congress, September 1951. Manuscript received by the Editor August 12, 1954.

† Compagnie Générale de Géophysique, Paris, France.

object of this paper. The surface elevations in that zone range from 350 m in the Possera valley to 650 m in the hills on each side of the river.

The Permian which is very thick is also the oldest horizon. It is formed chiefly of compact schists and of quartziferous sandstones. They are usually topped by very cavernous, fissured, and brecciated limestones of Rhaetic age, which constitute an excellent storing rock. This formation was submitted to extensive erosion by atmospheric and mechanical agents and its thickness does not exceed 150 to 200 meters. In some places it has completely disappeared leaving the Permian directly in contact with the overburden on some of the higher parts of the structures.

In the area situated southwest of Castelnuovo, there are found Macigno Oligocene sandstone strata with alternations of clay shales resting on the Rhaetic.

The overburden consists chiefly of shaly clays sometimes encasing large masses of limestone (Alberese) and ophitic rocks. This flowage mass constitutes a splendid impervious cover.

From the tectonical point of view the structural examination of Primary and Mesozoic outcrops and mining operations had shown the existence of numerous fractures which appeared during the Miocene. The main direction is that of the Apennine thrusts, that is, northwest-southeast with accompanying faults which are more or less perpendicular to that direction. Consequently, the tectonic style of the basement is a horsts and grabens mosaic and the very special nature of the sedimentary allochthonous overburden does not allow the reconstitution of its elements by a geological study of the surface.

It was obvious that the fractures provide natural active channels through which steam rises from depth to be stored in the permeable layers (Rhaetic calcareous formations, Permian quartziferous sandstone, and even some Eocene calcareous masses). These feeder faults were formerly not well known and were difficult to locate, so that in practice borings were carried out rather empirically according to the results of drillings in the vicinity.

At that stage, in 1950, electrical methods of prospecting were introduced in an endeavor to clarify tectonics and establish a more rational drilling program.

The problem was analyzed and simplified and the following working hypothesis was presented: determination of the main faults, search for horsts, borings on the horsts and preferably in the vicinity of the main faults.

A large electrical sounding, involving an output line 21 km (13 miles) long, was carried out in 1949 between Larderello and Serrazzano to determine approximately the depth of the magmatic basin which was the supposed generator of steam. The problem was not completely solved but measurements indicated that it was possible to rely on excellent electric differentiation between the overburden and the basement.

Scagliose clays are conductive (3 to 20 ohms m) in comparison with Rhaetic limestones and Permian schists, the resistivity of which is greater than 100 ohms m. Stratigraphic conditions are thus favorable and this compensates to a certain extent for the important perturbations caused by the hilly topography and the many overburden heterogeneities. A fairly considerable difficulty is caused by the blunting of

the substratum by erosion, mentioned earlier, which causes the partial or complete disappearance of the steps caused by fractures on the top of the resistive substratum. The result is a certain lack of precision in the outline of the faults in relation to the subsurface morphology and the relief of the basement.

On the other hand, electrical methods of prospecting will not distinguish in the substratum between the Rhaetian and the Permian and will therefore be unable to determine the areas, a priori less favorable, where scagliose clays are in direct contact with schists.

The technique used was the electrical sounding (Schlumberger quadripole) with output lines reaching up to 1,000 to 3,000 m depending on the thickness of the overburden. Some typical electrical soundings (E.S.) are given in Figure 1. Geophysical estimations and results of boring carried out subsequently are shown under each diagram.

A detailed reconnaissance of the Larderello-Castelnuovo region was carried out in this manner. The study involved nearly 300 E.S. spread over an area of approximately 1,200 hectares, that is a station per 4 hectares (10 acres).


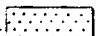


The results are shown on a contour map of the resistant substratum (equidistance 50 m) in Figure 2. The map shows the large horst which extends over a length of 4 km (2.5 miles) from Castelnuovo to Larderello. The main fractures, which border it to the east and to the west, were traced together with a large transversal thrust in the Larderello zone proper. A number of secondary fractures were certainly missed by electrical prospecting, given the adopted density of stations. It is permissible to accord to some of them a rather small part in the problem of steam production.

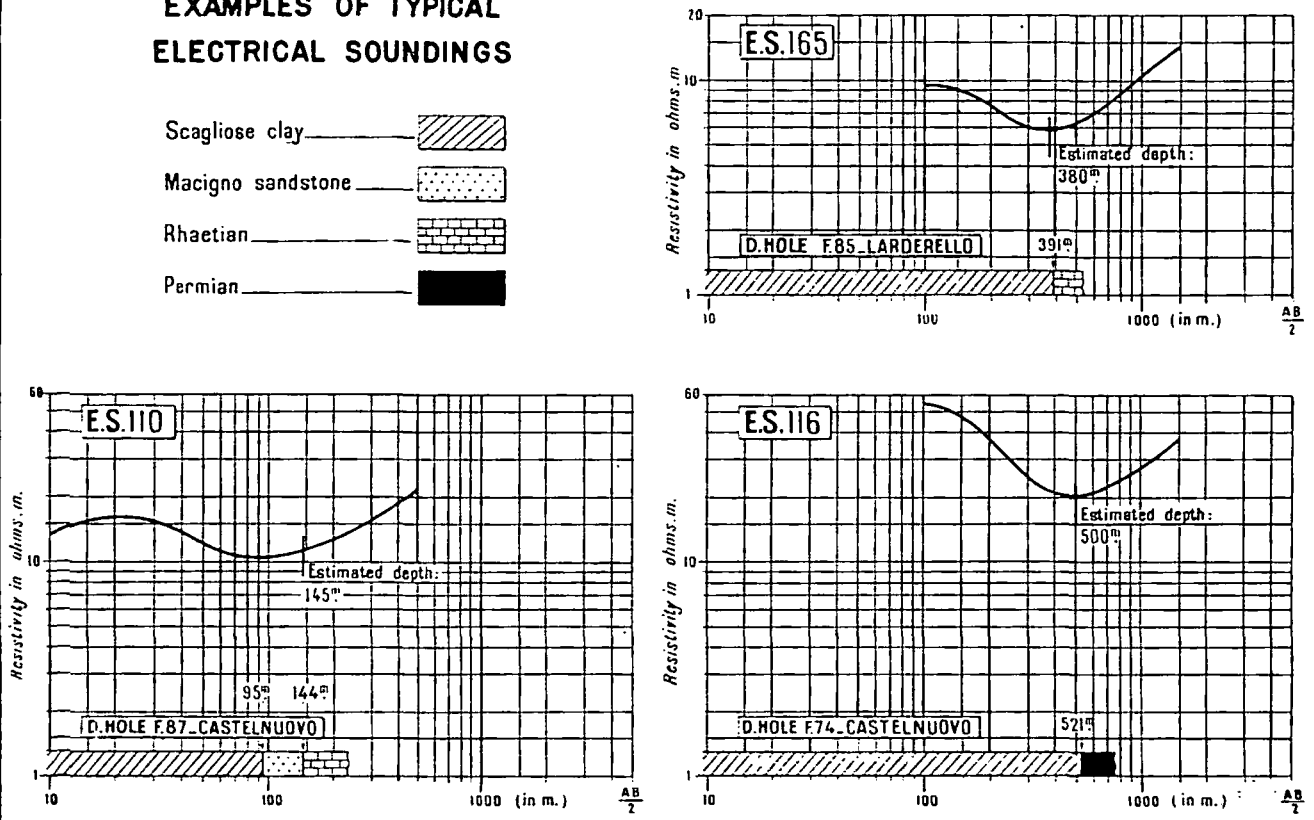
Before presenting verifications and results obtained from this geophysical study, it is advisable to indicate the important phenomenon clearly shown by this survey. It is the investigation of warm zones by the lower resistivity of the bottom layers of the overburden under the action of temperature. This phenomenon which is well known in theory had never been given, to our knowledge, a practical application on the field. In Larderello it was possible to conceive that the lower part of the overburden in contact with the storing rocks was heating up by conduction, therefore causing a lowering of its resistivity and creating locally conductive zones in the general map of the true resistivity of the lower layers of the overburden (Fig. 3).

Comparison with the preceding map is rather striking. It shows that equiresistivity curves outline the general shape of the structure, the 5 ohms m curve roughly enveloping the high productivity area. Naturally, this map should not be considered too literally as resistivity is equally affected by the lithologic variations of the scagliose clays, which may have an action just as important as the one caused by rise in temperature. However, the fact that the productive horst of Larderello-Castelnuovo is clearly indicated on the equiresistivity map of the lower layers of the overburden, in spite of its chaotic conditions, constitutes an encouraging element. It gives some hope that electrical methods of prospecting may be used in the search for hot zones.

FIG. 1

EXAMPLES OF TYPICAL ELECTRICAL SOUNDINGS

- Scagliose clay 
- Macigno sandstone 
- Rhaetian 
- Permian 



N° 17.642 P

FIG. 1

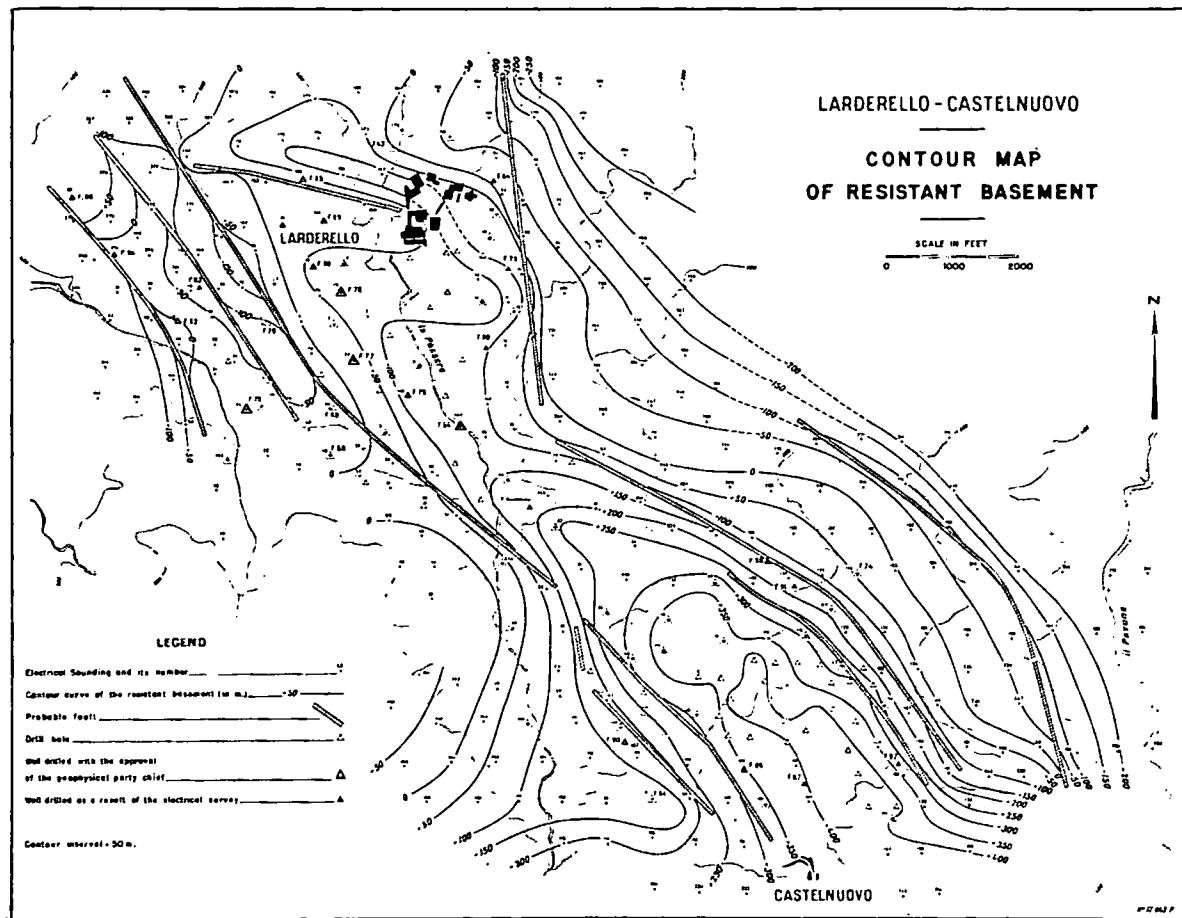


FIG. 2

We shall conclude with a chart showing the results of verifications by borings and steam production obtained over a period slightly less than two years. Among the wells one must differentiate between those located before the arrival of the geophysical party and approved by the party chief later on before their execution, and those, more numerous, which were located as a result of electrical prospecting only.

CHART SHOWING RESULTS OBTAINED

No. of E.S.	No. of well	Estimated depth to basement (in metres)	True depth	Production in tons/hour
<i>A—Larderello</i>				
147	F.56*	300	312	70
25	F.75*	515	517	130
70	F.76*	370	370	130
77	F.77†	455	427	94
149	F.78†	390	340	25
14 (at 80 m)	F.79†	380	350	23
16	F.80†	360	353	42
18	F.82†	440	453	303
20	F.83†	450	—	drilling stopped
93 (at 90 m)	F.84†	375	454	30
165	F.85†	380	391	202
10	F.88†	380	307	50
160	F.89†	410	—	drilling stopped
<i>B—Castelnuovo</i>				
109	F.86†	170	228	10
102-110	F.87†	145	144	0
367	F.90†	340	418	0
121	F.91†	430	430	62
188-195 (at 50 m)	F.92†	145	160	in course of drilling

* Well drilled with the approval of the geophysical party chief.

† Well drilled as a result of the electrical survey.

It should be noted that basement depths were checked with an error of less than 5 percent computed over 14 wells. This excellent accuracy is the result of numerous calibration measurements which were carried out on the old borings. In the case of new areas which have not yet been explored, the error should assume the normal value reached in the course of such electrical prospecting, that is 10 to 15 percent.

It should also be noted that we have left out of the average error calculations borings F.86 and F.90, situated southwest from Castelnuovo. Determination of the thickness of the overburden was much less accurate in their particular cases. The cause lies in the presence of thick Oligocene limestone (Macigno), the lower electrically resistant part of which cannot be distinguished from the underlying substratum. Under these conditions, the F.90 boring which was supposed to be car-

ried out at the limit of the horst was unfortunately situated west of the bordering fault, in the graben, and remained sterile. It is located the same way as borings F.43, F.49, F.64, F.70 and F.74, which are drilled over grabens and whose productivity is nil, or very small.

We may say, in conclusion, that electrical prospecting has greatly advanced the technical problem of the search for steam. As studies and borings progress, the working hypothesis justifies itself increasingly.

Prospecting is at present responsible for a production of 2,300 tons of steam per hour. Let us mention at Larderello a "soffionissimo" of 292 tons/hour at the F.85 boring, tonnage which had not been equalled to date, at Castelnuovo boring F.91, the largest producer, with 62 tons/hour and, finally, on a new structure found west of Larderello, boring F.82, found a second "soffionissimo" yielding 303 tons/hour.

Mineral Chemistry and Petrogenetic Aspects of the Vico Lavas, Roman Volcanic Region, Italy

A. Cundari

School of Geology, University of Melbourne, Parkville, Victoria 3052, Australia

Abstract. A detailed study of the phase chemistry of selected lavas from Vico shows that the "excess silica" in leucite is a significant and widespread crystal-chemical characteristic which may be interpreted in terms of an extended solubility of KAlSi_3O_8 and/or differential loss of potassium from the leucite structure. Plagioclase geothermometer data suggest increasing plagioclase control in the differentiation with decreasing $\text{Mg}/\text{Mg}+\text{Fe}^{2+}$ ratios for the bulk rocks. The pyroxene compositions show moderate amounts of ferri-Tschermak's and Ca-Tschermak's molecules, probably controlled by temperature and compositional variations in the cooling liquids. Both microphenocrystal and late-crystallizing micas correspond to phlogopite compositions throughout the suite.

The phase chemistry is discussed in relation to the differentiation of the suite and current petrogenetic models.

Introduction

The object of this investigation is primarily to provide complementary mineralogical data to the petrochemistry of the Vico leucite-bearing lavas, occurring in the northern part of the Roman volcanic region (cf. Mattias and Ventriglia, 1970), and to attempt a correlation between the phase chemistry and the differentiation of the host rocks.

The compositional variation of the Vico lava suite extends from tephritic leucitite through phonolitic tephrite and tephritic phonolite variants to leucite-trachyte compositions (Cundari and Mattias, 1974). The chronological succession of the lavas indicates that the chemical evolution of the magma was recurrent throughout its eruptive history, the most recent lavas virtually retracing the compositional variation of the earlier ones.

Bulk-rock analyses and estimated modal compositions are provided by Cundari and Mattias (1974, Table 1). The specimens selected for detailed mineral chemistry represent leucite-trachytes (LTR-156, LTR-29 and LTR-180), tephritic leucite-phonolites (TLP-18 and TLP-191) and phonolitic leucite-tephrites (PLT-176) along the predominant compositional "spread" of the Vico lava suite, which compounds 72.6% of the total variance; as deduced by a principal component analysis (Cundari and Mattias, 1974).

UNIVERSITY OF UTAH
RESEARCH INSTITUTE
EARTH SCIENCE LAB.

Table 1. Chemical analyses and structural formulae of leucite and alkali feldspar

wt. %	Leucite							
	(g.m.) 18/1	(pxl.rim) 18/2	(pxl.core) 18/3	(pxl.core) 18/9	(g.m.) 29/4	(pxl.core) 29/7	(pxl.core) 156/8	(pxl.core) 176/3
SiO ₂	56.2	56.2	56.8	56.6	56.9	56.9	56.4	55.9
TiO ₂	0.04	0.04	*	0.04	0.07	0.05	0.03	0.04
Al ₂ O ₃	23.8	24.0	23.8	23.2	22.5	22.8	23.8	24.1
Fe ₂ O ₃ ^a	0.36	0.36	0.42	0.23	0.31	0.22	0.30	0.31
MnO	*	*	*	*	0.04	*	*	*
MgO	*	*	*	*	*	*	*	*
CaO	*	*	*	*	*	*	*	*
Na ₂ O	0.37	0.43	0.38	0.43	0.17	0.18	0.31	0.42
K ₂ O	19.2	19.2	18.8	19.7	20.0	20.0	19.0	18.6
Σ	99.97	100.23	100.20	100.20	99.99	100.15	99.84	99.37
Cation Content: (6 oxygen atoms).								
Si	2.012	2.008	2.022	2.027	2.044	2.040	2.018	2.007
Al	1.005	1.011	0.999	0.979	0.953	0.963	1.004	1.020
Fe ³⁺	0.010	0.010	0.011	0.006	0.008	0.006	0.008	0.008
Mn	—	—	—	—	0.001	—	—	—
Ti	0.001	0.001	—	0.001	0.002	0.001	0.001	0.001
Mg	—	—	—	—	—	—	—	—
Ca	—	—	—	—	—	—	—	—
Na	0.026	0.030	0.026	0.030	0.012	0.013	0.022	0.029
K	0.877	0.875	0.854	0.900	0.917	0.915	0.867	0.852
XYZ	3.93	3.94	3.91	3.94	3.94	3.94	3.92	3.92
Y	1.02	1.02	1.01	0.99	0.96	0.97	1.01	1.03
X	0.90	0.91	0.88	0.93	0.93	0.93	0.89	0.88
Qz	31.9	31.7	33.1	31.0	31.4	31.3	32.6	32.8
wt. % Ne	1.7	2.0	1.8	2.0	0.8	0.8	1.5	2.0
Ks	66.4	66.3	65.1	67.0	67.8	67.8	65.9	65.2

* Below limit of detection (TiO₂, MnO, MgO, CaO=0.02% wt., respectively).

Y=Σ(Al+Fe³⁺+Mn+Ti+Mg+Ca).

X=Σ(Na+K).

^a Total iron as Fe₂O₃.

Analyst: A.K. Ferguson.

Analytical Methods

The chemical analyses were obtained from polished-thin sections of the analyzed bulk rocks by means of an automated JXA-5A electron microprobe operated at 15 Kv (accelerating voltage) and 0.02–0.03 μA (specimen current), the latter suitably reduced to minimize volatilization during the analysis of alkali-rich phases. Chemical standards were selected from natural mineral sets to approach the composition of the analyzed phases. The results were corrected according to the method of Mason *et al.* (1969) and are considered accurate to within 2–3 percent for major elements and better than 9 percent for minor elements.

Table 1 (continued)

(g.m.) 176/4	(pxl. core) 180/5
56.0	55.8
0.09	*
24.7	25.0
0.37	0.43
*	*
*	*
0.05	*
0.35	0.43
19.0	18.8
100.56	100.46
1.991	1.985
1.035	1.048
0.010	0.012
—	—
0.002	—
—	—
0.002	—
0.024	0.030
0.862	0.853
3.93	3.93
1.05	1.06
0.89	0.88
32.1	32.2
1.7	2.1
66.2	65.7

Leucite and Alkali

Leucite is ubiquitous, within and between (e.g. LTR-185A). The absence of resorptive leucites are seldom and are opaque and

Table 1. (continued)

						Alkali feldspar		
(g.m.)	(pxl. core)	(pxl. rim)	(pxl. core)	(g.m.)	(pxl. core)	(g.m.)	(pxl.)	
176/4	180/5	180/8	180/9	191/1	191/4	156/2	156/9	
56.0	55.8	56.5	55.1	59.8	55.2	65.0	65.0	
0.09	*	0.04	0.04	0.05	0.03	0.12	0.06	
24.7	25.0	25.1	24.1	24.4	24.1	19.5	19.8	
0.37	0.43	0.36	1.04	0.37	0.37	0.52	0.23	
*	*	*	*	*	0.04	*	*	
*	*	*	*	*	*	*	*	
0.05	*	0.03	*	*	*	0.79	0.78	
0.35	0.43	0.31	0.62	0.57	0.44	3.3	2.3	
19.0	18.8	17.7	19.4	15.0	19.0	11.0	12.0	
100.56	100.46	100.04	100.30	100.19	99.18	100.23	100.17	
						(32 oxygen atoms)		
1.991	1.985	2.000	1.979	2.070	1.994	11.797	11.813	
1.035	1.048	1.048	1.021	0.995	1.026	4.172	4.242	
0.010	0.012	0.010	0.028	0.010	0.010	0.071	0.031	
—	—	—	—	—	0.001	—	—	
0.002	—	0.001	0.001	0.001	0.001	0.016	0.008	
0.002	—	0.001	—	—	—	—	—	
0.024	0.030	0.021	0.043	0.038	0.031	0.154	0.152	
0.862	0.853	0.800	0.889	0.662	0.876	1.161	0.810	
3.93	3.93	3.88	3.96	3.78	3.94	2.548	2.783	
1.05	1.06	1.06	1.05	1.01	1.04	Z	16.06	16.09
0.89	0.88	0.82	0.93	0.70	0.91	X	3.86	3.75
32.1	32.2	35.3	30.0	42.7	31.4	Or	67.1	75.3
1.7	2.1	1.5	2.9	2.8	2.1	wt.% Ab	28.8	20.6
66.2	65.7	63.2	67.1	54.4	66.5	An	4.1	4.1

$$Z = \Sigma(\text{Si} + \text{Al} + \text{Fe}^{3+} + \text{Ti})$$

$$X = \Sigma(\text{Na} + \text{K} + \text{Ca})$$

Leucite and Alkali Feldspar

Leucite is ubiquitous in the Vico lava suite and shows variable crystal development, within and between flows, from microcrystalline, typical of leucite trachytes (e.g. LTR-185A, LTR-192, LTR-156), to $1\frac{1}{2}$ cm across (e.g. TLP-185B). Evidence of resorption, particularly in the larger crystals, is not infrequent. Vico leucites are seldom translucent with vitreous luster. More commonly, the crystals are opaque and pseudomorphed to various degrees by mixtures of analcime

i feldspar

core)	(pxl. core)	(pxl. core)
156/8	176/3	
56.4	55.9	
0.03	0.04	
23.8	24.1	
0.30	0.31	
*	*	
*	*	
*	*	
0.31	0.42	
19.0	18.6	
99.84	99.37	

2.018	2.007
1.004	1.020
0.008	0.008
0.001	0.001
0.022	0.029
0.867	0.852
3.92	3.92

1.01	1.03
0.89	0.88
32.6	32.8
1.5	2.0
65.9	65.2

(ely).

analyzed bulk rocks by accelerating voltage) and volatilization during the mineral sets to approach according to the method of for major elements and

REPRODUCED FROM THE ORIGINAL MANUSCRIPT

and/or clay minerals (Cundari and Graziani, 1964). Microscopic observation shows glassy, presumed fresh leucite, as colourless eu-subhedra with complex twinning and weak positive birefringence, while altered crystals are cloudy, fractured to granulated and show the development of a brownish pseudomorph with low, speckly birefringence.

Phenocrystal (pxl.) and groundmass (g.m.) analyses of glassy leucites are given in Table 1 with relative structural formulae and recalculated compositions in the system $\text{NaAlSi}_3\text{O}_8\text{—KAlSi}_3\text{O}_8\text{—SiO}_2$. The reduction of the analyses shows a systematic cation deficiency, generally less than 0.07 from the stoichiometric value of 4.00, but reaching deficiencies of 0.12 and 0.22 in 180/8 and 191/1, respectively. In particular, the X-groups are 7–12% lower than the expected value of 1.00 and as low as 18% and 36% in 180/8 and 191/1, respectively. Except for the latter composition, the potash contents fall within the range 17.6–20.0% K_2O (mean (7) = 18.3% K_2O) calculated from the K determinations (flame photometry) reported by Barbieri *et al.* (1968, Table 2) for Vico leucites. The Na/K ratio varies significantly (0.013–0.057), even for leucites in the same rock specimen. The phenocrystal cores generally show higher Na/K ratios than the coexisting rim and groundmass compositions, in agreement with the data reported by Carmichael *et al.* (1974, Figs. 5–13) for leucites in similar lava types from the Roman Region. However, the compositions of the Vico leucites differ from the latter analogues in their large "excess silica" over the experimentally determined leucite solid solution in the system $\text{NaAlSi}_3\text{O}_8\text{—KAlSi}_3\text{O}_8\text{—SiO}_2\text{—H}_2\text{O}$ (Fudali, 1963). This is illustrated in Fig. 1 by the resulting trend toward the alkali feldspar join, the extent of $\text{NaAlSi}_3\text{O}_8$ substitution in KAlSi_3O_8 solid solutions being relatively minor (1.1–5.0% wt. $\text{NaAlSi}_3\text{O}_8$). On the other hand, the $\text{NaAlSi}_3\text{O}_8$ solid solubility in coexisting phenocrystal and groundmass alkali feldspars (156/9 and 156/2, respectively; Table 1) is comparatively high (20.6–28.8% wt. $\text{NaAlSi}_3\text{O}_8$) and, contrary to leucite, increases for late-crystallizing compositions.

The "silica excess" in Vico leucites is by no means unique. Similar, if less conspicuous, stoichiometric "anomalies" are reported for leucites from the Leucite Hills (Carmichael, 1967a), Korath Range (Brown and Carmichael, 1969), New South Wales (Cundari, 1973) and Bufumbira (generalized in Fig. 1). It seems, therefore, plausible to consider such "silica excess" in leucite as a widespread crystal-chemical characteristic, rather than a regional peculiarity.

In the light of the data on Vico, it is suggested that the "silica excess" may be due, at least partly, to an extended solid solubility of KAlSi_3O_8 in leucite. The common occurrence of sanidine in the analcime pseudomorphs after Vico leucites (Cundari and Graziani, 1964) may derive from the subsolidus breakdown of leucite solid solutions with a high KAlSi_3O_8 component. It should be noted that "...leucite solid solutions were made which contained about 8 weight percent KAlSi_3O_8 " (Fudali, 1963, p. 1105) and no evidence is so far available to the writer that this is in fact an upper limit of KAlSi_3O_8 solid solubility in natural leucites. Notably, this limit is exceeded by the leucite compositions from Vico and the other localities mentioned above.

Alternatively, a differential loss of potassium from leucite will indirectly increase the weight percent of silica in the leucite compositions. Such loss is not

Petrogenetic

unreasonable
to Rb. Li

$$\frac{[\text{K/Rb}]^{\text{total}}}{[\text{K/Rb}]^{\text{pxl}}}$$

may be used
South Wales
Vico leucites
et al. (1968):
bearing rock

Plagioclase

Typically a
in the Vico

Table 2. Chemi

wt. %	(pxl.) 18/7
SiO_2	45.8
TiO_2	*
Al_2O_3	34.0
Fe_2O_3	0.74
MnO	0.06
MgO	*
CaO	18.4
Na_2O	1.23
K_2O	0.11
Σ	100.34
Cation content (3)	
Si	8.443
Al	7.388
Fe^{3+}	0.103
Mn	0.009
Ti	—
Mg	—
Ca	3.635
Na	0.440
K	0.026
Z	15.94
X	4.10
Or	0.7
Ab	10.4
An	88.9

* Below limit of de

* Total iron as Fe^{3+}

Analyst: A.K. Fers

ic observation shows
h complex twinning
cloudy, fractured to
domorph with low,

ssy leucites are given
ed compositions in
the analyses shows
the stoichiometric
n 180/8 and 191/1,
than the expected
191/1, respectively.
thin the range 17.6-
terminations (flame
Vico leucites. The
es in the same rock
a/K ratios than the
th the data reported
lar lava types from
leucites differ from
xperimentally deter-
SiO₄—SiO₂—H₂O
g trend toward the
in KAlSi₂O₆ solid
On the other hand,
groundmass alkali
relatively high (20.6-
or late-crystallizing

que. Similar, if less
leucites from the Leu-
Carmichael, 1969),
alized in Fig. 1). It
n leucite as a wide-
peculiarity.
the "silica excess"
ty of KAlSi₃O₈ in
pseudomorphs after
the subsolidus break-
nponent. It should
contained about 8
evidence is so far
Si₃O₈ solid solubility
leucite compositions

e will indirectly in-
s. Such loss is not

unreasonable in view of the poor K-retentivity of leucite in the subsolidus, relative to Rb, Li and Cs (Fornaseri and Penta, 1960). The ratio:

$$\frac{[K/Rb]^{leucite}}{[K/Rb]^{lava}}$$

may be used indicatively to contrast the near-stoichiometric leucites from New South Wales (0.7–1.0; mean (4)=0.88; Cundari, 1973, p. 480) to the low-K Vico leucites, averaging 0.60, deduced from independent data reported by Barbieri *et al.* (1968; Table 2: leucite mean (7) K/Rb=85; Table 1: leucite and feldspar-bearing rocks mean (28) K/Rb=141).

Plagioclase

Typically a microphenocrystal phase, occasionally glomerophytic, the plagioclase in the Vico lavas is strongly zoned and seldom resorbed. It is commonly observed

Table 2. Chemical analyses and structural formulae of plagioclase feldspar

wt. %	(pxl. rim) 18/7	(pxl. core) 18/8	(pxl. core) 29/2	(g. m.) 29/3	(pxl. core) 156/3	(pxl. rim) 156/4	(pxl. core) 176/9	(pxl. core) 180/6	(pxl. rim) 191/2
SiO ₂	45.8	46.3	47.4	52.7	46.1	47.2	48.1	45.9	47.5
TiO ₂	*	*	0.02	0.07	*	*	*	*	*
Al ₂ O ₃	34.0	34.0	32.0	29.0	33.0	32.0	32.0	34.0	34.0
Fe ₂ O ₃ *	0.74	0.75	0.58	0.72	0.75	0.73	0.71	0.41	0.84
MnO	0.06	*	0.04	0.04	*	0.02	*	*	0.02
MgO	*	*	0.04	0.06	*	0.04	0.04	0.03	0.04
CaO	18.4	17.5	17.1	12.2	18.3	17.8	16.0	17.8	16.1
Na ₂ O	1.23	1.50	2.3	3.9	1.63	2.3	2.9	1.29	1.96
K ₂ O	0.11	0.21	0.35	0.73	0.14	0.38	0.15	0.23	0.28
Σ	100.34	100.26	99.83	99.42	99.92	100.47	99.90	99.66	100.74
Cation content (32 oxygen atoms)									
Si	8.443	8.520	8.771	9.634	8.543	8.709	8.861	8.495	8.662
Al	7.388	7.375	6.980	6.250	7.209	6.960	6.949	7.418	7.309
Fe ³⁺	0.103	0.104	0.081	0.099	0.105	0.101	0.098	0.057	0.115
Mn	0.009	—	0.006	0.006	—	0.003	—	—	0.003
Ti	—	—	0.003	0.010	—	—	—	—	—
Mg	—	—	0.011	0.016	—	0.011	0.011	0.008	0.011
Ca	3.635	3.451	3.391	2.390	3.634	3.519	3.159	3.530	3.146
Na	0.440	0.535	0.825	1.382	0.586	0.823	1.036	0.463	0.693
K	0.026	0.049	0.083	0.170	0.033	0.089	0.035	0.054	0.065
Z	15.94	16.00	15.85	16.02	15.86	15.78	15.92	15.98	16.10
X	4.10	4.04	4.30	3.94	4.25	4.43	4.23	4.05	3.90
Or	0.7	1.2	2.2	4.5	0.9	2.4	0.9	1.4	1.7
Ab	10.4	12.4	18.2	34.1	13.0	17.3	22.8	10.8	16.9
An	88.9	86.4	79.6	61.4	86.1	80.3	76.3	87.8	81.4

* Below limit of detection (TiO₂, MnO, MgO=0.02% wt., respectively).

* Total iron as Fe₂O₃.

Analyst: A.K. Ferguson.

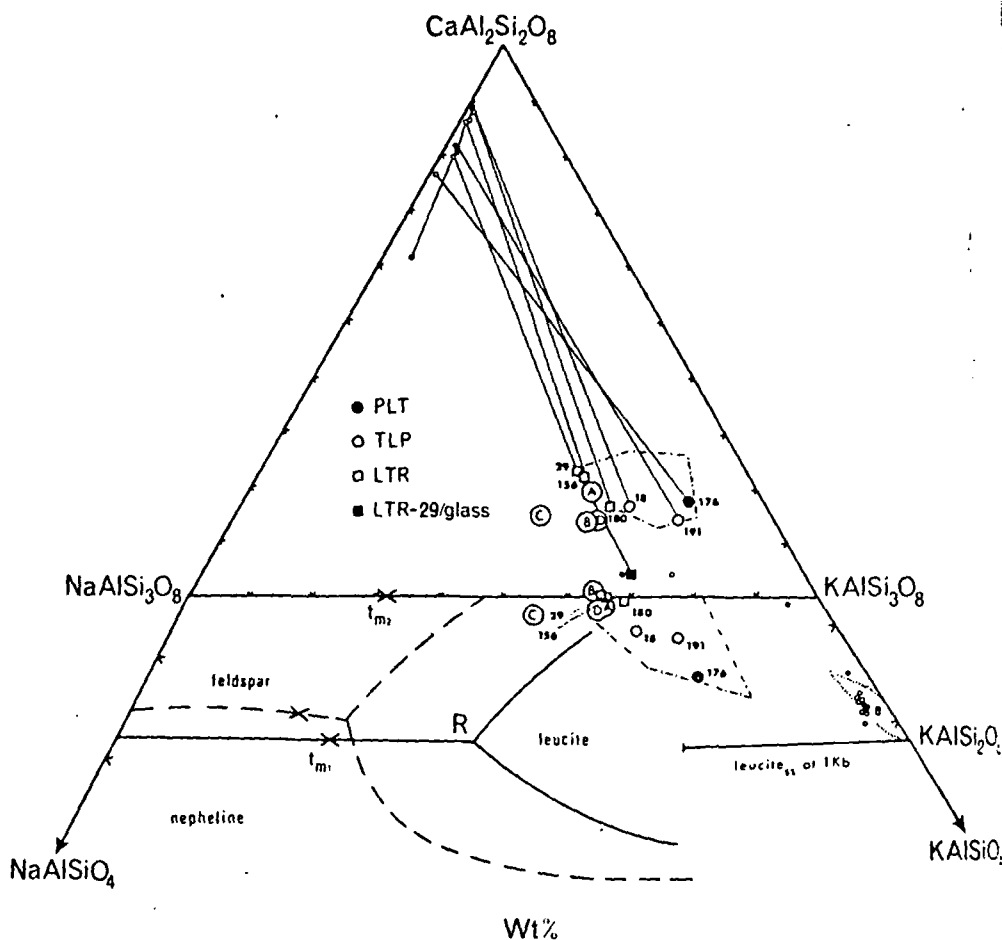


Fig. 1. Salic normative constituents of the Vico lavas (Cundari and Mattias, 1974, Table 1; large symbols and generalized fields indicated by dash-dot line) and their constituent leucite, alkali feldspar and plagioclase (small open symbols: phenocrystal core compositions; small filled symbols: phenocrystal rim and groundmass compositions. Analyses in Tables 1 and 2), projected onto the $CaAl_2Si_2O_8 - NaAlSi_3O_8 - KAlSi_3O_8$ and part of the $NaAlSi_3O_8 - KAlSi_3O_8 - SiO_2$ joins of the phonolite pentahedron (Carmichael *et al.*, 1974; Figs. 5-10). Coexisting plagioclases and a residual glass are joined by tie-lines to the respective bulk-rock compositions, corrected for the pyroxene contributions in the $CaAl_2Si_2O_8 - NaAlSi_3O_8 - KAlSi_3O_8$ join. Lettered circles represent mean pumice and "foam lava" compositions, calculated from Locardi and Mitterpergher (1967, Table 1; A: 7 analyses; B: 5 analyses; C: 8 analyses) and from Locardi (1965, Table 1; D: 2 analyses). Experimental phase boundaries and leucite solid solution in the system $NaAlSi_3O_8 - KAlSi_3O_8 - SiO_2 - H_2O$ at 1 Kb H_2O (Fudali, 1963) are indicated by continuous line; dashed line refers to the analogue dry system (Schairer, 1957). The field of the Bufumbira leucites (A.K. Ferguson, pers. comm.) is represented by dotted line

as euhedral inclusions in the larger leucite phenocrysts, but it is also a notable groundmass constituent throughout the suite (e.g. TL-30, PLT-176, TLP-191, LTR-156).

Chemical analyses and relative structural formulae of representative plagioclases are given in Table 2 and plotted in the join $NaAlSi_3O_8 - KAlSi_3O_8 - CaAl_2Si_2O_8$

Si_2O_8 (Fig. 1) (up to ca 6% $CaAl_2Si_2O_8$), and high Al_2O_3 as well as FeO .

Plagioclase geothermometry

Some indications can be obtained by plagioclase compositions following the results of Differentiation for the relative

Pxl. plagioclase

18/7
180/6
156/3
29/2
176/9

In view of the Weill, 1970: 1 the estimated correlation coefficient = 0.914) may be the plagioclase entropies of α may have been Vico lavas, i.e.

Pyroxene

The pyroxene along the c-axis monoclinic, p scheme:

$\alpha = \beta < \gamma$. Oscillations both sharp and Analyses of tural formulae

Si_2O_8 (Fig. 1). The phenocrystal compositions show significant concentric zoning (up to ca 6% wt. An variation), both normal (156/3–156/4) and reversed (18/8–18/7), and high anorthite contents (76.3–88.9% wt. An.) in the trachytic (29, 156, 180) as well as tephritic phonolite (18, 191) and phonolite tephrite (176) assemblages.

Plagioclase geothermometer

Some indications of the plagioclase-liquid relationships in the Vico lavas may be obtained by estimating the crystallization temperatures of the analyzed plagioclases, following the method proposed by Mathez (1973) for basaltic (dry) rocks. The results of the calculations are summarized below with the values of the Differentiation Index (Thornton and Tuttle, 1960) and the $\text{Mg}/\text{Mg} + \text{Fe}^{2+}$ ratios for the relative bulk rock compositions:

Pxl. plagioclase	An% mol.	T °C	D.I.	Mg/Mg + Fe ²⁺
18/7	89.2	1312	70.4	0.59
180/6	88.4	1265	65.0	0.60
156/3	86.1	1262	62.7	0.66
29/2	80.4	1217	59.5	0.68
176/9	75.3	1165	49.9	0.71

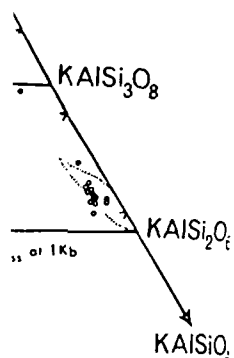
In view of the assumptions and limitations of the above method (Kudo and Weill, 1970; Mathez, 1973) and since the Vico lavas are not strictly basalts, the estimated crystallization temperatures may not be accurate in detail. However, the correlation of these temperatures with the Differentiation Indices (correlation coefficient = 0.988) and with the $\text{Mg}/\text{Mg} + \text{Fe}^{2+}$ ratios (correlation coefficient = -0.914) may be petrologically significant. From these data it is expected that the plagioclase crystallization temperatures are depressed in the lavas with higher entropies of melting. Consequently, the plagioclase control in the differentiation may have been more significant in the most differentiated compositions of the Vico lavas, i.e. the leucite-trachytes.

Pyroxene

The pyroxene is an ubiquitous microphenocrystal phase, seldom reaching $1/2$ cm along the c-axis, as well as a common groundmass constituent. It is exclusively monoclinic, pale-green (e.g. LTR-29) to distinctly pleochroic according to the scheme:

α =pale green; β =yellowish green; γ =deep green; the absorption being $\alpha < \beta < \gamma$. Oscillatory zoning showing concentric and sector-like geometries with both sharp and gradational contacts are commonly observed.

Analyses of representative pyroxenes are given in Table 3, with relative structural formulae and normative compositions calculated according to Kushiro's



974, Table 1: large
ite, alkali feldspar
ymbols: phenocrys-
the $\text{CaAl}_2\text{Si}_2\text{O}_8$ -
phonolite pentahed-
al glass are joined
e contributions in
umice and "foam
1: A: 7 analyses:
xperimental phase
 H_2O at 1 Kb H_2O
alogic dry system
m.) is represented

also a notable
176, TLP-191.

tative plagioc-
 Si_3O_8 - CaAl_2

Table 3. Chemical analyses, structural formulae and normative compositions of clinopyroxene

wt. %	(core) 18/4	(inner rim) 18/6	(rim) 18/5	(core) 29/13	(inner rim) 29/12	(rim) 29/5	(core) 156/6	(outer core) 156/7	(rim) 156/2
SiO ₂	49.5	48.8	45.8	50.2	49.9	50.5	51.8	47.7	49.5
TiO ₂	0.72	0.64	1.39	0.45	0.75	0.74	0.39	0.87	0.7
Al ₂ O ₃	5.3	4.6	6.7	3.6	3.8	3.9	3.1	6.2	4.4
Cr ₂ O ₃	*	*	*	0.11	*	*	0.39	0.19	*
FeO ^a	6.1	8.6	9.3	8.5	8.4	9.4	4.1	8.7	6.3
MnO	0.18	0.29	0.31	0.28	0.27	0.24	0.06	0.20	0.17
MgO	13.8	11.9	10.9	13.3	13.2	12.6	15.7	12.4	14.3
NiO	0.10	*	*	*	*	0.05	*	*	0.04
CaO	23.8	24.2	24.5	23.4	23.0	22.0	23.5	23.1	23.7
Na ₂ O	0.21	0.36	0.39	0.35	0.37	0.31	0.12	0.28	0.22
K ₂ O	*	0.02	0.02	*	*	0.02	*	*	0.02
Σ	99.71	99.41	99.31	100.19	99.69	99.76	99.16	99.64	99.42
FeO ^b	3.5	4.7	3.0	4.8	5.4	8.60	3.4	4.6	2.7
Fe ₂ O ₃ ^b	2.9	4.3	7.0	4.1	3.3	0.87	0.77	4.6	4.0
Cation content (6 oxygen atoms)									
Si	1.832	1.833	1.727	1.863	1.862	1.893	1.912	1.782	1.835
Al ^{iv}	0.168	0.167	0.273	0.137	0.138	0.107	0.088	0.218	0.165
Al ^{vi}	0.063	0.036	0.025	0.020	0.029	0.065	0.046	0.055	0.021
Ti	0.020	0.018	0.039	0.013	0.021	0.021	0.011	0.024	0.021
Fe ³⁺	0.081	0.122	0.199	0.114	0.093	0.024	0.021	0.129	0.112
Cr	—	—	—	0.003	—	—	0.011	0.006	—
Fe ²⁺	0.108	0.148	0.095	0.149	0.169	0.270	0.105	0.144	0.082
Mn	0.006	0.009	0.010	0.009	0.009	0.008	0.002	0.006	0.005
Mg	0.761	0.666	0.613	0.736	0.734	0.704	0.863	0.690	0.790
Ni	0.003	—	—	—	—	0.002	—	—	0.001
Ca	0.944	0.974	0.990	0.930	0.920	0.883	0.929	0.925	0.942
Na	0.015	0.026	0.029	0.025	0.027	0.023	0.009	0.020	0.016
K	—	0.001	0.001	—	—	0.001	—	—	0.001
Normative components (%wt.)									
NaCrSi ₂ O ₆	—	—	—	0.32	—	—	1.09	0.55	—
KFeSi ₂ O ₆	—	0.09	0.09	—	—	0.09	—	—	0.08
NaFeSi ₂ O ₆	1.44	2.53	2.77	2.11	2.58	2.17	—	1.41	1.51
CaFe ₂ Si ₂ O ₆	2.62	3.87	6.86	3.69	2.62	0.04	0.85	4.67	3.74
CaTiAl ₂ O ₆	1.86	1.70	3.72	1.17	1.97	1.95	0.99	2.29	1.99
CaAl ₂ Si ₂ O ₆	9.66	8.58	11.28	6.75	6.38	6.67	5.67	11.45	7.55
Ca ₂ Si ₂ O ₆	37.73	39.60	36.56	38.55	38.44	38.21	40.00	34.99	37.90
Mg ₂ Si ₂ O ₆	41.94	37.02	34.25	40.71	40.62	39.13	46.96	38.27	43.45
Fe ₂ Si ₂ O ₆	4.76	6.62	4.47	6.70	7.40	11.73	4.43	6.36	3.77

* Below limit of detection (Cr₂O₃, NiO=0.03%wt., respectively; K₂O=0.02%wt.)^a Total iron as FeO.^b Calculated values assuming Σ(WXYZ)=4.00 and Z=2.00 on the basis of 6 oxygen atoms.

Analyst: A.K. Ferguson.

(1962) method after forming the NaCrSi₂O₆ component (Binns *et al.*, 1970). The ferric ion contents are deduced assuming that the pyroxenes are stoichiometric (4.00 cations) on the basis of 6 oxygen atoms. Data extracted from a computer

Table 3 (continued)

(m.) 56/1	(core) 176/2	(rim) 176/1
49.8	48.7	50.1
0.63	0.85	0.76
3.4	4.0	4.2
*	*	0.17
8.8	9.6	5.1
0.26	0.27	0.08
13.3	13.2	15.1
0.10	*	*
22.6	23.1	23.8
0.37	0.37	0.15
0.02	*	0.02
92.28	100.09	99.48
5.3	3.9	2.3
3.9	6.3	3.1
1.866	1.813	1.848
0.134	0.176	0.152
0.016	—	0.031
0.018	0.024	0.021
0.110	0.177	0.086
—	—	0.005
0.166	0.121	0.071
0.008	0.009	0.003
0.743	0.733	0.830
0.003	—	—
0.908	0.922	0.941
0.027	0.027	0.011
0.001	—	0.001
—	—	0.48
0.09	—	0.08
2.59	2.58	0.55
3.27	6.11	3.11
1.66	2.23	1.94
5.85	6.55	7.07
37.88	36.39	38.28
41.29	40.67	45.37
7.37	5.48	3.12

library of published
tical) - FeO (calcula
pyroxene compositi

inopyroxene

(core) 156/6	(outer core) 156/7	(rim) 156/8
51.8	47.7	49.5
0.39	0.87	0.7
3.1	6.2	4.4
0.39	0.19	*
4.1	8.7	6.3
0.06	0.20	0.1
15.7	12.4	14.3
*	*	0.04
23.5	23.1	23.7
0.12	0.28	0.22
*	*	0.02

99.16	99.64	99.42
3.4	4.6	2.7
0.77	4.6	4.0

1.912	1.782	1.833
0.088	0.218	0.166
0.046	0.055	0.02
0.011	0.024	0.02
0.021	0.129	0.112
0.011	0.006	—
0.105	0.144	0.084
0.002	0.006	0.005
0.863	0.690	0.796
—	—	0.001
0.929	0.925	0.942
0.009	0.020	0.016
—	—	0.001

1.09	0.55	—
—	—	0.08
—	1.41	1.51
0.85	4.67	3.74
0.99	2.29	1.99
5.67	11.45	7.55
3.00	34.99	37.90
5.96	38.27	43.45
1.43	6.36	3.77

oms.

is *et al.*, 1970),
stoichiometric
on a computer

Table 3. (continued)

(m.) 176/1	(core) 176/2	(rim) 176/1	(core) 176/6	(rim) 176/5	(green core) 176/7	(core) 180/3	(rim) 180/4	(core) 180/10	(rim) 180/13	(core) 191/7	(rim) 191/6
48.7	48.7	50.1	46.4	49.7	48.7	49.7	50.6	51.5	49.5	49.2	47.7
0.85	0.85	0.76	0.76	0.85	0.78	0.74	0.65	0.41	0.64	0.69	0.95
4.0	4.0	4.2	7.1	4.8	4.5	4.1	3.9	3.5	5.1	4.6	5.9
*	*	0.17	*	0.07	*	*	*	0.07	0.04	*	*
9.6	9.6	5.1	10.8	6.5	9.7	9.6	7.0	5.5	6.9	7.7	9.1
0.27	0.27	0.08	0.27	0.27	0.24	0.31	0.19	0.10	0.07	0.14	0.19
13.2	13.2	15.1	11.2	14.6	11.6	12.4	14.2	15.5	14.5	13.7	12.3
*	*	*	*	*	*	0.03	*	*	*	*	*
23.1	23.1	23.8	23.2	22.9	23.4	22.5	23.2	23.6	22.7	23.0	23.1
0.37	0.37	0.15	0.36	0.30	0.54	0.43	0.23	0.14	0.19	0.25	0.35
0.02	*	0.02	*	*	*	*	0.02	*	0.03	*	0.02
100.09	100.09	99.48	100.09	99.99	99.46	99.81	99.99	100.32	99.67	99.28	99.61
3.9	3.9	2.3	4.5	3.2	5.5	6.8	4.7	3.3	3.8	4.3	4.5
6.3	6.3	3.1	7.0	3.7	4.7	3.1	2.5	2.4	3.4	3.8	5.1
1.866	1.813	1.848	1.737	1.830	1.832	1.861	1.871	1.885	1.831	1.835	1.785
0.134	0.176	0.152	0.263	0.170	0.168	0.139	0.129	0.115	0.169	0.165	0.215
0.016	—	0.031	0.050	0.039	0.031	0.042	0.041	0.036	0.053	0.037	0.045
0.018	0.024	0.021	0.021	0.024	0.022	0.021	0.018	0.011	0.018	0.019	0.027
0.110	0.177	0.086	0.197	0.103	0.133	0.087	0.070	0.066	0.095	0.107	0.144
—	—	0.005	—	0.002	—	—	—	0.002	0.001	—	—
0.166	0.121	0.071	0.141	0.099	0.173	0.213	0.145	0.101	0.118	0.134	0.141
0.008	0.009	0.003	0.009	0.008	0.008	0.010	0.006	0.003	0.002	0.004	0.006
0.743	0.733	0.830	0.625	0.801	0.650	0.692	0.783	0.845	0.799	0.761	0.686
0.003	—	—	—	—	—	0.001	—	—	—	—	—
0.908	0.922	0.941	0.931	0.904	0.943	0.903	0.919	0.925	0.900	0.919	0.926
0.027	0.027	0.011	0.026	0.021	0.039	0.031	0.016	0.010	0.014	0.018	0.025
0.001	—	0.001	—	—	—	—	0.001	—	0.001	—	0.001
—	—	0.48	—	0.20	—	—	—	0.19	0.11	—	—
0.09	—	0.08	—	—	—	—	0.08	—	0.13	—	0.09
2.59	2.58	0.55	2.54	1.85	3.82	3.02	1.58	0.75	1.19	1.73	2.45
3.27	6.11	3.11	6.91	3.32	3.85	2.24	2.10	2.31	3.28	3.57	4.75
1.66	2.23	1.94	2.02	2.18	2.08	1.95	1.68	1.04	1.65	1.80	2.50
5.85	6.55	7.07	13.93	8.15	7.98	7.13	6.78	6.46	9.43	8.30	10.57
37.88	36.39	38.28	33.28	35.93	38.34	37.68	38.39	38.72	35.41	36.85	35.36
41.29	40.67	45.37	34.92	43.95	36.24	38.51	43.02	46.14	43.81	41.97	38.07
7.37	5.48	3.12	6.41	4.43	7.71	9.46	6.38	4.37	4.99	5.77	6.20

library of published pyroxene analyses shows that the mean difference FeO (analytical) - FeO (calculated) = 0.08% wt. (S.D. = 2.55% wt.) for a sample of 580 clinopyroxene compositions (A.K. Ferguson, pers. comm., 1975).

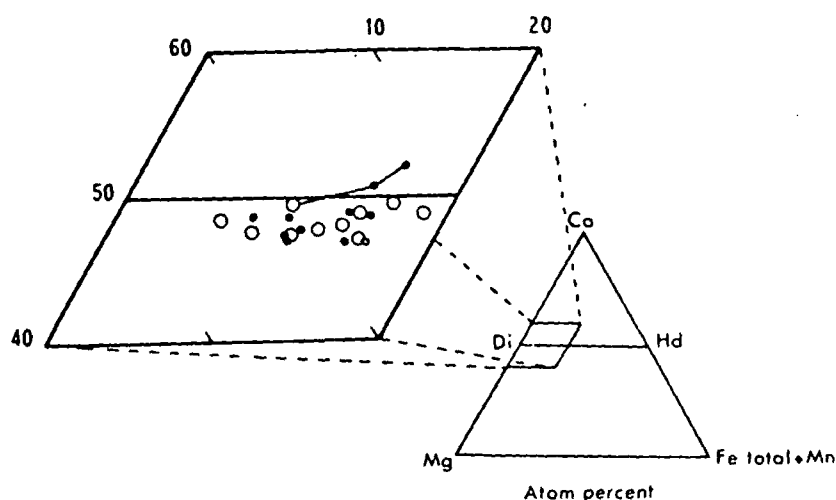


Fig. 2. Pyroxene phenocrystal core (open circles), rim and groundmass (filled circles) compositions (Table 3), plotted in the conventional Ca—Mg— Σ (Fe total+Mn) variation diagram. Coexisting compositions in TLP-18 are joined by tie-lines (see text)

In the conventional Ca—Mg—Fe total+Mn diagram (Fig. 2), the pyroxene compositional variation falls mainly within the salite domain and shows a general Fe-enrichment trend parallel to the diopside-hedenbergite join, with no clear distinction between core and rim compositions for the various rock types. Only the pyroxene in a tephritic leucite phonolite (18/4.6.5), indicated by tie-lines, shows a distinct Ca-enrichment trend (cf. Carmichael *et al.*, 1974, Figs. 5–31). This may be influenced by competing plagioclase crystallization, which would generally tend to reduce the amount of calcium available to the pyroxene. Significantly, calcium and concomitant sodium enrichment trends characterize similar pyroxene compositions from plagioclase-free leucites (Cundari, 1973).

The Si-deficiency in the Z-sites (5.7–13.6 atoms percent) is lower than 20.3 atoms percent reported by Carmichael *et al.* (1974, Table 5–5) for groundmass pyroxene in leucite phonolite, and sufficient aluminium is available in all but one composition (176/2) to make the Z-groups up to 2.00. Generally, the percentage of total aluminium atoms in the Z-groups (Al_z) is greater than 80. Lower values (76–77 atoms percent) are obtained for the pyroxene compositions (180/3,4,10,13) in a relatively differentiated leucite trachyte (LTR-180; DI=65.0). However, the small range of SiO_2 -undersaturation for the selected lavas (negative C.I.P.W. $Q=9.15-1.72$) does not encourage conclusions on the correlation of Al_z with differentiation (Le Bas, 1962).

The distribution of Ti relative to Al_z in coexisting core and rim compositions generally shows contrasting trends, suggesting a complex history of multiple equilibrations in the pyroxene-liquid relationships (cf. Thompson, 1972; Ferguson, 1973). This may be influenced by temperature and/or water content fluctuations in the relatively viscous Vico lavas ($SiO_2=49-58\%$ wt.) during the protracted crystallization of the pyroxene.

The normativ Si_2O_6 , resulting in Si_2O_6 is formed molecule ($CaFe_2^{3+}$ contents (5.7–13.9 amounts (1.2–3.8) is also present in :

The variation the same lava, co the solubility of be primarily sensit chemistry (Hollis volcanic regime. L mak's molecule a lavas ($Na_2O=1.6$ - lase is expected to in the liquid durin

Mica and Fe-Ti O

Mica is a common roded, as well as in to the scheme: $z=1$ tion being $z < \beta \approx 7$ are given in Table structural formula. Except for analyti attributed to the t Z-groups are made

Surprisingly for

Mg/Fe ratio of th compositions. The (176/8) is also within mean (4)=2.88) ar bearing lavas (cf. C: ally decrease for lat

The Fe-Ti oxid

lavas, generally oc

the groundmass (e

the crystals are gene

sentative chemical a

ponents (Carmicha

are best recast on t

γ -phase in the "mag

Relatively high alu

the compositions o

The normative compositions are notable for the absence of jadeite ((Na,K)AlSi₂O₆), resulting from an excess of Fe³⁺ over (Na + K) after acmite ((Na,K)Fe³⁺Si₂O₆) is formed. This leads to the presence of significant ferri-Tschermak's molecule (CaFe³⁺SiO₆) in the normative compositions, combined with moderate contents (5.7–13.9% wt.) of Ca-Tschermak's molecule (CaAl₂SiO₆) and accessory amounts (1.2–3.8% wt.) of acmite. The titan pyroxene component (CaTiAl₂O₆) is also present in accessory amounts (less than 2.5% wt.).

The variation in Ca-Tschermak's content within and between pyroxenes in the same lava, coexisting with calcium-rich plagioclase, supports the view that the solubility of the Ca-Tschermak's molecule in the Vico pyroxenes should be primarily sensitive to crystal-liquid equilibria and related chemistry and crystal chemistry (Hollister and Gancarz, 1971) rather than pressure changes in the volcanic regime. Likewise, the factors controlling the solubility of the ferri-Tschermak's molecule are probably the relatively low sodium contents in the host lavas (Na₂O = 1.6–2.7% wt.), for which the concomitant crystallization of plagioclase is expected to compete, and the oxidizing conditions prevailing, rhythmically, in the liquid during pyroxene crystallization (cf. Huckenholz *et al.*, 1969).

Mica and Fe-Ti Oxide Minerals

Mica is a common accessory occurring both as microphenocrysts, generally corroded, as well as interstitially in the groundmass. Pleochroism is strong according to the scheme: α = pale yellow; $\beta \approx \gamma$ = deep brown to greenish brown, the absorption being $\alpha < \beta \approx \gamma$. The chemistry and structural formulae of the analyzed micas are given in Table 4. Because of the undetermined fluorohydroxyl groups, the structural formulae are calculated on the anhydrous basis of 22 oxygen atoms. Except for analytical error, the deficiencies in the X and Y groups may be attributed to the undetermined elements, particularly Fe³⁺ and Ba, after the Z-groups are made up to 8.00.

Surprisingly for intermediate rock compositions (LTR-180, TLP-191), the Mg/Fe ratio of the analyzed micas is greater than 2:1, indicating phlogopite compositions. The mica in the groundmass of a basic phonolitic leucite tephrite (176/8) is also within the phlogopite range. However, the Mg/Fe ratios (2.66–3.05; mean (4) = 2.88) are lower than the values for analogues in more basic leucite bearing lavas (cf. Carmichael, 1967a, Table 6; Cundari, 1973, Table V) and generally decrease for late-crystallizing compositions.

The Fe-Ti oxide minerals are ubiquitous accessory constituents of the Vico lavas, generally occurring as equant microphenocrysts as well as microlites in the groundmass (e.g. PLT-176). In polished-thin section under reflected light the crystals are generally homogeneous and isotropic with high reflectivity. Representative chemical analyses (Table 4) and calculated ulvöspinel and ilmenite components (Carmichael, 1967b) show in all cases that the FeO and Fe₂O₃ values are best recast on the ilmenite basis. This points to substantial contents of the γ -phase in the "magnetite" solid solutions and suggests oxidation of the β -spinel. Relatively high aluminium and low magnesium and chromium contents reflect the compositions of the host lavas.

REPRODUCED FROM THE ORIGINAL MANUSCRIPT

Table 4. Chemical analyses and structural formulae of mica and iron-titanium oxides

wt%	Mica				Iron-titanium oxides				
	(g.m.) 176/8	(pxl.) 180/1	(pxl.) 180/2	(pxl.) 191/3	(pxl.) 18/10	(pxl.) 29/1	(pxl.) 176/10	(pxl.) 191/8	
SiO ₂	40.2	39.0	39.6	36.8	0.83	0.51	0.38	0.42	
TiO ₂	1.88	4.99	4.63	4.94	11.0	17.5	13.0	12.3	
Al ₂ O ₃	11.8	13.5	13.5	14.6	2.8	2.7	3.1	2.5	
Cr ₂ O ₃	0.03	*	*	*	*	*	0.06	0.05	
FeO*	10.8	10.7	10.7	10.5	72.0	71.0	76.0	77.0	
MnO	0.11	0.10	0.08	0.09	1.5	0.80	0.67	1.1	
MgO	16.1	18.3	18.0	16.6	0.21	0.20	0.66	0.19	
NiO	*	*	*	*	0.04	*	0.09	*	
CaO	2.1	0.04	*	0.09	4.4	0.05	0.29	0.16	
Na ₂ O	0.61	0.42	0.22	0.37	0.11	0.06	*	0.06	
K ₂ O	8.9	9.4	9.5	8.6	0.17	0.07	*	0.13	
Σ	92.53	96.45	96.23	92.59	93.06	92.89	94.25	93.91	
Cation content (22 oxygen atoms)					Ulvöspinel basis				
Si	6.067	5.640	5.726	5.530	Fe ₂ O ₃	41.5	28.0	38.4	39.9
Al ^{iv}	1.933	2.301	2.274	2.470	FeO	34.6	45.8	41.4	41.0
Al ^{vi}	0.166	—	0.027	0.116	Σ	97.2	95.7	98.1	97.9
Ti	0.213	0.543	0.504	0.558	Ulvöspinel	36.8	56.5	41.3	39.1
Fe ²⁺	1.363	1.294	1.294	1.320	(Mol.%)				
Mn	0.014	0.012	0.010	0.011	Ilmenite basis				
Cr	0.004	—	—	—	Fe ₂ O ₃	76.6	62.2	73.5	74.7
Mg	3.622	3.944	3.879	3.718	FeO	3.0	15.0	9.8	9.7
Ca	0.340	0.006	—	0.014	Σ	100.7	99.1	101.6	101.4
Na	0.178	0.118	0.062	0.108	Ilmenite	24.0	36.8	26.8	25.6
K	1.714	1.735	1.753	1.649	(Mol.%)				
Z	8.00	8.00	8.00	8.00					
Y	5.38	5.31	5.71	5.72					
X	2.23	1.86	1.82	1.77					
Mg/Fe	2.66	3.05	3.00	2.82					

* Below limit of detection (Cr₂O₃, NiO, Na₂O=0.03%wt., respectively; CaO, K₂O=0.02%wt., respectively).

* Total iron as FeO.

Analyst: A.K. Ferguson.

The Phonolite Pentahedron

The investigated lavas and pertinent phase assemblages are projected onto the NaAlSi₃O₈—KAlSi₃O₈—CaAl₂Si₂O₈ and part of the NaAlSi₃O₈—KAlSi₃O₈—SiO₂ join (Fig. 1) of the phonolite pentahedron (Carmichael *et al.*, 1974, p. 241ff.). The selected lava compositions (numbered symbols) are corrected for the CaAl₂Si₂O₈ contributions of the respective pyroxene, where the range of the CaAl₂Si₂O₈ component in the NaAlSi₃O₈—KAlSi₃O₈—CaAl₂Si₂O₈ join is 75.6-

93.4% wt. Mean-
ciated to the lave
Locardi (1965). a
alkali feldspar jo
SiO₄=37.4% wt
SiO₄=36.8% wt
join.

Although this
data from Vico m
et al. (1974, Figs
fields of the suite
a course of the ty
descent controllec
gioclase. In the l
directly away fro
conforming with
in the system Na
noted that the "s
differentiating liqu
salic derivatives.

Plagioclase fra
dominant differen
tie-lined bulk-roc
phenocrysts coexis
cur with the plag
end of the suite, as
1974).

The compositio
with the establish
of the suite, akin t

In summary, th
for the observed
possible crystalliza
ent data on similar

The stability of
near-atmospheric
250ff.) in the syst
regarded as a mal
however, that the
suite may develop
tephrite magma a
(Cundari and Le M

It is concluded t
related liquids deri
composition. The r
of the eruptions m
of the parental mag

oxides		
n oxides		
	(pxl.)	(pxl.)
	176/10	191/8
Si	0.38	0.42
Ti	13.0	12.3
Al	3.1	2.5
Fe	0.06	0.05
Mn	76.0	77.0
Mg	0.67	1.1
Ca	0.66	0.19
Na	0.09	*
K	0.29	0.16
P	*	0.06
As	*	0.13
Sum	94.25	93.91
sis		
	38.4	39.9
	41.4	41.0
	98.1	97.9
	41.3	39.1
	73.5	74.7
	9.8	9.7
	101.6	101.4
	26.8	25.6

l. K₂O=0.02%wt.,

93.4% wt. Mean compositions of the analyzed pumices and "foam lava" associated to the lava suite, calculated from Locardi and Mittempergher (1967) and Locardi (1965), are included for comparison. Two compositions straddling the alkali feldspar join (LTR-29; SiO₂=44.1% wt., NaAlSiO₄=18.5% wt., KAlSiO₄=37.4% wt.; and B: SiO₂=44.6% wt., NaAlSiO₄=18.6% wt., KAlSiO₄=36.8% wt.) plot in fact on the SiO₂ side of the NaAlSiO₄-KAlSiO₄-SiO₂ join.

Although this system is as yet undetermined experimentally, the available data from Vico may be discussed in the light of the model proposed by Carmichael *et al.* (1974, Figs. 5-14). The selected lava compositions and the generalized fields of the suite show that the dominant differentiation trend of Vico follows a course of the type PLT→TLP→LTR, along a possible liquid path of thermal descent controlled by the early and protracted crystallization of leucite and plagioclase. In the NaAlSiO₄-KAlSiO₄-SiO₂ join this path is slightly curved, directly away from KAlSi₂O₆ and toward the leucite-alkali feldspar boundary, conforming with the fractionation curves predicted by Fudali (1963, Fig. 10) in the system NaAlSiO₄-KAlSiO₄-SiO₂-H₂O at $P_{H_2O}=1$ Kb. It should be noted that the "silica excess" of leucite may influence the SiO₂ content in the differentiating liquids and, ultimately, the level of silica-saturation in the extreme salic derivatives.

Plagioclase fractionation could produce K-enrichment variations across the dominant differentiation trend of the suite, as illustrated by LTR-29/glass and tie-lined bulk-rock composition. Fractionation of the aluminous pyroxene phenocrysts coexisting with the early-crystallized plagioclase will essentially concur with the plagioclase control in this system and may prevail at the basic end of the suite, as indicated by crystal extract calculations (Cundari and Mattias, 1974).

The compositions of the pumices and "foam lava" are generally consistent with the established trends and may be regarded as possible salic differentiates of the suite, akin to the leucite-trachytes.

In summary, the leucite and plagioclase differentiation controls can account for the observed variations of the Vico suite in this system, consistently with possible crystallization paths experimentally deduced or inferred from independent data on similar assemblages.

The stability of phlogopite, coexisting with leucite and alkali feldspar under near-atmospheric pressure regime, is predicted by Carmichael *et al.* (1974, p. 250ff.) in the system NaAlSiO₄-KAlSiO₄-Mg₂SiO₄-H₂O, which may be regarded as a mafic variant of the phonolite pentahedron. It should be noted, however, that the major role of phlogopite in the differentiation of the Vico suite may develop at depth, where the crystal fractionation processes in a leucite-tephrite magma are controlled largely by phlogopite+pyroxene assemblages (Cundari and Le Maitre, 1970; Ferguson and Cundari, 1975).

It is concluded that the Vico suite may be interpreted as a series of genetically related liquids derived from a common parental magma of tephritic (*sensu lato*) composition. The recurrent chemistry of the rocks in the chronological succession of the eruptions may well reflect distinct but reproducible cycles of evolution of the parental magma.

ected onto the
4-KAlSiO₄-
1974, p. 241ff.).
for the CaAl₂
of the CaAl₂
join is 75.6-

Discussion

The dominant differentiation trend of the Vico suite is consistent with the general variation found by Locardi and Mittempergher (1969, Fig. 2) and conforms to Appleton's (1972, Fig. 6 and p. 437) "Trend B" for the lavas of the Roman Region. However, the petrogenetic model advocated by Locardi and Mittempergher (1969) for Vico is based on two distinct but genetically related differentiation trends attributed to the lavas (tephrite-basanite-leucitite) and to the "pyroclastic" materials (trachyandesite-latitude-trachyte-alkali trachyte), respectively. Neither of these trends nor the invoked carbonate syntexis hypothesis can be substantiated by the available data. Also, the alleged influence of the volcanic structures and related magma feeders on the course of magmatic differentiation and relative quantity of erupted differentiates (Locardi and Mittempergher, 1967, 1969) is singularly unsatisfactory for Vico, where the recurrent chemistry of the volcanic rocks erupted from major and minor vents in various amounts conforms to the dominant differentiation trend.

The carbonate-syntexis hypothesis (Rittmann, 1933, 1963; Marinelli and Mittempergher, 1966; Locardi and Mittempergher, 1969; Burri, 1968) is rejected as a viable petrogenetic model for the Vico suite. Notably, the advocates of this hypothesis fail to produce for Vico any supporting evidence of magma-carbonate rock interaction bearing on the development of the elusive "syntectic magma", alleged to be parental to the lava suite. Considering the shallow magma reservoir deduced for Vico from geophysical data (1-13 Km; Molina and Sonaglia, 1969) and the large volume of erupted materials (ca. 14 Km³ for the "pyroclastic" rocks alone, according to Locardi and Mittempergher, 1967, Table 1), it seems unlikely that concrete evidence of the "syntectic" process escaped sampling by the extended activity of Vico. Additional limitations of the carbonate syntexis hypothesis in the petrogenesis of the leucite-bearing lavas are discussed elsewhere (e.g. Savelli, 1967, 1968; Watkinson and Wyllie, 1969; Bell and Powell, 1969) and the available evidence strongly points to crystal-liquid relationships *within* the magma as the essential differentiation controls of the derivative lavas (cf. Brown and Carmichael, 1969; Appleton, 1972; Cundari, 1973). In conclusion, the differentiation trends of the leucite-bearing lavas and associated "pyroclastic" materials from Vico depend on reproducible crystal-differentiation processes, consistent within the Roman Volcanic Region (Cundari and LeMaitre, 1970) and similar to the Bufumbira analogues (Ferguson and Cundari, 1975).

Acknowledgments. The author gratefully acknowledges the continuing support of the Australian Research Grants Committee and the assistance of A.K. Ferguson in providing unpublished mineral data and computer programmes for the calculations of the plagioclase geothermometer. Professor Kenzo Yagi kindly reviewed the manuscript.

References

- Appleton, J.D.: Petrogenesis of potassium-rich lavas from the Roccamonfina volcano, Roman Region, Italy. *J. Petrol.* 13, 425-456 (1972)
- Barbieri, F., Fornasari, M., Penta, A.: Rubidium and potassium relationship in some volcanoes of Central Italy. *Chem. Geol.* 3, 189-197 (1968)

- Bell, K., Powell, J.: Birunga and T. (1969)
- Binns, R.A., Dugg: Northeastern N
- Brown, F.H., Carr: tephrite series of
- Burri, C.: Potentie kunst des Vesuv
- Carmichael, I.S.E.: Wyoming, Con
- Carmichael, I.S.E.: sian silicates. C
- Carmichael, I.S.E.: 1974
- Cundari, A.: *Petro* 20, 465-492 (19
- Cundari, A., Graz: Mineral. (Rome)
- Cundari, A., LeMa: Birunga volcani
- Cundari, A., Mattia: 38, 98-114 (197
- Ferguson, A.K.: O (1973)
- Ferguson, A.K., Ci: Bufumbira, Sou
- Fornasari, M., Penta: di analcimizzazi
- Fudali, R.F.: Exper of alkalic rock s
- Hollister, L.S.: Gas Italy. *Am. Mine*
- Huckenholz, H.G.: Soc. Amer. Spec
- Kudo, A.M., Weill: (1970)
- Kushiro, I.: *Pyrox* Trans. 33, 213-2
- Le Bas, M.J.: *The* Am. J. Sci. 260.
- Locardi, E.: *Tipi d* Soc. Toscana. S
- Locardi, E., and M: processes. *Geol.*
- Locardi, E., and M: volcanoes of Cer
- Marinelli, G., and I: (potassic) suite. 1
- Mason, P.K.: Frost: tive X-ray micro
- Mathez, E.A.: *Refin* rocks. *Contrib. A*
- Mattias, P.P., Vent: It. 9, 331-384 (15
- Molina, F., Sonaglia: Ann. Geofis. (RC

- Bell, K., Powell, J.L.: Strontium isotopic studies of alkali rocks: the potassium-rich lavas of the Birunga and Toro-Ankole regions, East and Central Equatorial Africa. *J. Petrol.* **10**, 536-572 (1969)
- Binns, R.A., Duggan, M.B., Wilkinson, J.F.G.: High pressure megacrysts in alkaline lavas from Northeastern New South Wales. *Am. J. Sci.* **269**, 132-198 (1970)
- Brown, F.H., Carmichael, I.S.E.: Quaternary volcanoes of the Lake Rudolf Region: I. The basanite-tephrite series of the Korath Range. *Lithos* **2**, 239-260 (1969)
- Burri, C.: Potentielle Mineralbestände Kalitrichybasaltisch-karbonatischer Syntektika und die Zukunft des Vesuvmagmas. *Geol. Rundschau* **57**, 744-765 (1968)
- Carmichael, I.S.E.: The mineralogy and petrology of the volcanic rocks from the Leucite Hills, Wyoming. *Contrib. Mineral. Petrol.* **15**, 24-66 (1967a)
- Carmichael, I.S.E.: The iron-titanium oxides of salic volcanic rocks and their associated ferromagnesian silicates. *Contrib. Mineral. Petrol.* **13**, 36-64 (1967b)
- Carmichael, I.S.E., Turner, F.J., Verhoogen, J.: *Igneous Petrology*, 739 pp. New York: McGraw-Hill 1974
- Cundari, A.: Petrology of the leucite-bearing lavas in New South Wales. *J. Geol. Soc. Australia* **20**, 465-492 (1973)
- Cundari, A., Graziani, G.: Prodotti di alterazione della leucite nelle vulcaniti vicane. *Periodico Mineral. (Rome)* **33**, 35-53 (1964)
- Cundari, A., LeMaitre, R.W.: On the petrogeny of the leucite-bearing rocks of the Roman and Birunga volcanic regions. *J. Petrol.* **11**, 33-47 (1970)
- Cundari, A., Mattias, P.P.: Evolution of the Vico lavas, Roman Volcanic Region, Italy. *Bull. Volcanol.* **38**, 98-114 (1974)
- Ferguson, A.K.: On hour-glass sector zoning in clinopyroxene. *Min. Mag. (London)* **29**, 321-325 (1973)
- Ferguson, A.K., Cundari, A.: Petrological aspects and evolution of the leucite-bearing lavas from Bufumbira, South West Uganda. *Contrib. Mineral. Petrol.* **50**, 25-46 (1975)
- Fornaseri, M., Penta, A.: Elementi alcalini minori negli analcimi e loro comportamento nel processo di analcimizzazione della leucite. *Periodico Mineral. (Rome)* **29**, 85-102 (1960)
- Fudali, R.F.: Experimental studies bearing on the origin of pseudoleucite and associated problems of alkalic rock systems. *Bull. Geol. Soc. Am.* **74**, 1101-1126 (1963)
- Hollister, L.S., Gancarz, A.J.: Compositional sector zoning in clinopyroxene from the Narce area, Italy. *Am. Mineralogist* **56**, 959-979 (1971)
- Huckenholtz, H.G., Schairer, J.F., Yoder, H.S. Jr.: Synthesis and stability of ferri-diopside. *Mineral. Soc. Amer. Spec. Pap.* **2**, 163-177 (1969)
- Kudo, A.M., Weill, D.F.: An igneous plagioclase thermometer. *Contrib. Mineral. Petrol.* **25**, 52-65 (1970)
- Kushiro, I.: Pyroxene solid solutions. Pt. I. The $\text{CaAl}_2\text{SiO}_6$ component. *Jap. J. Geol. Geography Trans.* **33**, 213-220 (1962)
- Le Bas, M.J.: The role of aluminium in igneous clinopyroxenes with relation to their parentage. *Am. J. Sci.* **260**, 267-288 (1962)
- Locardi, E.: Tipi di ignimbriti di magmi mediterranei. Le ignimbriti del vulcano di Vico. *Atti. Soc. Toscana. Sci. Nat.* **72**, 55-173 (1965)
- Locardi, E., and Mittempergher, M.: Relationship between some trace elements and magmatic processes. *Geol. Rundschau* **57**, 313-334 (1967)
- Locardi, E., and Mittempergher, M.: The meaning of magmatic differentiation in some Recent volcanoes of Central Italy. *Bull. Volcanol.* **33**, 1089-1100 (1969)
- Marinelli, G., and Mittempergher, M.: On the genesis of some magmas of typical mediterranean (potassic) suite. *Bull. Volcanol.* **29**, 113-140 (1966)
- Mason, P.K., Frost, M.T., Reid, S.J.B.: Computer programs for calculating correlations in quantitative X-ray microanalysis. *Nat. Phys. Lab. (U.K.) I.M.S. Rep.* **2**, (1969)
- Mathez, E.A.: Refinement of the Kudo-Weill plagioclase thermometer and its application to basaltic rocks. *Contrib. Mineral. Petrol.* **41**, 61-72 (1973)
- Mattias, P.P., Ventriglia, U.: La Regione Vulcanica dei Monti Sabatini e Cimini. *Mem. Soc. Geol. It.* **9**, 331-384 (1970)
- Molina, F., Sonaglia, A.: Rilevamento geomagnetico degli apparati vulcanici Vicano e Sabazio. *Ann. Geofis. (Rome)* **22**, 147-162 (1969)

- Rittmann, A.: Die geologisch Evolution und Differentiation des Somma-Vesumagma. *Z. Vulk.* 15, 8-94 (1933)
- Rittmann, A.: Les Volcans et leur activité. 461 pp. Paris: Masson, 1963
- Savelli, C.: The problem of rock assimilation by Somma-Vesuvius magma. I. Composition of Somma and Vesuvius lavas. *Contrib. Mineral. Petrol.* 16, 328-353 (1967)
- Savelli, C.: The problem of rock assimilation by Somma-Vesuvius magma. II. Composition of sedimentary rocks and carbonate ejecta from the Vesuvius area. *Contrib. Mineral. Petrol.* 18, 43-64 (1968)
- Schairer, J.F.: Melting relations of the common rock-forming silicates. *Am. Ceram. Soc. Bull.* 40, 215-235 (1957)
- Thompson, R.N.: Oscillatory and sector zoning in augite from a Vesuvian lava. *Carnegie Inst. Yearb.* 71, 463-470 (1972)
- Thornton, C.P., Tuttle, O.F.: Chemistry of igneous rocks. I. Differentiation Index. *Am. J. Sci.* 258, 664-684 (1960)
- Watkinson, D.H., Wyllie, P.J.: Phase equilibrium studies bearing on the limestone-assimilation hypothesis. *Bull. Geol. Soc. Am.* 80, 1565-1576 (1969)

Accepted August 29, 1975

Introdu multidis guide to

SCII

Now you can en
cles on any sub
year the Index
(ISR™) will
reviews select
2,700 of the v
tant journals.

Broad Coverage

Over 100 discipli
ence are covered
Agricultural
Environmental
Engineering,
Sciences
Medical & Li
Physical & C
Social & Bel

So you won't hav
references to loca
jects in any of
index—the ISR—
nary lines and re
no matter where
the literature. The
literature publish
nual "review" pr
Review of Genet

Effectively Indexed

The Index to Sci

I'd like to know m
Please send full inf

Name _____

Organization _____

Address _____

City _____

Zip _____

ISI Institut
325 Chestnut St., Ph
European Headc
132 High Street, Uxt